

ETD Archive

Fall 1-1-2019

Role of Tumor Necrosis Factor-stimulated Gene-6 In Cutaneous Wound Healing And Inflammation

Sajina Shakya
Cleveland State University

Follow this and additional works at: <https://engagedscholarship.csuohio.edu/etdarchive>
How does access to this work benefit you? Let us know!

Recommended Citation

Shakya, Sajina, "Role of Tumor Necrosis Factor-stimulated Gene-6 In Cutaneous Wound Healing And Inflammation" (2019). *ETD Archive*. 1312.
<https://engagedscholarship.csuohio.edu/etdarchive/1312>

This Dissertation is brought to you for free and open access by EngagedScholarship@CSU. It has been accepted for inclusion in ETD Archive by an authorized administrator of EngagedScholarship@CSU. For more information, please contact library.es@csuohio.edu.

ROLE OF TUMOR NECROSIS FACTOR-STIMULATED GENE-6 IN
CUTANEOUS WOUND HEALING AND INFLAMMATION

SAJINA SHAKYA

Bachelor of Engineering in Biomedical Engineering

Purbanchal University- NEPAL

December 2009

Submitted in partial fulfillment of requirements for the degree of
DOCTOR OF PHILOSOPHY IN APPLIED BIOMEDICAL ENGINEERING

at the

CLEVELAND STATE UNIVERSITY

December 2019

We hereby approve this dissertation

for

Sajina Shakya

Candidate for the Doctor of Philosophy in Applied Biomedical Engineering degree for the

Department of Chemical and Biomedical Engineering

and CLEVELAND STATE UNIVERSITY'S

College of Graduate Studies by

Dissertation Chairperson, Edward V. Maytin, M.D., Ph.D.

Department of Chemical & Biomedical Engineering October 14, 2019

Department & Date

Dissertation Committee Member, Nolan B. Holland, Ph.D.

Department of Chemical & Biomedical Engineering October 22, 2019

Department & Date

Dissertation Committee Member, Mark Aronica, M.D.

College of Science & Health Professions October 07, 2019

Department & Date

Dissertation Committee Member, Margot Damaser, Ph.D.

Department of Chemical & Biomedical Engineering October 14, 2019

Department & Date

Dissertation Committee Member, Carol de la Motte, Ph.D.

College of Science & Health Professions October 11, 2019

Department & Date

Student's Date of Defense: August 26, 2019

DEDICATION

In memory of my maternal grandmother, Nhuchche Maya Shakya (1936-2019).

I will miss you Aji.

ACKNOWLEDGEMENTS

My adventurous journey to this PhD dissertation would not have been as rewarding or fun filled without many people. I would like to take this opportunity to acknowledge all of those inspirational and supportive individuals.

First of all, I would like to express my deepest appreciation to my research advisor and mentor Dr. Edward Maytin, for his continuous guidance and support during these years. Your unwavering encouragement kept me motivated to push through all the challenges in the way.

I would like to extend my sincere thanks to my committee members for their invaluable suggestions and guidance throughout. Thanks to Dr. Carol de la Motte for her knowledgeable insights, Dr. Margot Damaser for her constructive criticisms, Dr. Mark Aronica for his helpful advices, and my academic advisor Dr. Nolan Holland for helping me keep track of the coursework, among other things. I would also like to acknowledge the Maytin laboratory family- Dr. Judith Mack, Dr. Yan Wang, Dr. Sanjay Anand, and Minou Alipour, for their advices and support in the lab and beyond. My deepest gratitude to Judy for being with me in each and every step of this journey, playing multiple roles, as a patient teacher, a strict supervisor, and at times a firm defender.

Last but not the least, I would like to extend my warmest acknowledgements to my family and friends for their unrelenting love and support during these years and always. I am extremely grateful to my parents for being my strongest support system, and my aunt and siblings for being on my side all the time. Special thanks to my dear friends Savita, Hala and Shataakshi for their advices, care and support.

Finally, I would like to thank my loving husband, Safal, for being beside me in this journey, cheering me up whenever I was down, and helping me see beyond the problems.

ROLE OF TUMOR NECROSIS FACTOR-STIMULATED GENE-6 IN
CUTANEOUS WOUND HEALING AND INFLAMMATION

SAJINA SHAKYA

ABSTRACT

Controlled inflammation is crucial for normal wound healing. Our main aim in this study was to investigate the effect of loss of *tumor necrosis factor-stimulated gene-6* (TSG-6) in cutaneous wound closure and inflammation. TSG-6 by its enzymatic action modifies the extracellular matrix molecule, *hyaluronan* (HA), through the transfer of *heavy chain* (HC) proteins from inter- α -trypsin inhibitor to form HC-HA complexes. Both TSG-6 and HC-HA have been associated with inflammation. Here, we showed that loss of endogenous TSG-6 and HC-HA in TSG-6 null mice results in significantly delayed wound closure and differential neutrophil recruitment compared to wildtype mice. Both of these phenotypes were successfully rescued by reintroduction of TSG-6 into null wounds. We also observed leukocyte recruitment behavior upon chemical injury and propose interesting differences between wildtype and TSG-6 null animals. Further, we showed that levels of the pro-inflammatory cytokine $\text{TNF}\alpha$, and the presence of M1 proinflammatory macrophages, were elevated in TSG-6 null wounds compared to wildtype wounds. To facilitate the analysis of wound macrophages, we have described a detailed protocol to isolate single cells from cutaneous wounds. In a nutshell, our study indicates that TSG-6 is required for normal wound closure and plays an important role in regulating inflammation during wound repair.

TABLE OF CONTENTS

	Page
ABSTRACT	vi
LIST OF TABLES.....	xiii
LIST OF FIGURES.....	xiv
CHAPTER	
I. INTRODUCTION	1
1.1 Overview.....	1
1.2 Wound treatments, and our limited understanding of the biology of wound healing	3
1.3 TSG-6, an important protein that regulates the status of hyaluronan in the extracellular matrix, the availability of cytokines, and the course of inflammation during the course of wound repair.....	5
1.4 Specific Aims	5
II. BACKGROUND	8
2.1 The Skin: A brief overview	8
2.2 Wound healing: General introduction	10
2.3 Hyaluronan: Introduction.....	22
2.4 Inter- α -trypsin inhibitor (α 1)	26
2.5 TSG-6 overview	26

2.6	TSG-6 and HC-HA complexes in diseases.....	32
2.7	Summary	34
III. CUTANEOUS WOUNDS IN MICE LACKING TUMOR NECROSIS		
FACTOR-STIMULATED GENE-6 EXHIBIT DELAYED CLOSURE		
AND AN ABNORMAL INFLAMMATORY RESPONSE.....		
		35
3.1	Introduction	35
3.2	Materials and Methods	39
3.2.1	Animals	39
3.2.2	Wounding experiments	40
3.2.3	Histological assessment of wound closure	40
3.2.4	Western Blotting.....	41
3.2.5	Evaluation of HC modification of hyaluronan (HC-HA analysis).....	42
3.2.6	Immunostaining for neutrophils and macrophages	42
3.2.7	Immunostaining for macrophage phenotypes.....	43
3.2.8	Recombinant TSG-6 injection	44
3.2.9	Flow cytometric analysis for M1 and M2 macrophages.....	44
3.2.10	Statistical analysis.....	45
3.3	Results.....	46

3.3.1	TSG-6 protein is present in unwounded murine skin and increases post wounding	46
3.3.2	There are no redundant enzymes that transfer HC to HA in the skin	47
3.3.3	Absence of TSG-6 results in delayed wound closure	48
3.3.4	Delayed wound closure verification: TSG-6 null wounds displayed slower re-epithelialization	49
3.3.5	The absence of TSG-6 results in differential regulation of neutrophil infiltration into wound bed	53
3.3.6	TSG-6 null mice develop an abnormally pro- inflammatory wound milieu	57
3.3.7	No difference in absolute macrophage number in TSG-6 null wounds compared to WT wounds	58
3.3.8	TSG-6 null mice wound macrophages are polarized towards the pro-inflammatory M1 phenotype at Day 7 post wounding.....	59
3.3.9	Reintroduction of recombinant TSG-6 into TSG-6 knockout wounds restores normal healing.....	61
3.4	Discussion	63
3.5	Limitations.....	68

IV. ISOLATION OF SINGLE CELLS FROM CUTANEOUS WOUNDS FOR FLOW SORTING AND FLOW CYTOMETRIC ASSESSMENT OF MACROPHAGES.....	69
4.1 Introduction.....	69
4.2 Method details	71
4.2.1 Step 1: Wounding and wound collection.....	71
4.2.2 Step 2: Tissue Digestion and single cell preparation	73
4.2.3 Step 3: Cell staining with fluorophore markers for FACS sorting or flow cytometric analysis.....	81
4.3 Method validation.....	95
4.3.1 Validation of FACS sorting.....	95
4.3.2 Validation of flow cytometric analysis	98
4.4 Summary	100
4.5 Limitations.....	101
V. IN-VIVO ASSESSMENT OF LEUKOCYTE ROLLING AND ADHESION UPON CHEMICAL INJURY IN THE PRESENCE OR ABSENCE OF TUMOR NECROSIS FACTOR-STIMULATED GENE- 6 USING INTRAVITAL MICROSCOPY	102
5.1 Introduction.....	102
5.2 Materials and Methods	105
5.2.1 Animals	105

5.2.2	Croton oil-induced ear inflammation	105
5.2.3	Validation of croton oil-induced inflammation	106
5.2.4	Intravital microscopy	106
5.2.5	Analysis of leukocyte behavior.....	108
5.2.6	Statistical analysis.....	109
5.3	Results.....	109
5.3.1	Croton oil induces inflammation at 4 hours after application.....	109
5.3.2	The number of rolling cells induced by chemical injury is lower in TSG-6 null ears than in WT ears.	110
5.3.3	The number of adherent cells induced by chemical injury appears to be higher in TSG-6 null ears compared to WT ears.	111
5.4	Discussion	115
5.5	Limitations.....	118
VI.	CONCLUSIONS AND RECOMMENDATIONS.....	120
6.1	Introduction	120
6.2	Findings	121
6.3	Recommendation for future research	123
6.4	Conclusion	125

BIBLIOGRAPHY.....	126
APPENDIX	149

LIST OF TABLES

Table	Page
2-1 Three different types of HASs produce different sized hyaluronic acid (HA) in mammals	24
5-1 Table detailing the different measurements and calculations for each group	114
6-1 Summary of the specific aims and the results from the hypotheses explored in the thesis	122

LIST OF FIGURES

Figure	Page
2-1 Skin is conventionally divided into two layers.	10
2-2 Wound healing is a complex process.	14
2-3 The extravasation of leukocytes involves a cascade of events.	17
2-4 Neutrophils play important roles in wound healing and tissue repair.....	18
2-5 Macrophages perform several functions in cutaneous wound healing.	19
2-6 Wound macrophages are broadly categorized into two phenotypes: the pro-inflammatory M1 and the anti-inflammatory M2 phenotype.....	21
2-7 Abnormal inflammation results in improper wound healing.	22
2-8 The disaccharide unit of hyaluronic acid.....	23
2-9 Structure for Versican and Aggrecan showing the HA binding region (HBR).....	25
2-10 Modular structure of TSG-6	27
2-11 TSG-6 is a multifunctional protein.....	28
2-12 Schematics for transfer of $\alpha 1$ HC to HA.....	29
3-1 TSG-6 protein and HC-HA are present in unwounded murine skin and increase post wounding.	47
3-2 TSG-6 HC transfer activity is non-redundant in skin.....	48
3-3 Loss of TSG-6 results in delayed wound closure.....	49
3-4 Delayed wound closure phenotype in TSG-6 null wounds were confirmed by histological analysis of re-epithelialization.....	51
3-5 Loss of TSG-6 results in an abnormal inflammatory response.....	54

3-6	Absence of TSG-6 results to a more pro-inflammatory wound milieu.....	58
3-7	No difference in macrophage recruitment observed in TSG-6 null wounds compared to WT.	58
3-8	Loss of TSG-6 polarizes cutaneous macrophages to more pro-inflammatory and less anti-inflammatory phenotype.....	60
3-9	Introduction of rTSG-6 into TSG-6 null wounds rescues the delayed closure and abnormal neutrophil recruitment.....	62
4-1	Wounds on the shaved back of a mouse.	73
4-2	Schematic for step 2-10.	79
4-3	Schematic showing preparation of control tube with cells.	84
4-4	Control and experimental tubes for FACS sorting.	89
4-5	Control and experimental tubes for flow cytometric analysis.	92
4-6	Representative dot plots for FACS sorting.....	96
4-7	Evaluation of Adgre1 expression for the two FACS sorted cell populations.....	98
4-8	Gating strategy for flow cytometric analysis and representative dot plots for experimental samples.....	99
5-1	Positioning of the mice for microscopy.	107
5-2	Croton oil induces neutrophil recruitment after 4 hours of application.	110
5-3	Rolling behavior of leukocytes.	111
5-4	Adhesion behavior of leukocytes.	112
5-5	Representative images for intravital microscopy of croton oil or acetone treated ear vessels.....	113

CHAPTER I

INTRODUCTION

1.1 Overview

A wound in simplest terms is any kind of disruption, shallow or deep, of the protective epithelial barrier of the skin. The most common causes of wounds are trauma or accidents, including burns, surgical intervention due to various underlying conditions, and ulcers due to long-term pressure, shear, or chronic diseases such as diabetes and vascular insufficiency. Depending upon the length of time required for healing, wounds are basically categorized as either acute or chronic. While acute wounds heal normally, chronic wounds are the kind that do not heal and remain open for more than one month (Lindholm and Searle 2016; Sen 2019).

Chronic wounds generally do not occur in healthy individuals, and are instead connected to some underlying pathological condition such as diabetes or cardiovascular disease. Because of this, the cost of wound care management has not been as well defined as other health conditions (Sen et al. 2009). However, recently available studies show that management of wound care makes up a substantial portion of the health care economies of the USA and Europe (the two

largest wound-dressing markets in the world). Thus, an estimated 6.5 million people in the USA and 2 million people in Europe are affected by chronic wounds at any one time (Lindholm and Searle 2016; Sen 2019).

A retrospective analysis of the Medicare 5% Limited Data Set for 2014 by Nussbaum et al. of different categories of acute and chronic wounds, published in 2018, found that ~15% of Medicare users, equating to 8.2 million people, had at least one type of wound or infection. The most prevalent cause of wounds was found to be surgical wounds at 4%, followed by diabetic infections at 3.4%. The resultant total Medicare expense for all analyzed wounds was projected at between \$28.1 and \$96.8 billion (Nussbaum et al. 2018). Considering that chronic wounds are most common in the elderly and in people with underlying conditions (such as diabetes), both populations that are on the rise, costs can be expected to increase even more in the coming years. Overall, about 2% of the total U.S. population is estimated to be affected by chronic wounds (Sen 2019).

Another retrospective cohort analysis of the Healthy Improvement Network Database for wound management in the U.K. during 2012-2013 found that an estimated 2.2 million wounds were treated during that time period, amounting to a cost ranging from £4.5 to £5.1 billion. The most common wound type observed in that population was leg ulcers (uncharacterized etiology) at 19%, followed by leg ulcers (venous etiology) at 13% (Guest et al. 2015).

The costs of wound management include expenses related to wound care products and devices, to hospital stays and outpatient hospital visits, and to fees from health care professionals. Wounds also have a significant impact on the

quality of life, both for the injured person and for caregivers including family members; the multiple stressors involving pain, anxiety, social isolation, and loss of financial income. Due to the hidden effects of chronic wounds not only upon the patient but also the people around them, the phenomenon of non-healing wounds has been called 'the silent epidemic' (Lindholm and Searle 2016).

1.2 Wound treatments, and our limited understanding of the biology of wound healing

Depending upon the extent and type of the wound, wound healing involves various types of cells including epidermal cells, inflammatory cells, endothelial cells and connective tissue cells. Importantly proper wound healing requires the timely and controlled activation of all cells and tissues involved. For successful wound management, the main purpose is to attain fast wound closure while avoiding any kind of infection while attaining the least scar possible (Martin 1997). Several developments have been made in the field of wound healing to fulfill this purpose. Some of these include wound dressings, surgical (grafts) and non-surgical innovations, growth factors, and (most recently) stem cell therapy (Ather et al. 2019).

Wound dressings or bandages, along with topical ointments, are the simplest category of wound healing methodology and has been in practice for a long time. While the ancient Egyptians used honey-soaked linens as rather effective antimicrobial wound dressings, newer developments have been made in the field by introducing interactive dressings made of hydrophilic materials such as hydrogels, alginates, polyurethane foams, and hydrocolloids which can retain

moisture, thereby making a more favorable environment to improve wound healing. Dressings made of semi-permeable films are now available, which are permeable to water vapor and oxygen but not to water and infectious microorganisms. (Ather et al. 2019; Dhivya et al. 2015). Bioengineered grafts and tissue engineered skin substitutes including auto-, allo-, or xeno-grafts (epidermal or dermal) are under investigation, designed to be surgically applied to the injured area. Other, non-surgical methodologies such as negative pressure wound therapy, hyperbaric oxygen,, and electrical stimulation to restore electrical potential of the cells, are also available (Ather et al. 2019). Additionally, studies are being conducted to understand the application of protein growth factors, such as epidermal growth factor (EGF), fibroblast growth factor (FGF), and platelet derived growth factors (PDGF), that were shown to promote wound healing in murine models. Most recently, the use of stem cells that can release a number of these growth factors is also being investigated (Ather et al. 2019; Yamakawa and Hayashida 2019).

Unfortunately (and rather disappointingly), none of the above-mentioned advancements in wound treatment methodologies have made a significant difference in reducing current rates of morbidity and mortality in the setting of chronic human wounds. The inescapable conclusion is that only by obtaining a better understanding of the critical underlying biological events in the wound micro-environment, can we hope to achieve better wound healing outcomes. Conversely, when armed with improved understanding of basic biology, there will be hope for developing more efficient treatments for chronic wounds.

1.3 TSG-6, an important protein that regulates the status of *hyaluronan* in the extracellular matrix, the availability of cytokines, and the course of inflammation during the course of wound repair.

Our purpose here is to understand the underlying biology of wound healing with respect to the ubiquitous extracellular matrix *hyaluronan* (HA) which is known to play important roles in wound healing (Maytin 2016). In this thesis we investigate the role of *tumor necrosis factor-stimulated gene-6* (TSG-6) protein during cutaneous wound healing by employing a mouse model which lacks the gene that encodes TSG-6. More details on these molecules and their roles in wound healing are discussed in Chapters 2 and 3.

1.4 Specific Aims

Specific Aim 1: To determine how loss of TSG-6 affects wound closure and recruitment of inflammatory cells. [Chapter 3]

Rationale: Faster wound closure is a prime goal in wound management, to prevent infection and loss of body fluids. Literature suggests that TSG-6 plays an anti-inflammatory role by inhibiting neutrophil recruitment and by promoting the appearance of tissue-reparative macrophages. Also, studies show that exogenous sources of TSG-6 promote faster wound closure. For these reasons, the absence of TSG-6 in TSG-6 null mice are expected to make cutaneous wounds heal slower, accompanied by exacerbated inflammation, when compared to wounds in wild-type (WT) mice.

Hypotheses: (1) Absence of anti-inflammatory TSG-6 protein will cause a delay in wound closure in TSG-6 null mice. (2) TSG-6 null mice will have increased neutrophil recruitment and abnormal macrophage polarization. (3) Re-introduction of TSG-6 to the null wounds by addition of recombinant TSG-6 will rescue both the wound closure delay and the proinflammatory phenotype in TSG-6 null mice.

Specific Aim 2: To develop a viable protocol to isolate single cells from cutaneous wounds for flow sorting and flow cytometric assessment of leukocytes in WT and TSG-6 null wounds, with a particular emphasis on macrophages. [Chapter 4]

Rationale: Flow sorting and flow cytometric analysis are sensitive ways to analyze individual cells or a certain population of cells. However, a detailed protocol to isolate single cells from cutaneous wounds is lacking. Availability of a comprehensive protocol, describing all the minute details of single leukocyte cell isolation, will further the understanding of the wound microenvironment.

Hypothesis: (1) The flow-sorted population of wound macrophages will express the macrophage-specific adhesion G protein-coupled receptor E1 (*Adgre1*) gene, while the non-macrophage population will not express this gene. (2) Flow cytometric analysis will allow us to analyze each cell in the single cell suspension and help us determine the different levels of macrophage polarization.

Specific Aim 3: To determine how the absence of TSG-6 affects rolling and adhesion behavior of leukocytes *in vivo* after chemical injury using intravital microscopy. [Chapter 5]

Rationale: Literature indicates that TSG-6 plays an anti-inflammatory role by inhibiting neutrophil recruitment. However, direct evidence regarding the details of neutrophil transmigration behavior within small blood vessels at sites of injury in the skin is missing. Intravital microscopy allows the assessment of leukocytes *in vivo*, and therefore should make it possible to understand the effects that loss of TSG-6 exerts upon leukocyte rolling and adhesion behavior.

Hypothesis: (1) Upon chemical injury, leukocyte rolling behavior in cutaneous blood vessels in TSG-6 null mice will be differentially regulated as compared to WT mice. (2) Upon chemical injury, leukocyte adhesion (arrest) behavior in the blood vessels of TSG-6 null mice will be differentially regulated as compared to WT mice.

CHAPTER II

BACKGROUND

The purpose of this chapter is to provide the reader with sufficient background information to understand the following main concepts: (1) The different stages of cutaneous wound healing; (2) the inflammatory cells involved in wound healing, including how these cells get recruited to the wound site and what roles they play; and (3) how tumor necrosis factor-stimulated gene-6 (TSG-6) modifies hyaluronan (HA) and affects inflammation in the skin.

2.1 The Skin: A brief overview

The skin is a large organ that covers the entire body of an animal, forming a physical barrier between the organism and its environment. The skin is conventionally described as consisting of two layers- the outer epithelial tissue layer (epidermis), and the inner connective tissue layer (dermis) (Figure 2-1). Under the skin is a layer of adipose tissue called the subcutaneous layer, or hypodermis (McLafferty et al. 2012; Odland and Goldsmith 1991).

The epidermis comprises several stratified layers of keratinizing epithelium, which are named (from outermost to innermost) as the *stratum corneum*, the *stratum granulosum*, the *stratum spinosum*, and the *stratum basale*. The major cell

type of the epidermis is the keratinocyte. Keratinocytes in the basal layer are cuboidal and are actively dividing. With maturation, these cuboidal cells differentiate and undergo physical changes as they migrate upwards, forming the upper layers of the epidermis. In addition to keratinocytes, other cell types are dispersed within the different layers of the epidermis; these include *melanocytes*, *Langerhans cells*, and *Merkel cells*, with each cell type performing specific functions. Also embedded within the skin are various appendages, such as the hair follicle, the sebaceous gland, and the sweat gland. These appendages are vital for thermoregulation and environmental sensing. Thus, the skin forms a protective, semi-permeable envelope that aids in the regulation of body homeostasis (Proksch et al. 2008; Sotiropoulou and Blanpain 2012). Under the epidermis is a layer of extracellular matrix known as the *basement membrane* that separates the epidermis from the underlying dermis.

The *dermis* is a connective tissue layer composed of structural components, such as collagen fibers (predominantly Types I and III), elastic fibers (elastin and fibrillin), and glycosaminoglycans (GAGs, including hyaluronan) that provide physical strength to the skin. The major cell type of the dermis is the fibroblast which is primarily responsible for the maintenance of the structural elements of the dermis. Other cell types in the dermis are resident dermal macrophages and dendritic cells. The dermis also contains a network of vasculature, nerves, and the appendages mentioned above. With the aid of all of these cellular and structural components, the dermis provides mechanical strength and nutrients to the skin (McLafferty et al. 2012; Odland and Goldsmith 1991).

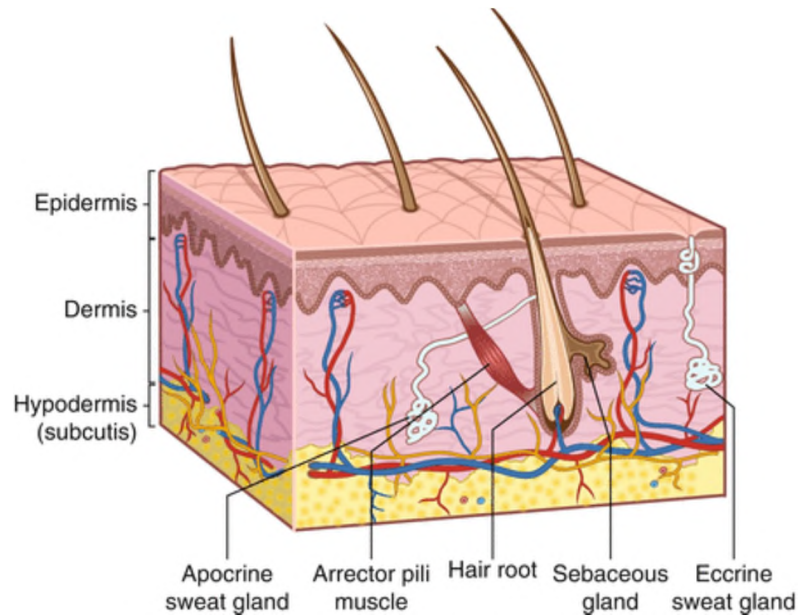


Figure 2-1. Skin is conventionally divided into two layers.

The upper epithelial tissue layer called the epidermis provides a semi-permeable barrier, and the lower connective tissue layer called the dermis provides mechanical strength. [Adapted from (Rehfeld et al. 2017)]

2.2 Wound healing: General introduction

As the skin is the first layer of protection for the body against the outside environment, the presence of an intact barrier layer is critical. Loss of integrity of skin, for any reason, is termed as skin wound. Skin wounds can be caused by accidents (trauma), burns, surgery, or as a result of chronic diseases such as diabetes. Depending upon the level of injury and the time it takes to heal, wounds can be grossly categorized as acute wounds or chronic wounds (Lindholm and Searle 2016).

While the main goal of wound care management, in general, is to attain fast and efficient wound closure with the least scar, not all wounds heal normally (Martin 1997). Abnormal wound healing is an important medical issue (as discussed in Chapter 1), whether the problem is a non-healing wound (chronic

ulcer) or an imperfectly healing wound (e.g., hypertrophic scars or keloid). To understand the many possible reasons for abnormal wound healing, a basic understanding of normal wound healing biology is essential. The next section gives a brief picture of this complex process.

2.2.1 Phases of cutaneous wound healing

Wound healing is an intricate affair, involving a timely and controlled action of many different cell types and molecules. To better conceptualize this complex process, the events in wound healing are divided into three major phases that partially overlap in time. These steps are, a) the *inflammatory* phase, b) the *tissue formation* phase, and c) the *tissue remodeling* phase. Figure 2-2 illustrates the various events that occur during the three phases of wound healing, which are also described briefly below.

2.2.1.1 Inflammatory phase

In the first part of the inflammatory phase, the injured endothelial cells release signals that initiate vasoconstriction immediately after wounding. Circulating platelets aggregate at the wound site, forming a physical plug (blood clot) that helps to stop blood loss and achieve hemostasis. This platelet plug further acts as a provisional matrix (a scaffold) for later events. Also, platelets release essential growth factors, such as platelet-derived growth factor (PDGF) and transforming growth factor (TGF- β), along with cytokines such as tumor necrosis factor (TNF)- α and interleukin (IL) -1 that promote migration (chemotaxis) of leukocytes and fibroblasts (Kirsner and Eaglstein 1993; Singer and Clark 1999).

The next event in the inflammatory phase is the influx of inflammatory leukocytes into the wound site following the release of the cytokines and growth factors by the platelets and endothelial cells. Neutrophils are the first of the leukocytes to reach the wound site, coming in as early as the first few hours (Clark 2001; Diegelmann and Evans 2004). These cells release proteases from their cytotoxic granules that attack any infectious agents in the wound. The neutrophils in normal wounds are short-lived and quickly undergo apoptosis. Following closely behind, monocytes reach the site in about 2-3 days and differentiate into macrophages which phagocytose the debris, including dead neutrophils and bacteria (Broughton et al. 2006). Macrophages are further categorized into pro-inflammatory M1 phenotypes and anti-inflammatory M2 phenotypes, which will be discussed further in detail in a separate section below. Briefly, M1 macrophages release the toxic agent *nitric oxide*, thus promoting inflammation, whereas M2 macrophages produce *polyamines* essential for cell functions (Martinez and Gordon 2014). Activated leukocytes also release several inflammatory cytokines, continuing the cascade of events.

2.2.1.2 Tissue formation phase

The second phase in wound healing is the tissue formation phase, which starts around 3 days after injury and continues for about a week. It is characterized by epithelial migration and proliferation, along with fibroblast migration, proliferation and differentiation. In this phase, cross-talk (between macrophages and fibroblasts primarily) initiate fibroblast proliferation; migration of keratinocytes occurs; and synthesis of collagens and GAGs by activated fibroblasts begins.

Additionally, keratinocytes express VEGF, resulting in the proliferation of endothelial cells and the formation of new vessels, termed as neovascularization. Collectively, this newly formed tissue is called *granulation tissue*, so-called because of the granular appearance of the small hemorrhagic dots (neovascularization) that are visible when a newly-forming scab is picked off the skin (Broughton et al. 2006; Diegelmann and Evans 2004; Kirsner and Eaglstein 1993).

2.2.1.3 Tissue remodeling phase

The tissue remodeling phase starts at about the first week after injury. During this last phase of wound healing, the fibroblasts phenotypically differentiate into myofibroblasts. Myofibroblasts are activated fibroblasts that contain microfilaments of alpha smooth muscle actin (α -SMA) which enable them to contract. Thus, wound contraction is made possible by fibroblast-to-myofibroblast conversion. Additionally, the deposition of extracellular matrix (ECM) continues and eventually replaces the granulation tissue with a mature and organized matrix rich in collagen. Inflammation gradually resolves, and the newly formed vessels start to retract (Olczyk et al. 2014; Schafer and Werner 2008). The tissue remodeling phase can continue from weeks to months.

Hyaluronan (HA) is an important extracellular matrix molecule in skin that is known to play important roles in all different phases of wound healing (Figure 2-2). HA is known to facilitate neutrophil infiltration into the wound site, to maintain vascular integrity by modifying the endothelial glycocalyx, to modify epithelial migration, to affect the expression of pro-inflammatory cytokines like TNF α , and to

regulate angiogenesis (Aya and Stern 2014). More about HA will be discussed in Section 2.3 below.

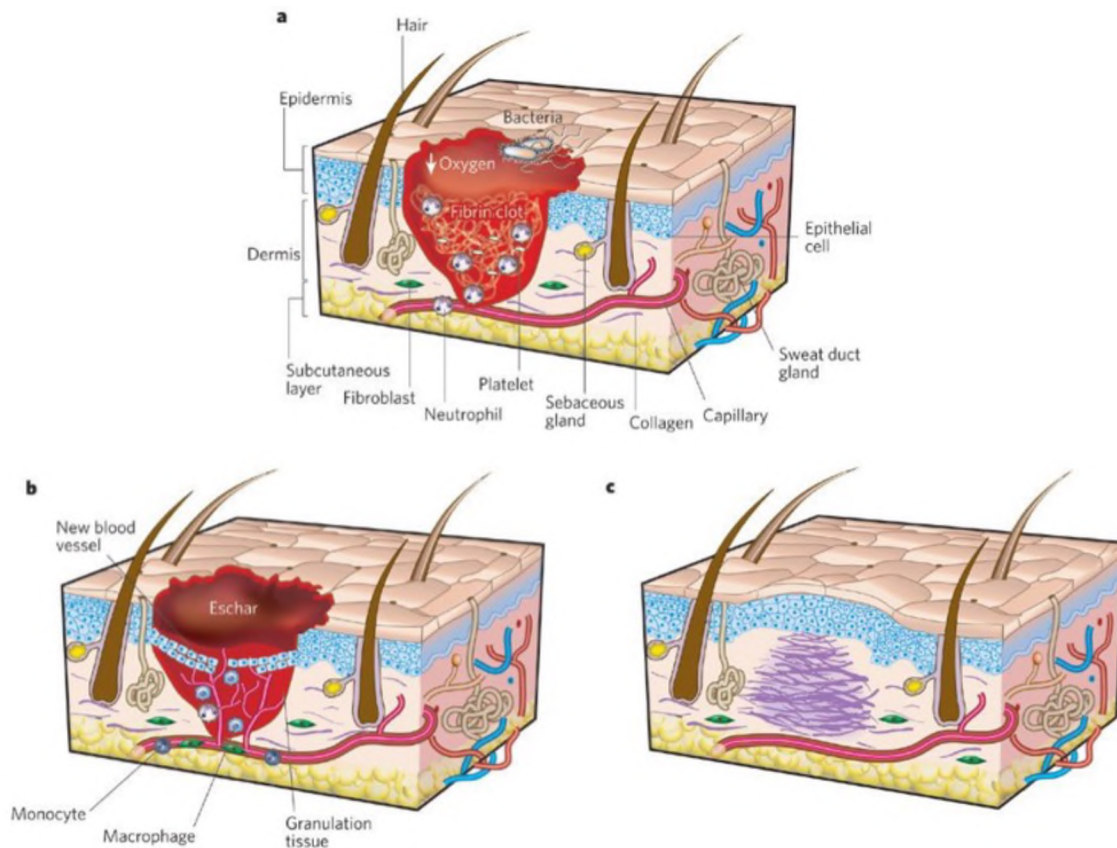


Figure 2-2. Wound healing is a complex process.

Depicted are the sequence of events during normal cutaneous wound healing. Each of the three phases- (a) inflammation, (b) tissue formation, and (c) remodeling, consists of multiple events happening simultaneously. [Adapted from (Gurtner et al. 2008)]

2.2.2 Inflammatory cells in wound healing

2.2.2.1 Recruitment of inflammatory leukocytes

A large part of this Thesis revolves around the second part of the inflammatory phase of wound healing, i.e. the recruitment of inflammatory leukocytes into wounds, specifically neutrophils and macrophages. Inflammatory cells are not normally present outside the blood vessels in normal skin, but after

injury, leukocytes invade the extravascular tissue in large numbers in response to different cytokines and chemokines. Leukocyte export is facilitated by different chemotactic factors and their interaction with the endothelial cells (Diegelmann and Evans 2004). Different cytokines and chemokines produced by injured tissue cell types, including endothelial cells and the macrophages and activated neutrophils themselves, facilitate the recruitment of leukocytes from the circulating blood. Once out of the vessels, leukocytes are stimulated to act as phagocytic cells and/or release their contents, causing cytotoxic effects. Recruitment of circulating leukocytes from the blood circulation to the injury site entails multiple steps (Figure 2-3), and involves the sequential activation of different adhesion molecules and their corresponding ligands on leukocytes and endothelial cells (Wagner and Roth 2000). The specificity of leukocyte migration is mostly determined by the type of adhesion molecules expressed.

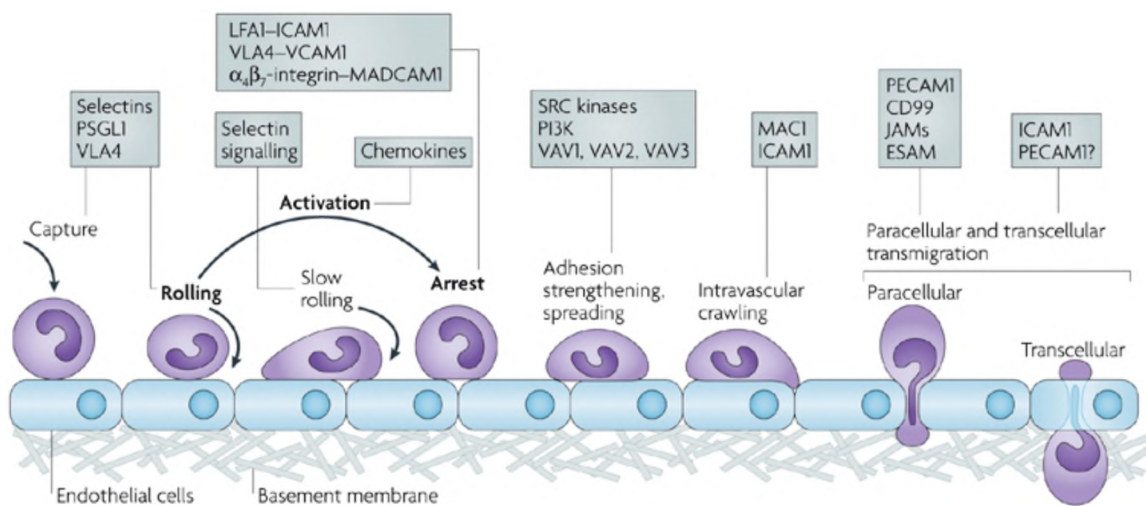
Events in Leukocyte extravasation:

The first step in the migration of leukocytes is capture/tethering and rolling (Ley et al. 2007), which is mediated by a kind of transmembrane glycoprotein adhesive molecule called *selectin*. Three different types of selectins are responsible for this process, causing the leukocytes to slowly roll on the vessel wall. When suitable inflammatory stimuli are present, *P-selectins* on platelets and endothelial cells can efficiently capture neutrophils from the flow by binding to their ligands on the neutrophils (Stone and Nash 1999). The next selectin type is *L-selectin* which is present on the surface of leukocytes and binds to its ligand on endothelial cells (Kishimoto et al. 1995). The third type of selectin, *E-selectin*, is

expressed on endothelial cells upon stimulation by inflammatory cytokines, and binds to its ligand on the surface of neutrophils. Selectin-induced binding of neutrophils to the endothelial cells is a weak and reversible interaction. Binding decreases the velocity of the blood cells and helps in margination. A firmer type of binding, known as adhesion, needs to occur before leukocytes can transmigrate from the circulation (Ley et al. 2007).

The next step in the migration of leukocytes is adhesion, in which leukocytes adhere more strongly to the vessel wall. The process is mediated by two groups of molecules, namely, integrins and cellular adhesion molecules (CAMs). *Integrins* are glycoproteins on migrating cells, that play an important role in intercellular binding as well as in mediating interactions between migrating cells and the extracellular tissue (Von Andrian et al. 1992; Wagner and Roth 2000). The second group of adhesion molecules, CAMs, such as intercellular adhesion molecule (ICAM-1) and vascular cell adhesion molecule-1 (VCAM-1), act as ligands on the endothelial cells for the integrin molecules (Sadik et al. 2011). These adhesion molecules are activated by different inflammatory cytokines such as tumor necrosis factor (TNF)- α and interleukin-1 (IL-1), as well as the selectin-mediated interaction between leukocytes and endothelial cells (Lawrence and Springer 1991; Reinhardt et al. 1997; Von Andrian et al. 1992; Wagner and Roth 2000). Once activated, the integrin-mediated cell-cell interaction is strong and stable. With time, as more signals are received, more integrin-ligand binding occurs. This causes a stronger and more stable binding between the two types of cells, preparing leukocytes to escape from the blood vessels.

Adhesion is then followed by diapedesis or transmigration. This is the movement of leukocytes through the endothelial cell layer by either transcellular or paracellular migration. Numerous cytokines and chemotactic factors are responsible for this. One of the major mediators of trans-endothelial migration is Platelet/endothelial cell adhesion molecule 1 (PECAM-1 or CD31). It was shown that when PECAM-1 was blocked using anti-PECAM, transmigration of neutrophils was inhibited (Muller et al. 1993; Wagner and Roth 2000).



Nature Reviews | Immunology

Figure 2-3. The extravasation of leukocytes involves a cascade of events.

Upon receiving chemical signals from the wound bed, the freely flowing leukocytes in the blood vessels start slowing down, roll on the endothelium, adhere, and finally transmigrate. [Adapted from (Ley et al. 2007)]

2.2.2.2 Functions of inflammatory leukocytes in cutaneous wound healing and repair

Neutrophils, also known as *polymorphonuclear leukocytes* (PMNs), are the first circulating inflammatory cells to be recruited to the wound bed after injury. Recruitment of neutrophils starts within a few minutes after injury, mediated by chemokines such as IL-8 and monocyte chemoattractant protein-1 (MCP-1)

(Engelhardt et al. 1998). Figure 2-4 below depicts the functions of neutrophils in wound healing and repair.

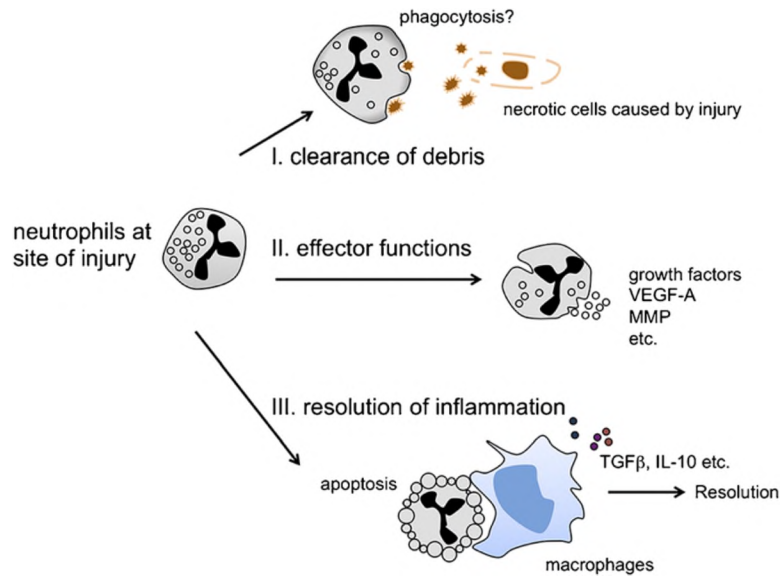


Figure 2-4. Neutrophils play important roles in wound healing and tissue repair.

Neutrophils are the first inflammatory cells to get to the injury site and play critical roles in proper wound healing and repair. [Adapted from (Wang 2018)]

The recruited neutrophils remove necrotic cells and phagocytose any foreign/infectious agents in the injured tissue by releasing active antimicrobial substances, such as reactive oxygen species (e.g., nitric oxide and hydrogen peroxide), cationic peptides, and proteases such as elastase and proteinases. This is critical for preventing any possible infection, as delayed neutrophil recruitment has been associated with compromised wound healing in humans as well as mice (Eming et al. 2007; Hampton et al. 1998; Nishio et al. 2008; Wang 2018). Another important role of neutrophils is the production of cytokines that activate macrophages and augment inflammatory response. After performing these functions, the recruited neutrophils die (become apoptotic) and are removed by macrophages. Those macrophages also release a variety of growth factors and

anti-inflammatory cytokines. The timely removal of neutrophils is critical, since the toxic factors that neutrophils secrete (although useful for removing infectious agents) can also harm host tissues. Thus, prolonged neutrophil recruitment is linked to impaired wound healing and chronic inflammation (Hampton et al. 1998; de Oliveira et al. 2016; Smith 1994; Wang 2018).

Monocytes are the next group of inflammatory cells recruited from the circulation. The monocytes mature and differentiate into macrophages once they complete their transmigration through the endothelium. Macrophage recruitment in the wound bed is mediated by different chemotactic growth factors and cytokines, including chemokines such as *macrophage inflammatory protein* (MIP) 1 α , MCP-1, and RANTES (Eming et al. 2009). Macrophages first appear around 2-3 days post injury and phagocytose the apoptotic neutrophils. They also contribute to matrix reformation and remodeling by secreting various growth factors and by activating fibroblasts and supporting angiogenesis (Figure 2-5).

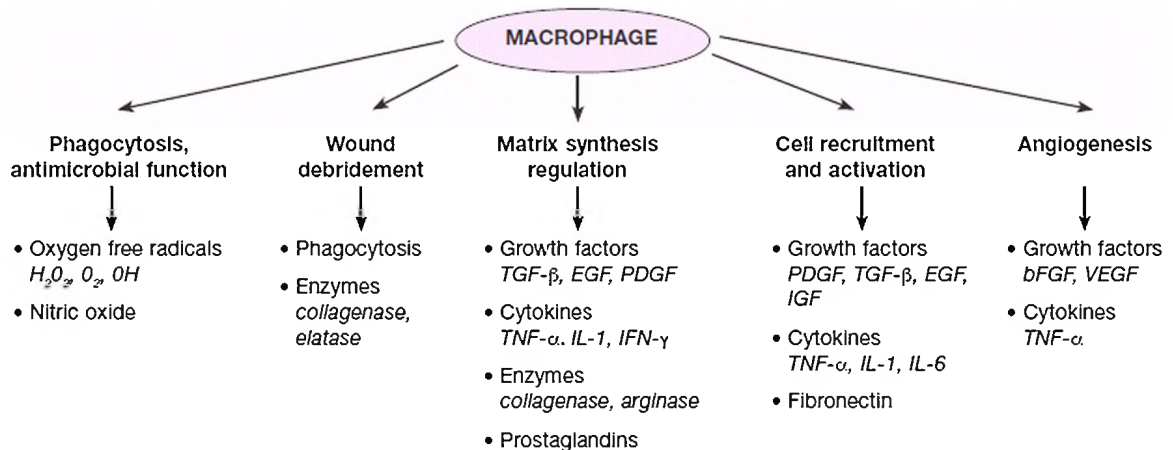


Figure 2-5. Macrophages perform several functions in cutaneous wound healing.

The second type of inflammatory cells, macrophages, appear around 2 days post injury and last for weeks, playing important roles in different events of wound healing. [Adapted from (Chhabra et al. 2017)]

Wound macrophages (Φ) are broadly categorized, based upon their activation stimuli, the markers they express, and the functions they perform, into two phenotypes. These are the classically activated/ pro-inflammatory M1 macrophages, and the alternatively activated/ anti-inflammatory M2 macrophages, also called as tissue reparative macrophages (Figure 2-6) (Hesketh et al. 2017a). Polarization (differentiation) of macrophage into the M1 phenotype is mediated by pro-inflammatory factors such as interferon (IFN)- γ , TNF- α , lipopolysaccharide (LPS), and *damage associated pattern molecules* (DAMPs). In turn, M1 macrophages produce a myriad of pro-inflammatory cytokines, chemokines, and other mediators including TNF- α , IL-6, IL-1 β , IL-12, chemokine [C-X-C motif] ligand 10 (CXCL10), CXCL11, and inducible nitric oxide synthase (iNOS), thus promoting inflammation. M1 macrophages normally appear in the early stages of inflammation and are characterized by the expression of these pro-inflammatory markers (High levels of iNOS, TNF α , IL-12, and IL-6; Low levels of IL-10). On the other hand, M2 macrophage activation (also called 'alternative activation') is mediated by anti-inflammatory cytokines and factors such as, IL-4, IL-10, IL-13, and glucocorticoids. M2 macrophages secrete anti-inflammatory cytokines and growth factors such as, IL-10, transforming growth factor (TGF)- β , VEGF, and insulin-like growth factor-1. The M2 macrophages are responsible for the phagocytosis of apoptotic neutrophils, and execution of tissue reparative functions. Common markers used to identify M2 macrophages are high levels of Arginase-1 and IL-10, along with low levels of TNF- α and IL-12 (Hesketh et al. 2017a; Koh and DiPietro 2011; Martinez and Gordon 2014).

An important thing to note here is that the M1 and M2 phenotypes do not exactly represent two distinct cell populations. Instead, the idea of M1/M2 represents a range of population characteristics that depends upon the macrophage microenvironment, and the maturation of macrophages according to the available stimulation (Brancato and Albina 2011; Koh and DiPietro 2011).

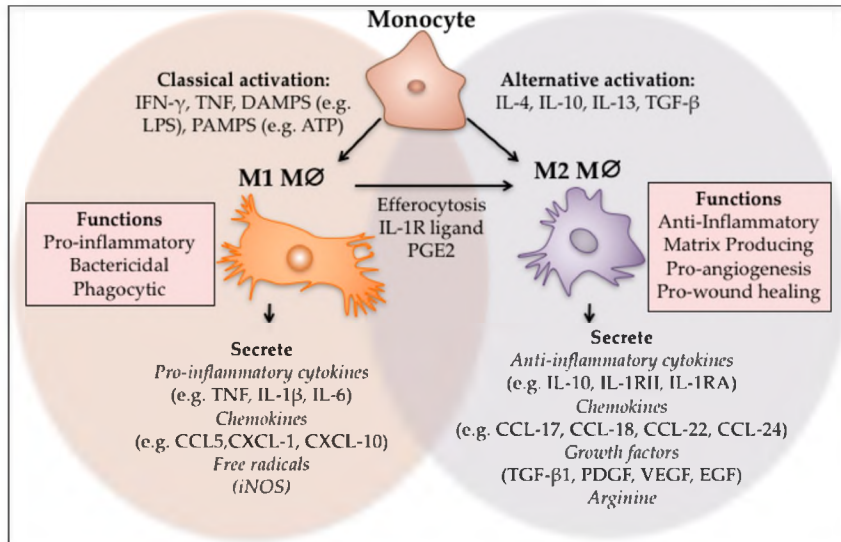


Figure 2-6. Wound macrophages are broadly categorized into two phenotypes: the pro-inflammatory M1 and the anti-inflammatory M2 phenotype.
[Adapted from (Hesketh et al. 2017a)]

2.2.3 Abnormal inflammation and cutaneous wound healing

As explained in earlier sections, a controlled inflammatory response is critical for proper cutaneous wound healing. Figure 2-7 illustrates the effects of abnormal inflammation on the quality of wound repair. The important take-away from this diagram is that persistent inflammation can lead to non-healing wounds, such as occurs in diabetic ulcers or pressure ulcers (Eming et al. 2009).

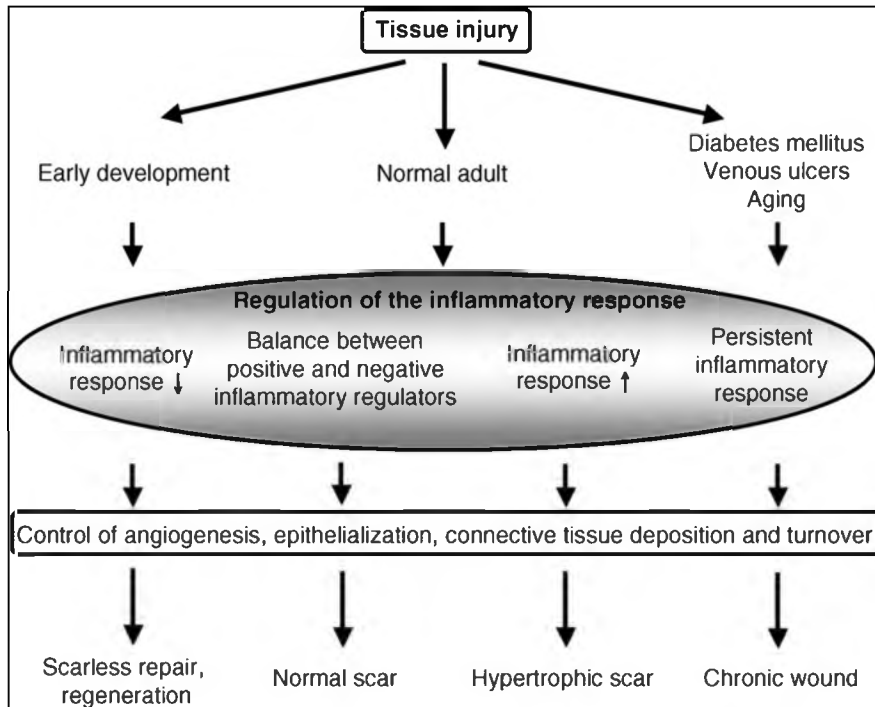


Figure 2-7. Abnormal inflammation results in improper or insufficient wound healing.
 [Adapted from (Eming et al. 2009)]

2.3 Hyaluronan: Introduction

As mentioned above, HA is an important molecule of the extracellular matrix that regulates different phases of wound healing. HA is a high molecular weight, non-sulfated glycosaminoglycan (GAG), composed of long chains of repeated disaccharide sub-units of glucuronic acid (GlcA) and N-acetylglucosamine (GlcNAc) as shown in Figure 2-8 (Hascall and Esko 2009). Unlike other GAGs, HA is not synthesized in the Golgi apparatus, but is instead synthesized on the cytosolic side of the plasma membrane of cells, and then extruded into the extracellular space (Itano and Kimata 2002; Wang and Hascall 2004). Three different membrane-bound enzymes are present in mammals and synthesize HA. The hyaluronan synthase (HAS) genes are: HAS1, HAS2 and HAS3. In contrast,

another group of enzymes called hyaluronidases (HYALs) degrade HA (Fraser and Laurent 1989; Stern and Jedrzejewski 2006; Tammi et al. 1988). The most widely expressed members of the human hyaluronidase (HYAL) family are HYAL 1, 2, 3 and 4, and are highly tissue specific (Stern and Jedrzejewski 2006).

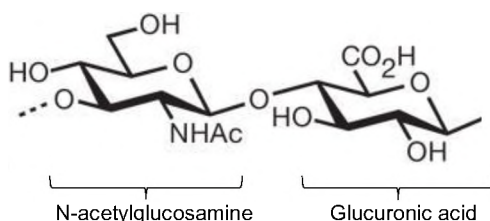


Figure 2-8. The disaccharide unit of hyaluronic acid.

This unit is repeated to form a molecule of tremendous size, up to 2×10^6 Daltons.

Each of the three HAS enzymes produce different-sized HA chains, ranging anywhere from 2×10^5 Da to more than 2×10^6 Da (Table 2-1) (Itano and Kimata 2002). Among these, HAS2 is known to produce the largest HA molecules. Also, it has been found that if the gene for HAS2 synthase is removed, it causes embryonic lethality in mice because of severe cardiac and vascular deformities (Camenisch et al. 2000). Removing HAS1 and/or HAS3 synthase genes, however, does not present any major phenotypic differences, indicating that HAS2 is the most important hyaluronan synthase during embryonic development. The size of HA is very significant in determining its effect. For example, high molecular weight HA (HMW-HA) plays protective functions in maintaining vessel integrity and endothelial permeability. HMW-HA can form a coiled structure on the endothelium, thus limiting direct access of blood cells and plasma factors to the endothelial cells (Lennon and Singleton 2011). Depending on its size, HA can also have pro- or anti-inflammatory functions (Rayahin et al. 2015; Weigel et al. 1986).

Table 2-1. Three different types of HASs produce different sized hyaluronic acid (HA) in mammals.

While HAS2 produces larger molecular weight HA, HAS1 and HAS3 are known to produce relatively smaller HA molecules.

Hyaluronan synthase (HAS)	Size of hyaluronic acid (HA) produced	Functions
HAS1	2×10^5 to 2×10^6 Da	Upregulation noted in inflammatory diseases such as osteoarthritis and rheumatoid arthritis Associated with tumor progression (Siiskonen et al. 2015)
HAS2	$> 2 \times 10^6$ Da	Source of HA in cardiac morphogenesis (Camenisch et al. 2000)
HAS3	2×10^5 to 2×10^6 Da	Plays crucial role in gut inflammation (Kessler et al. 2015)

HA is an important ECM component that is ubiquitously distributed in mammalian connective, epithelial, and neural tissue (Itano and Kimata 2002). A gooey material, HA is highly hydrophilic and capable of holding a large amount of water. Because of this, HA contributes to the viscoelastic properties of the vitreous humor in the eye, and to the lubricating properties of synovial fluid of articular joints (Sebag 1987; Swann et al. 1974). Similarly, HA helps to maintain the elasticity of skin tissue, and its hydrating properties makes HA a very popular ingredient in topical creams and cosmetics (Hascall and Esko 2009).

2.3.1 Hyaluronan in cutaneous wound healing

Originally, HA was considered to be just an inert extracellular matrix component, essentially a “filler”. However, HA has now been found to participate in the active regulation of many cellular behaviors (Maytin 2016; Noble 2002; Tammi et al. 2002; Turley et al. 2002). HA in the ECM participates in intracellular signaling by binding to cells via a plasma membrane receptors called CD44, and to a soluble protein called *Receptor for HA-mediated motility* (RHAMM, CD168)

(Turley et al. 2002; Underhill 1992). HA regulates cell proliferation and migration during embryogenesis (Toole 2001), wound healing (Nagy et al. 2010; Stenson 2010), and tumor growth (Toole et al. 2002). Additionally, HA is known to affect angiogenesis (Pardue et al. 2008), a process that involves activation of the HA receptors CD44 and RHAMM (Slevin et al. 2007).

HA has been shown to regulate keratinocyte migration in the epidermis, thus affecting cutaneous wound healing (Mack et al. 2003). Also, the role of HA in inflammation during wound healing is a highly researched area (Back et al. 2005; Mack et al. 2012; Nagy et al. 2010; Neudecker et al. 2004; Stenson 2010).

2.3.2 HA modification

Although structurally a very simple molecule, HA can be modified by binding to various glycoproteins (9). Proteoglycans such as aggrecan and versican contain an HA binding region (HBR) in their N-terminus which facilitates binding to HA (Figure 2-9). Versican, aggrecan, and similar molecules are therefore called *hyaladherins* (Iozzo and Murdoch 1996; Wight et al. 2013). Another more recently-identified hyaladherin, one that actually modifies HA, is a protein called *TNF α stimulated gene-6* (TSG-6). The latter is discussed in more detail below.

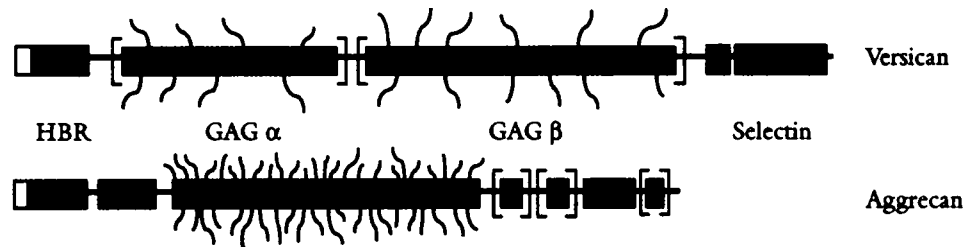


Figure 2-9. Structure for Versican and Aggrecan showing the HA binding region (HBR) (Adapted from (Iozzo and Murdoch 1996))

2.4 Inter- α -trypsin inhibitor ($I\alpha I$)

The $I\alpha I$ family of proteins are produced mostly in the liver, and are present in the blood in high amounts (Zhuo and Kimata 2008). These proteins are composed of a common light chain comprising a GAG chain, *chondroitin sulfate* (CS), covalently attached to a core protein (bikunin protein, decorated with two closely related *heavy chains* (HCs). There are 6 different known genes encoding human HCs. HC 1 and 2 are the predominant isoforms in human $I\alpha I$; HC3 along with CS and bikunin form the pre- α -trypsin inhibitor ($P\alpha I$). HC 4 and 5 are not as well-defined as the first three isoforms. HC 4 exist as a free HC in circulating blood and does not bind to bikunin. HC 5 is localized to only a few organs including mammary glands, ovaries, uterus, thyroid, and is most common in the placenta (Zhuo and Kimata 2008).

2.5 TSG-6 overview

2.5.1 Introduction, and TSG-6 regulation

TSG-6 protein is a member of the hyaluronan (HA) binding protein family, first characterized by Lee et al. in 1992 in $TNF\alpha$ treated normal human fibroblast cell lines (Lee et al. 1992). The TSG-6 gene codes for a glycoprotein of about 30-35 kDa, consisting of a *Link domain* at its N-terminus and a *CUB domain* (Complement components C1s/C1r, uEGF, BMP1) at the C-terminus (Milner and Day 2003). The Link domain contains a sequence similar to sequences in CD44, aggrecan, and versican, all of which bind HA (Lee et al. 1992; Neame et al. 1987). Figure 2-10 shows the modular structure of TSG-6, with the HA binding sequence

of amino acids in the Link domain in *purple*, and the CUB domain in *green*. The function of the CUB domain has not been determined yet.

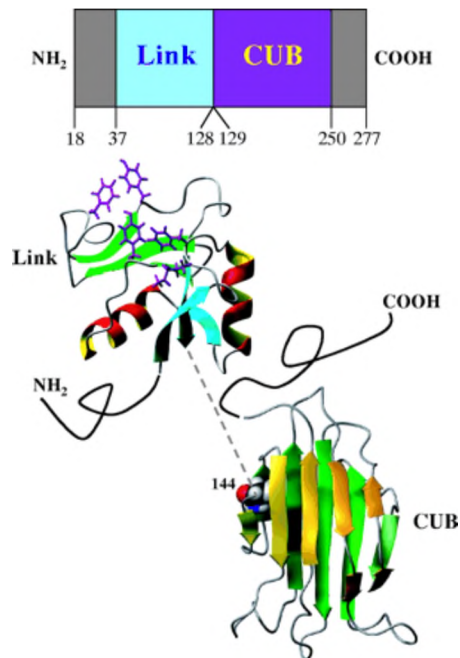


Figure 2-10. Modular structure of TSG-6
[Adapted from (Milner and Day 2003)]

TSG-6, as the name suggests, is induced by the inflammatory cytokine $\text{TNF}\alpha$, as well as interleukin (IL-1). TSG-6 is being widely investigated for its role in inflammation and inflammation-like conditions. While mostly absent in normal tissues, TSG-6 is constitutively present in cumulus cell-oocyte complexes (COCs) during their expansion (Fulop et al. 1997a). Along with its ability to bind to HA, TSG-6 can interact with inter-alpha trypsin inhibitor ($\text{I}\alpha\text{I}$, discussed later in this section) and enhances its plasmin proteolysis inhibition activity. These features of TSG-6 allow for its important role in the stabilization and expansion of the cumulus matrix in the ovary. Expansion of COCs is an important phenomenon for egg cell maturation; the absence of TSG-6 in TSG-6 null mice results in female infertility (Day and de la Motte 2005; Fulop et al. 1997a).

2.5.2 Functions of TSG-6

TSG-6 is known to play various functions in different inflammatory conditions (Day and Milner 2018). Here, we discuss a few of these roles of TSG-6 in inflammation as described in the literature (Figure 2-11).

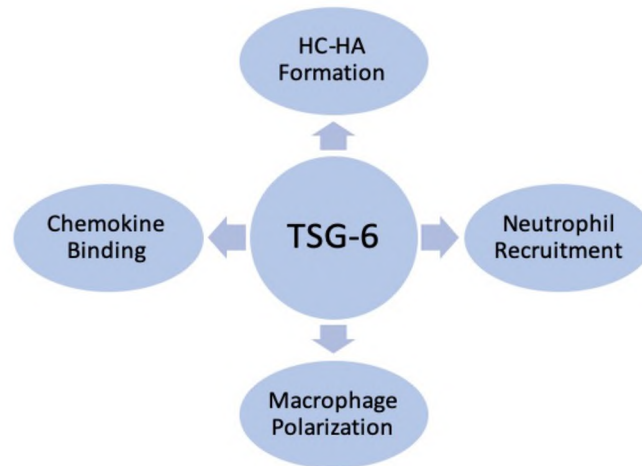


Figure 2-11. TSG-6 is a multifunctional protein.

Shown are some of the roles of TSG-6 that are interrelated and collectively affect inflammation.

2.5.2.1 TSG-6 in HA modification (HC-HA formation)

An important HA modification primarily attributed to the enzymatic activity of TSG-6 is the transfer of heavy chains (HC) from Inter- α -trypsin inhibitor ($I\alpha 1$) to HA (Day and de la Motte 2005). TSG-6 covalently binds to the HCs of $I\alpha 1$, and then catalyzes the transfer of HCs to HA (Figure 2-12). The covalent binding of TSG-6 to HA, and of HC to HA, have been implicated in the cross-linking of HA and the formation of HA cables. HC-HA complexes were thought to be present exclusively in inflammatory tissues (Baranova et al. 2011; Colon et al. 2009; Lauer et al. 2015a). However, our preliminary data show that HC-HA (and TSG-6) are present in normal, unperturbed skin. This is discussed in more detail later.

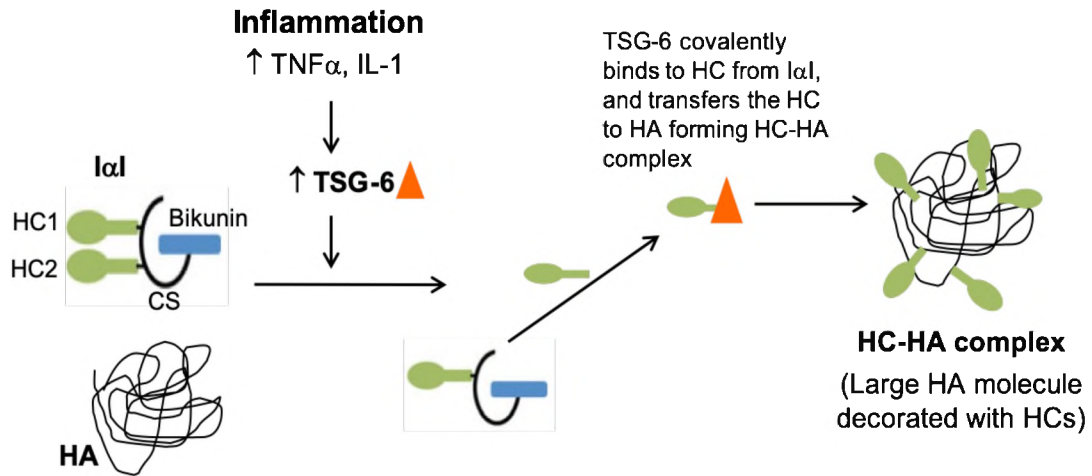


Figure 2-12. Schematics for transfer of IαI HC to HA.

(Figure legend: Green blobs= HC; Blue rectangle= Bikunin; Black C-shaped curve= CS; Orange triangle= TSG-6; Black consolidated structure= HA)

2.5.2.2 TSG-6 in neutrophil recruitment

TSG-6 is mostly known as an anti-inflammatory protein that is upregulated in inflammatory conditions as a protective feedback mechanism. It has been shown to inhibit neutrophil recruitment into the site of inflammation (Bardos et al. 2001; Choi et al. 2011). In an air-pouch model of inflammation in murine skin, injection of the Link module of TSG-6 caused attenuation of neutrophil migration into the tissue (Getting et al. 2002). Moreover, application of recombinant TSG-6 (rTSG-6) or mesenchymal stem cells (MSCs) in multiple models of skin wounds have shown to result in reduced neutrophil recruitment to the wound area (Qi et al. 2014; Wang et al. 2015). Similarly, in models of corneal wounding in mice and rabbits, treatment with either injection of rTSG-6 or TSG-6 producing stem cells were demonstrated to suppress neutrophil infiltration (Hertsenberg et al. 2017; Kim et al. 2014a; Oh et al. 2010). Additionally, loss of TSG-6 in TSG-6 null mice has been correlated to increased neutrophil migration in mouse peritonitis and arthritis models. This effect

of TSG-6 on neutrophil recruitment has been attributed to the ability of TSG-6 to interact with HA, which modulates CD44-mediated attachment of leukocytes to the endothelium (Szanto et al. 2004).

2.5.2.3 TSG-6 in chemokine binding

One of the mechanisms by which TSG-6 has been shown to inhibit neutrophil migration as described by Dyer et al. is by its ability to bind to multiple chemokines from the CXC and CC families with variable affinity, via its Link module (Dyer et al. 2016; Dyer et al. 2014). CXCL8 (or IL-8) is a major pro-inflammatory chemokine that regulates neutrophil migration. TSG-6 was preliminarily found to bind to CXCL8 at a site close to the GAG binding site on CXCL8 (Dyer et al. 2014). Thus, it was proposed that the interaction between TSG-6 and CXCL8 antagonizes the binding of CXCL8 to GAGs such as heparan sulfate on the vascular endothelium. Also, TSG-6/CXCL8 binding was thought to interfere with the interaction of the chemokine to its ligand, thus resulting in inhibited neutrophil migration. Further, Dyer et. al. (Dyer et al. 2016) showed that TSG-6 can bind to other chemokines such as, CXCL4, CCL2, and CCL5, again limiting their interaction with the GAGs. This causes a disturbance in chemotactic gradient which is required to direct the migration of leukocytes ultimately resulting to inhibited migration of the inflammatory cells.

2.5.2.4 TSG-6 in macrophage polarization

Macrophage, as explained in earlier sections, is an important type of inflammatory leukocyte performing various functions in inflammation and wound healing. TSG-6 has been shown to promote the polarization of inflammatory

macrophages to anti-inflammatory or tissue reparative M2 phenotype. In a study by Mittal et al., mice lacking TSG-6 were found to be more prone to LPS induced inflammatory lung injury with increased mortality, whereas, WT mice when treated with rTSG-6 had reduced inflammation. This was accompanied by macrophage population expressing higher level of M2 makers- CD206, Arginase-1 and Chi3l3 (Mittal et al. 2016). In a type 1 diabetic mouse model of corneal epithelial inflammatory wound, treatment with MSCs upregulated TSG-6 expression, reduced inflammation, and promoted healing, similar to rTSG-6 treatment. Flow analysis of F4/80+ macrophages from rTSG-6 or MSC treated corneas presented lower number of pro-inflammatory M1 phenotype macrophages and significantly higher number of M2 phenotype macrophages (Di et al. 2017). In a mouse model of dextran sulfate sodium induced inflammatory bowel disease, the intraperitoneally administered MSCs released TSG-6, reduced inflammatory response, and improved disease activity index, in conjunction with increased CD206+ M2 macrophages. The M2 macrophage polarization was reportedly abrogated when TSG-6 was silenced in MSCs using small interference RNA (siRNA) (Song et al. 2017).

Moreover, TSG-6 from cells have been shown to modulate macrophage phenotype in in-vitro cell cultures. Macrophages derived and differentiated from monocytes, when co-cultured with activated dermal fibroblasts or MSCs, were found to polarize more towards the M2 phenotype. This polarization was mediated by TSG-6 released by activated dermal fibroblasts or MSCs as verified by knockdown of TSG-6 with siRNA. (Ferrer et al. 2017; Song et al. 2017).

2.6 TSG-6 and HC-HA complexes in diseases

TSG-6, as mentioned above, is stimulated by inflammatory cytokines $\text{TNF}\alpha$, as well as by IL-1, in vivo (Wisniewski et al. 1993). Under stimulation by these cytokines, TSG-6 is produced by a variety of cell types including fibroblasts and inflammatory cells, specifically neutrophils. TSG-6 has been widely discussed as a protein having anti-inflammatory activity (Wisniewski et al. 1996; Wisniewski and Vilcek 1997) although its role during inflammation remains controversial. Also, the presence of TSG-6 and HC-HA complexes have been associated with different inflammatory conditions such as, arthritis (Szanto et al. 2004; Wisniewski et al. 1994), colitis (Sala et al. 2015), gingivitis (Beltran et al. 2015), peritonitis, and asthma related inflammation of airway epithelium (Lauer et al. 2013; Swaidani et al. 2013). The generation of the TSG-6 null mouse by Szanto *et al.* (Szanto et al. 2004) has provided a valuable platform to study its role in these inflammatory diseases.

Asthma/airway: Swaidani et al. (Swaidani et al. 2013) showed that TSG-6 null mice had decreased airway inflammation after induction of allergic airway diseases. This was marked by a decrease in the amount of pulmonary HA. Also, in comparison to wild-type (WT) littermates, TSG-6 null mice were resistant to airway hyperresponsiveness and presented improved lung mechanics after irritation induction. This suggests that TSG-6 aids in the pathogenesis of asthma. Lauer et al. (Lauer et al. 2013) showed that the amount of HA synthesis by airway smooth muscle cells is increased when recombinant human TSG-6 (rhTSG-6) is used in cell culture, which is consistent with the decreased HA seen in the TSG-6

null mouse. Moreover, the amount of HA was found to increase in a severe murine asthma model, but HC-HA was only found to increase in non-severe asthma, indicating the involvement of HC modification of HA in asthma severity (Lauer et al. 2015a).

Arthritis/Cartilage: Arthritis is one of the most studied diseases in terms of determining the role of TSG-6 in inflammation. Wisniewski et al. (Wisniewski et al. 1993) showed that TSG-6 is present in high levels in the synovial fluids of human arthritic patients. It was determined that the patient's synoviocytes constitutively produce TSG-6 protein, and that TSG-6 is increased after $\text{TNF}\alpha$ or IL-1 treatment. Another study by Bardos et al. (Bardos et al. 2001) in an autoimmune murine model of arthritis showed that addition of recombinant mouse TSG-6 (rmTSG-6) to acutely inflamed joints caused a reduction in edema, through immobilization of CD44-bound HA.

Skin/scarring: TSG-6 was characterized for the first time in human normal skin fibroblasts (Lee et al. 1992), where TSG-6 protein was found to be expressed when cells in culture were treated with inflammatory cytokines $\text{TNF}\alpha$ and IL-1. Recently, a few studies have been done to determine the effects of TSG-6 in scarring. Tan et al. (Tan et al. 2011) characterized the differential distribution of HA and TSG-6 in different scar types from human skin- normal scars, keloid scars, and adjacent unscarred skin. Immunohistochemistry performed on skin sections showed that scars as well as unscarred tissues stained positive for TSG-6, as well as for HC1, HC2, and bikunin, suggesting the presence of $\alpha 1$. However, the study is missing more quantitative data. Another study by Qi et al. (Qi et al. 2014) showed

that intradermally implanted MSCs release TSG-6 in murine skin; compared to control wounds, the MSC implanted wounds healed faster with less fibrosis. This phenotype was demonstrated to be accompanied by decreased macrophage activation, negative regulation of $\text{TNF}\alpha$, and reduced granulation tissue formation. Thus, TSG-6 could be anti-inflammatory in cutaneous wounds. Moreover, Wang et al. (Wang et al. 2015) investigated the effect of rhTSG-6 on rabbit ear wound models. Compared to sham injections, it was shown that wounds receiving rTSG-6 healed with less hypertrophic scar.

2.7 Summary

Understanding the normal underlying biology and microenvironment of the wound is crucial to understanding the possible abnormalities in wound healing. Such understanding will eventually aid in the development of new therapeutics and treatment modalities. As discussed above, the few studies available in cutaneous wound models suggest that TSG-6 plays an important role in cutaneous wound healing. The TSG-6 null mouse provides an ideal vehicle to define the mechanistic roles of TSG-6 in wound repair. Also, results from studies with the TSG-6 deficient model might provide further rationale for the possibility of using TSG-6 as a therapeutic tool to enhance wound healing.

CHAPTER III

CUTANEOUS WOUNDS IN MICE LACKING TUMOR NECROSIS FACTOR-
STIMULATED GENE-6 EXHIBIT DELAYED CLOSURE AND AN ABNORMAL
INFLAMMATORY RESPONSE

3.1 Introduction

Cutaneous wound healing is a complex process that involves inflammation, keratinocyte/fibroblast proliferation, migration, angiogenesis, extracellular matrix (ECM) deposition and remodeling, all orchestrated by the specific actions of cytokines, chemokines, growth factors, and enzymes (Barrientos et al. 2008; Clark 2001; Martin 1997; Singer and Clark 1999). One of these enzymes is Tumor necrosis factor (TNF)-stimulated gene-6 (TSG-6) protein, also known as TNF-induced protein 6 (Tnfp6 or Tnfaip6). *TSG-6*, first identified by Lee et al. (Lee et al. 1990) in human foreskin fibroblasts stimulated with the pro-inflammatory cytokine $TNF\alpha$, encodes a secretory glycoprotein with a molecular weight of ~30-35 kDa (Milner and Day 2003; Mittal et al. 2016; Wisniewski et al. 1993).

Functionally, TSG-6 appears to play important roles in ECM modification and in tissue inflammation. One of its important enzymatic activities is to catalyze the covalent transfer of heavy-chain (HC) protein from inter-alpha-trypsin inhibitor

(I α I) and pre- α -inhibitor (P α I) to hyaluronan (HA) forming HC-HA complexes (Colon et al. 2009; Jessen and Ødum 2003; Mukhopadhyay et al. 2004). Due to this activity, TSG-6 has an important role in the stabilization and expansion of cumulus cell-oocyte complexes (COCs), a phenomenon vital for egg cell maturation, and thus accounting for female sterility in the TSG-6 knock-out (KO) mouse (Fulop 2003; Fulop et al. 1997b; Salustri et al. 1999; Salustri and Fülöp 1998). Additionally, TSG-6 protein is able to inhibit neutrophil migration via the TSG-6 Link domain (Cao et al. 2004; Getting et al. 2002) which interacts with neutrophil chemokines such as human CXCL8, and with glycosaminoglycans on endothelial cell surfaces (Dyer et al. 2016; Dyer et al. 2014). Furthermore, TSG-6, as well as HC-HA complexes, have been shown to promote the polarization of macrophages to an alternatively activated/ anti-inflammatory M2 phenotype instead of the classically activated/ proinflammatory M1 phenotype (Ferrer et al. 2017; He et al. 2013; Mittal et al. 2016). Given the ability of TSG-6 to regulate the behavior of neutrophils and macrophages, we postulated that TSG-6 may be important in cutaneous wound healing. However, evidence for this prior to our study was largely indirect.

TSG-6, although is generally absent in normal tissues, has been reported to be constitutively present in human amniotic membrane epithelial and stromal cells (Zhang et al. 2012), in the normal murine pancreatic islets (Hull et al. 2012), and in astrocytes in rodent adult central nervous system (Coulson-Thomas et al. 2016). One hint to its possible importance in inflammation is the fact that TSG-6 expression can be greatly stimulated by pro-inflammatory cytokines and growth

factors including $\text{TNF}\alpha$, interleukin-1 (IL-1), and lipopolysaccharide (LPS), in fibroblasts, inflammatory cells, and endothelial cells among other cell types (Milner and Day 2003). Another fact that suggests a central role for TSG-6 is the manner in which it is regulated in inflammatory diseases such as arthritis. In a study by Wisniewski et al., the synovial fluids from rheumatoid and osteoarthritis patients were shown to have a high level of TSG-6 which was otherwise absent in non-arthritic joints. It was determined that the patient's synoviocytes constitutively produce TSG-6 protein, that it is increased after TNF or IL-1 treatment, and its activity exerts anti-inflammatory effects (Wisniewski et al. 1993). In murine models of experimental arthritis, the addition of recombinant TSG-6 (rTSG-6) to acutely inflamed joints lessened edema by immobilization of CD44-bound HA (Bardos et al. 2001) and had a chondroprotective effect. Another study with a cartilage-specific TSG-6 transgenic mouse showed less damage on articular cartilage upon induction of arthritis (Glant et al. 2002). Conversely, the absence of TSG-6 in a TSG-6 null arthritic mouse model led to more severe destruction of the articular cartilage and bone accompanied by increased neutrophil infiltration into the synovium (Szanto et al. 2004).

In a number of recent studies, the introduction of exogenous TSG-6 protein into various models of inflammation has mostly shown a protective effect. For example, in models of corneal injury in rabbits (Oh et al. 2010) or rats (Kim et al. 2014a), injection of rTSG-6 into the anterior chamber of eye exhibited reduced mRNA expression of pro-inflammatory cytokines, such as $\text{TNF}\alpha$ and IL-1, decreased level of myeloperoxidase, and reduced neutrophil infiltration in compare

to PBS only controls. In a mouse model of inflammation-related dry eye syndrome, application of rTSG-6 increased tear production while decreasing expression of pro-inflammatory cytokines (Lee et al. 2015). In a gingival wound model in rats, a relative reduction in levels of MPO, IL-1 β , IL-6, and neutrophils infiltration were observed after an injection of rTSG-6 into the wounds (Beltran et al. 2015). Activated mesenchymal stem cells (MSCs) are a good source of exogenous TSG-6, and have been explored for inflammation management (Lee et al. 2016; Prockop and Youn Oh 2012). In mouse models of myocardial infarction (Lee et al. 2009), peritonitis (Choi et al. 2011), or dextran sulfate sodium (DSS) induced colitis, injection of MSCs or rTSG-6 led to increased levels of serum TSG-6, decreased inflammation, decreased disease activity, and/or improved recovery, while knockdown of TSG-6 in MSCs negated these effects (Sala et al. 2015). In the DSS-induced colitis mouse, injection of MSCs appeared to improve colitis by lowering proinflammatory markers and increasing the proportion of anti-inflammatory (tissue protective) M2 macrophages (Song et al. 2017). In contrast with most inflammatory disease models in which TSG-6 appears to correlate with reduced inflammation, murine models of asthma are a notable exception, wherein the opposite appears to be true (Lauer et al. 2015b; Lauer et al. 2013; Swaidani et al. 2013).

In skin biology, very few studies on TSG-6 have been performed to date. One study used immunohistochemistry to demonstrate the presence of TSG-6, and heavy chains HC1 and HC2, in human scars and keloids, but was qualitative in nature (Tan et al. 2011). Another study showed that intradermally implanted

MSCs released TSG-6 in murine skin, and that relative to control wounds, the MSC-implanted wounds healed faster and had less fibrosis, less macrophage activation, lower TNF α levels, and reduced granulation tissue formation (Qi et al. 2014). A third study investigating the effect of rTSG-6 on rabbit ear wounds showed that, wounds injected with rTSG-6 healed with less hypertrophic scar than wounds receiving sham injections (Wang et al. 2015).

Thus, the few available studies suggest that TSG-6 may play an anti-inflammatory role in cutaneous wound healing. The aim of our study is to test this hypothesis by examining what consequences the elimination of endogenous TSG-6 might have upon the normal course of wound repair in a knockout (TSG-6 null), and to thereby gain more information about TSG-6 as possible therapeutic tool to enhance wound healing.

3.2 Materials and Methods

3.2.1 Animals

C57BL/6J wild-type (WT) mice were obtained from JAX Laboratories (Bar Harbor, ME). TSG-6 null mice, whose generation was described by Fülöp et al. (Fulop 2003), in C57BL/6 background was generously provided by Dr. Mark Aronica in our institute. All mice were maintained per guidelines of the American Association for the Accreditation of Laboratory Animal Care. All procedures were approved by the Cleveland Clinic Institutional Animal Care and Use Committee.

3.2.2 Wounding experiments

Mice (WT, or TSG-6 KO, male and female, 8–10 weeks of age) were anesthetized with an intraperitoneal injection of Ketamine-Xylazine and fur shaved from the upper back with an electric razor. After letting the skin recover overnight, two full-thickness excisional wounds were made using 5 mm punch biopsies (Acuderm, Fort Lauderdale, FL), under anesthesia. To follow wound closure, mice were anesthetized with isofluorane and photographed from a fixed distance using a digital camera on a stand at Days 0, 3, 5, 7 and 10 post wounding. The wound area (in pixels) was determined from the digital photos using IPLab Spectrum imaging software (Scanalytics, Rockville, MD). For histological examination, wounds were harvested at 12 hours, Days 1, 3, 5, 7 and 10 post wounding, along with unwounded skin. Tissues were fixed in Histochoice (Amresco, Solon, OH), paraffin embedded, and stored for later sectioning. Wounds were also harvested at different time points along with unwounded tissues, flash frozen in liquid nitrogen, and stored at - 80 °C for subsequent protein and RNA isolation.

3.2.3 Histological assessment of wound closure

Histochoice-fixed, paraffin embedded wound tissues from 12 hours to Day 10 post wounding were cut into 5-micron sections using microtome. After rehydration, the sections were stained for Hematoxylin and Eosin (H&E) using standard procedure. The mounted slides were then scanned using an Aperio AT2 slide-scanner (Leica Biosystems, Buffalo Grove, IL). The scanned images were analyzed for histological wound closure using Aperio ImageScope (Leica

Biosystems). Percentage re-epithelialization (or epidermal gap) was determined by measuring the length of epidermal tongue at both wound edges and the total wound length from wound edge-to-edge.

3.2.4 Western Blotting

Unwounded and excisional wound skin samples stored at - 80 °C were processed for protein isolation as follows – tissues were first pulverized in a chilled Bessman tissue pulverizer, resuspended in cell lysate buffer (Raybiotech, Inc., Peachtree Corners, GA) with 1X protease inhibitor cocktail (Sigma-Aldrich, St. Louis, MO), and then homogenized and sonicated. Protein in the supernatant was collected after centrifugation and quantified using Bradford assay. Chemiluminescent Western blotting was performed as per standard procedure. Protein lysates were electrophoresed in NuPage 4-12 % Bis-Tris gels (Invitrogen, Carlsbad, CA) and blotted onto PVDF membranes. The blots were probed overnight at 4 °C with one for the following primary antibodies: Anti-TSG-6 mouse monoclonal (1 µg/ml; Millipore, Burlington, MA); rat monoclonal TNF α (1 µg/ml; BioXCell, West Lebanon, NH); rabbit monoclonal Arg1 (1:1000, Cell Signaling Technology, Danvers, MA); rabbit anti-mouse Actin (1:1000; Santa Cruz Biotechnology, Dallas, TX). This was followed by 1.5-hour incubation at room temperature with an anti-rat or anti-rabbit horseradish peroxidase (HRP)-conjugated secondary antibodies (1:10,000; Jackson ImmunoResearch, West Grove, PA). Chemiluminescent detection was performed using Amersham™ ECL™, or ECL™ prime reagent kit (GE Healthcare, Chicago, IL). The protein bands were quantified using

IPLab Spectrum imaging software (Scanalytics) with actin as the loading control.

3.2.5 Evaluation of HC modification of hyaluronan (HC-HA analysis)

HC-HA analyses was performed as described by Lauer et al. (Lauer et al. 2015a). Briefly, unwounded and excisional wound skin tissues were collected, weighed and minced in PBS at 1 μ l volume per 0.33 mg of tissue. *Streptomyces* hyaluronidase (Millipore) was added at 20 TRU/ml for extraction of HCs, or equal volumes of PBS for No-hyaluronidase controls, incubated at 30 minutes on wet-ice followed by 30 minutes at 37 °C. After centrifugation at 13,000 x g, supernatants were collected into clean labeled tubes. Equal amounts of samples were electrophoresed in NuPage 4-12 % Bis-Tris gels and blotted onto PVDF membranes. Blots were then incubated with anti- α 1 rabbit polyclonal Dako antibody (1:8000; Agilent Technologies, Santa Clara, CA), followed by IRDye® 800CW donkey anti-rabbit secondary antibody (1:15,000; LI-COR Biosciences, Lincoln, NE). Blots were imaged on an Odyssey infrared imaging system and the bands for HC (at around 85 kDa) were quantified using ImageStudio™ (LI-COR Biosciences).

3.2.6 Immunostaining for neutrophils and macrophages

Histochoice-fixed, paraffin embedded wound tissues were cut into 5-micron sections using microtome. After rehydration, the sections were blocked with 3% normal goat serum for 30 minutes at room temperature. Sections were then incubated overnight at 4 °C with the respective primary antibodies in

blocking buffer: Anti-Ly6G rat monoclonal (1:100; Affymetrix, Santa Clara, CA) for neutrophils; anti-F4/80 rat monoclonal (1:100; Bio-Rad, Hercules, CA) for macrophages. A biotinylated goat anti-rat biotin secondary (1:300) was followed by Vectastain ABC reagent (Vector Laboratories, Burlingame, CA) for 30 minutes each. DAB peroxidase substrate kit was used for detection followed by VectaMount mounting medium for mounting.

For analysis, slides were scanned using an Aperio AT2 slide-scanner (Leica Biosystems). IPLab Spectrum imaging software (Scanalytics) was used to determine the positive staining for neutrophils or macrophages in the wound bed. A common threshold was set to encompass the pixels with dark brown DAB positive stains, and areas per unit wound length was determined using the Breadloaf method. Regions of interest (ROIs) 500 pixels wide were chosen across the wound length and four consecutive ROIs were averaged to get a data point. A minimum of 15 data points, derived from at least 4 wounds, were analyzed per condition.

3.2.7 Immunostaining for macrophage phenotypes

Serial wound sections were incubated overnight at 4 °C with the respective primary antibodies: rabbit anti-mouse CD38 (1:100; Bioss, Woburn, MA) for M1 macrophages; rat monoclonal F4/80 (1:100; Bio-Rad) for all macrophages; rabbit monoclonal Arg1 (1:100; Cell Signaling Technology) for M2 macrophages. Antigen retrieval using citrate buffer at pH 6.0 was performed for anti- CD38 and anti- Arg1 antibodies. Sections were then incubated with goat anti-rat or goat anti-rabbit biotinylated secondary antibody (1:300; 30 min;

Vector Laboratories) followed by incubation with Alexa Fluor 488 Streptavidin (1:500; 1.5 hour, Invitrogen), and mounted in VECTASHEILD mounting medium (Vector). Using a Leica DM upright microscope (Leica Biosystems), corresponding images were captured for each antibody type by tracing a common landmark. For each image captured, cells stained positively for macrophage phenotype marker (M1 or M2 marker) and the pan-macrophage F4/80 marker were counted, and the ratios determined.

3.2.8 Recombinant TSG-6 injection

Mice were shaved and anesthetized as described above and two full thickness excisional wounds were made using 5 mm punch biopsies. Recombinant human TSG-6 (rTSG6, R&D systems, Minneapolis, MN) was prepared at 2 µg in 100 µl PBS. The edge and center of wounds were injected with rTSG6 (+ rTSG6) or equal volume of PBS (Vehicle control, VC) right after wounding on Day 0 and on Day 4 post wounding. Wounds were photographed as above to evaluate wound closure. Wounds were also made and collected at 12 hours and Day 7 post wounding to evaluate for neutrophils and macrophages infiltration as above.

3.2.9 Flow cytometric analysis for M1 and M2 macrophages

Single cell suspensions from Day 5 wounds were prepared as described (Bannon et al. 2013) with modifications as explained in Chapter IV. Briefly, wounds were isolated from WT and TSG-6 null animals and weighed. Tissues were rinsed once each in 70 % ethanol and PBS, cut into 2 mm² pieces and incubated overnight (4 °C) in 20 µl HBSS per mg of wound tissue with 1 mg/mL

Dispase II (Sigma-Aldrich, St. Louis, MO), 3% FBS and 10 mg/mL G418 (Sigma-Aldrich). Tissues were transferred to 80 μ l HBSS per mg wound tissue with 1 mg/mL Collagenase I (Worthington, Lakewood, NJ), 75 U/mL DNaseI (Worthington) and 5 mg/mL G418 and incubated for 2 hours (37 °C) with shaking. Cell suspensions were filtered through a 40 μ m cell strainer (Corning Technology, Corning, NY) and washed twice with PBS buffer (PBS, 3% FBS, 0.1 mM EDTA), and centrifuged at 400 rpm. Cells were counted, resuspended at 1 million cells/ml in PBS buffer, and labeled with fluorescently tagged antibodies: Rat anti-mouse CD45 (1:200); rat anti-mouse F4/80 (1:80); rat anti-mouse TNF α (1:40; BioLegend, San Diego, CA); sheep anti-mouse Arg1 (1:10; Novus Biologicals, Centennial, CO) for 25 minutes (4 °C). Samples were analyzed on a BD LSRFortessa flow analyzer (BD Biosciences, Mississauga, ON, Canada).

3.2.10 Statistical analysis

Numerical data were expressed as Mean \pm SEM. All statistical analyses were performed using SigmaPlot 12 (Systat Software Inc., San Jose, CA). Normality of the data were tested using Shapiro-Wilk Normality test. Analyses for two group comparisons were performed using either the two-tailed Student's t-test or Mann-Whitney Rank Sum test. For multiple group comparisons, either One Way ANOVA or Two Way ANOVA with Bonferroni corrections were performed. P-value \leq 0.05 was considered statistically significant. (See Appendix for full analysis.)

3.3 Results

3.3.1 TSG-6 protein is present in unwounded murine skin and increases post wounding

To determine the endogenous expression of TSG-6 in normal and injured skin, Western analysis was performed on proteins from unwounded skin and full-thickness excisional wounds of wildtype (WT) mice (Figure 3-1a and b). TSG-6 is constitutively expressed at low levels in unwounded skin and increases by more than 4-fold as early as 12 h post-wounding. Expression peaks by 3 days, after which it drops, but remains above baseline until at least day 10 (Figure 3-1b). This shows that TSG-6 is upregulated after wounding, and suggests a possible functional role in wound repair.

As mentioned above, TSG-6 catalyzes the covalent and non-covalent transfer of heavy chains (HCs) from $\alpha 1$ and pre- $\alpha 1$ to HA, forming HC-HA complexes. HC-HA is thought to stabilize HA rich extracellular matrices, making it more adhesive to inflammatory cells (Lauer et al. 2014; Rugg et al. 2005; Zhuo et al. 2006; Zhuo et al. 2001). To quantify the levels of HC-HA in unwounded and wounded WT skin, the assay shown in Figure 3-1c was performed. In the absence of hyaluronidase, HC-HA complexes in the samples cannot enter the SDS-PAGE gel, and remain trapped in the well due to their large size (Figure 3-1c, lane 3, dashed box). However, after hyaluronidase treatment, HC-HA complexes are degraded and HC is released, appearing as a band at ~85 kDa. The presence of an HC band in the hyaluronidase-digested sample in lane 2 of Figure 3-1c shows that HC-HA is constitutively present in normal unwounded skin. At 3 days post-

wounding, the HC band intensity increases by ~3 fold (Figure 3-1c, lane 4; Figure 3-1d). These changes mirror changes in expression of TSG-6 protein pre- and post-wounding (Figure 3-1a and b).

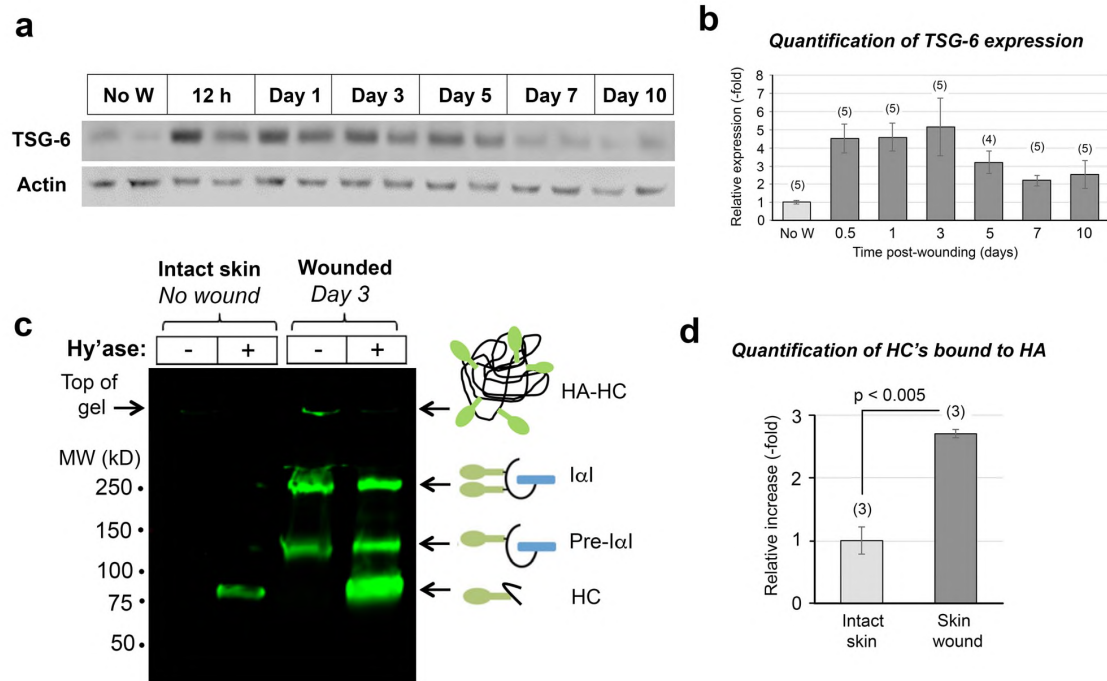


Figure 3-1. TSG-6 protein and HC-HA are present in unwounded murine skin and increase post wounding.

(a) Harvested wound sections were processed for protein extraction and analyzed using Western blot analysis with Actin as the loading control. (b) TSG-6 is present in unperturbed skin, significantly increases within 12 hours post wounding, peaks at Day 3 and is still increased at Day 10 post wounding relative to unwounded skin. (c) The presence of a HC band in the unwounded tissue extract treated with *Streptomyces hyaluronidase* (Hy'ase) indicate that HC-HA is present de novo in unperturbed skin (Lane 2) HC-HA levels are increased in a Day 3 wound (Lane 4) relative to uW skin. (d) When quantified using ImageStudio, HC-HA from Day 3 ExW wounds significantly increased by more than 3 folds. Statistical analysis was performed using One Way Repeated Measures ANOVA or Student's *t*-test. (n), number of animals.

3.3.2 There are no redundant enzymes that transfer HC to HA in the skin

To determine whether TSG-6 protein is the sole molecule responsible for HC-HA complex formation in skin, we assayed HC-HA in extracts from the skin of TSG-6 null mice biopsied pre- and post-wounding. TSG-6 protein expression was absent in TSG-6 null mice as expected (Figure 3-2a). In unwounded skin, the HC

band (85 kDa) normally seen in unwounded WT samples (Figure 3-2b, lane 2) was absent in samples from unwounded TSG-6 null skin (Figure 3-2b, lane 4). At Day 1 post-wounding, a time when HC-HA complexes are strongly induced in WT wounds (Figure 3-2b, lane 6), no HC band was detectable in TSG-6 null wounds (Figure 3-2b, lane 8). These data verify that the loss of TSG-6 is responsible for the inability to form HC-HA complexes, and no other molecule is induced that can compensate and transfer HC from αI to HA. Thus, this model was appropriate for our study to understand the effect of loss of TSG-6 and HC-HA complexes on cutaneous wound healing.

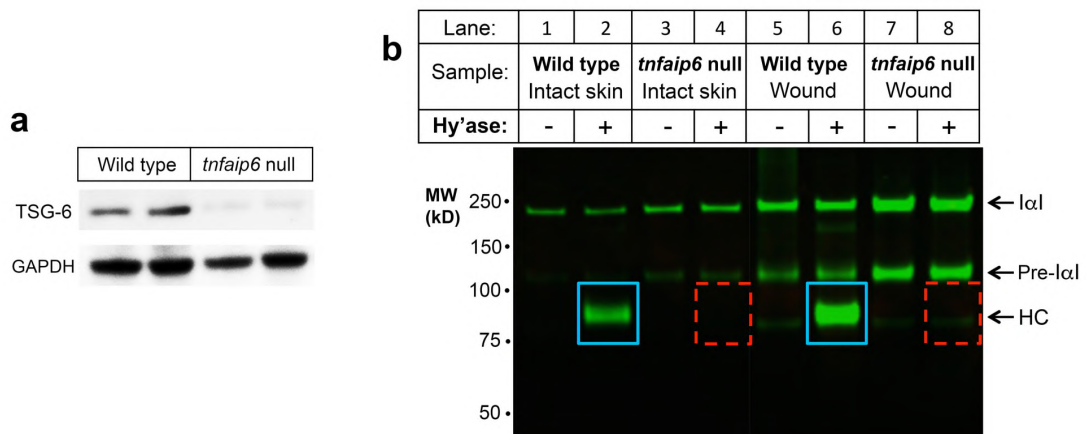


Figure 3-2. TSG-6 HC transfer activity is non-redundant in skin

(a) Western blot analysis of proteins from WT and TSG-6 null skin using anti TSG-6 antibody. GAPDH was used as the loading control. (b) HC-HA assay was performed on unwounded and Day 1 excisional wounded skin from TSG-6 null and WT controls. WT skin showed the presence of HC band in the hyaluronidase treated sample (Lane 2, boxed band), which increased after wounding (Lane 6) as expected. TSG-6 null samples were missing the HC band both before and after wounding (Lane 4 and 8, dashed boxes).

3.3.3 The absence of TSG-6 results in delayed wound closure

Wound closure rate is an important indicator of proper wound healing. To observe the effects of loss of TSG-6 upon cutaneous wound closure, excisional wound areas were monitored over time in WT and TSG-6 null mice (Figure 3-3a

and b). At all the time points post-wounding, the relative wound area was larger for TSG-6 null wounds compared to WT wounds, demonstrating that loss of TSG-6 delays wound closure. Differences were statistically significant at Days 5, 7 and 10 post-wounding.

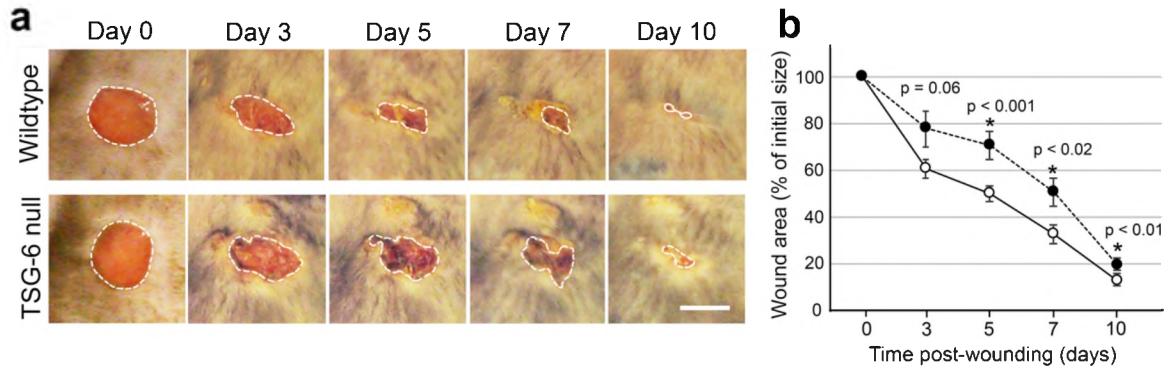


Figure 3-3. Loss of TSG-6 results in delayed wound closure

(a) Full-thickness excisional wounds in WT and TSG-6 null mice. White dotted lines denote the open wound area; Bar= 5mm (b) Wounds were photographed and measured using IPLab imaging software to determine the open wound area. Wound sizes are represented as the percentage of that on Day 0. The wound areas were larger for the TSG-6 null wounds compared to WT wounds for each time point post wounding. The difference was significant for Days 5 and 7 and 10. *Statistical analysis was performed using either Student's t-test or Mann-Whitney Rank Sum test. Dashed line with closed circles= TSG-6 null, Solid line with open circles=WT; N= 20 wounds, except for Day 10, N= 10 wounds.*

3.3.4 Delayed wound closure verification: TSG-6 null wounds displayed slower re-epithelialization

Histological analysis of WT and TSG-6 null wound sections was performed to verify the delayed wound closure phenotype seen above. The H&E stained slides were scanned, and epithelial tongue length was measured to determine the percentage re-epithelialization over the original wound length (Figure 3-4i). While negligible re-epithelialization was observed in 1-day wounds (image not shown), re-epithelialization was clearly observed starting at 3-day post wounding (Figure 3-4a and b). Difference in re-epithelialization were significant in 5-day (Figure 3-4c

and d) and 7-day post wounding (Figure 3-4e and f). By 10 days (Figure 3-4g and h), the wounds were almost completely epithelialized in both WT and TSG-6 null. Thus, TSG-6 null wounds have delayed wound closure as verified by delayed re-epithelization.

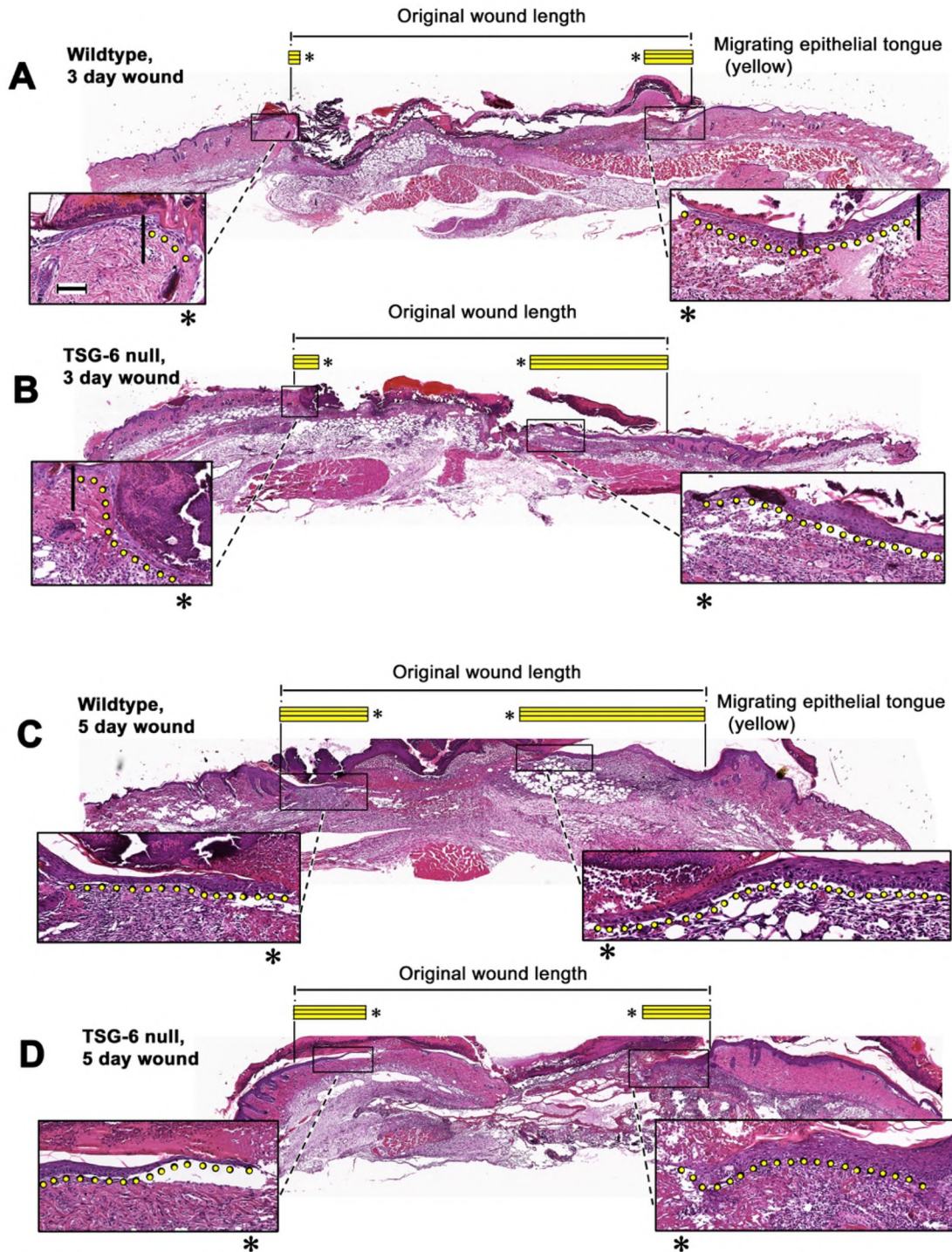


Figure 3-4. Delayed wound closure phenotype in TSG-6 null wounds were confirmed by histological analysis of re-epithelialization.

H&E staining of WT and TSG-6 null wounds. Representative images for (a, b) 3-day wounds, (c-d) 5-day wounds. Black lines above the full scans denote wound edges. Original wound lengths were measured by tracing the distance between these two lines. The insets show epithelial tongues on either side of the wound (black boxes in full scans). The yellow lines (in full scans) and yellow dots (in insets) denote where the epithelial tongues were measured. Scalebar (in the first inset)= 100 μ m

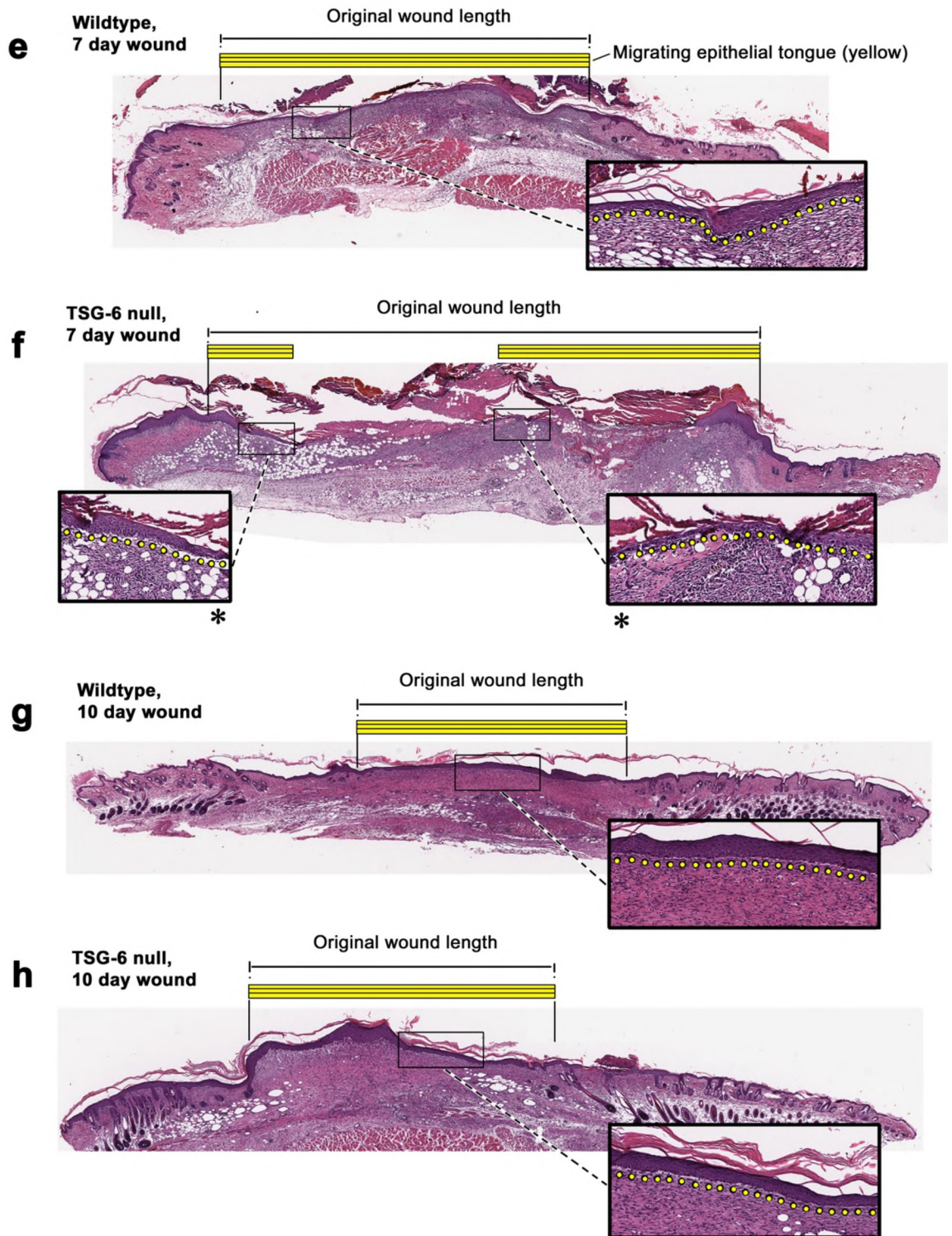


Figure 3-4. (Continued) H&E staining of WT and TSG-6 null wounds. Representative images for **(e, f)** 7-day wounds, **(g-h)** 10-day wounds. The black lines above the full scans denote wound edges. Original wound lengths were measured by tracing the distance between these two lines. Single inset per wound means the wounds were full re-epithelialized. Yellow lines (in full scans) and yellow dots (in insets) denote where the epithelial tongues were measured.

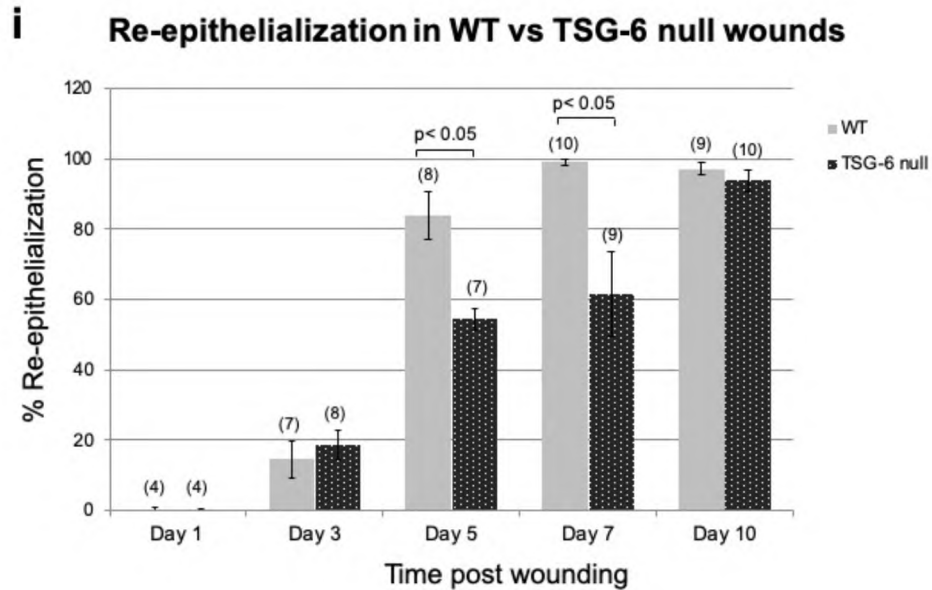


Figure 3-4. (Continued) **(i)** Percentage epithelialization is significantly lower in TSG-6 null wounds at Day 5 and 7 post wounding, indicating delayed wound closure compared to WT wounds. *Statistical analysis was performed using either Student's t-test or Mann-Whitney Rank Sum test. (n), number of wounds.*

3.3.5 The absence of TSG-6 results in differential regulation of neutrophil infiltration into wound bed

Another critical measure of proper wound healing is the orchestrated recruitment and clearance of inflammatory cells. Neutrophils are among the first to arrive at the site of injury (Figure 3-5a to m). Interestingly, sections from early wounds (at 12 h and 24 h) immunostained with the neutrophilic granule marker Ly6G showed significantly fewer neutrophils in the TSG-6 null mice compared to WT mice (Figure 3-5a to d). However, at later time points there were more neutrophils in TSG-6 null wounds, particularly at Day 7 where the difference was highly significant (Figure 3-5i and j). Thus, a differential pattern of neutrophil recruitment and/or clearance was observed in the presence versus absence of TSG-6 (and HC-HA) in cutaneous wounds (Figure 3-5m).

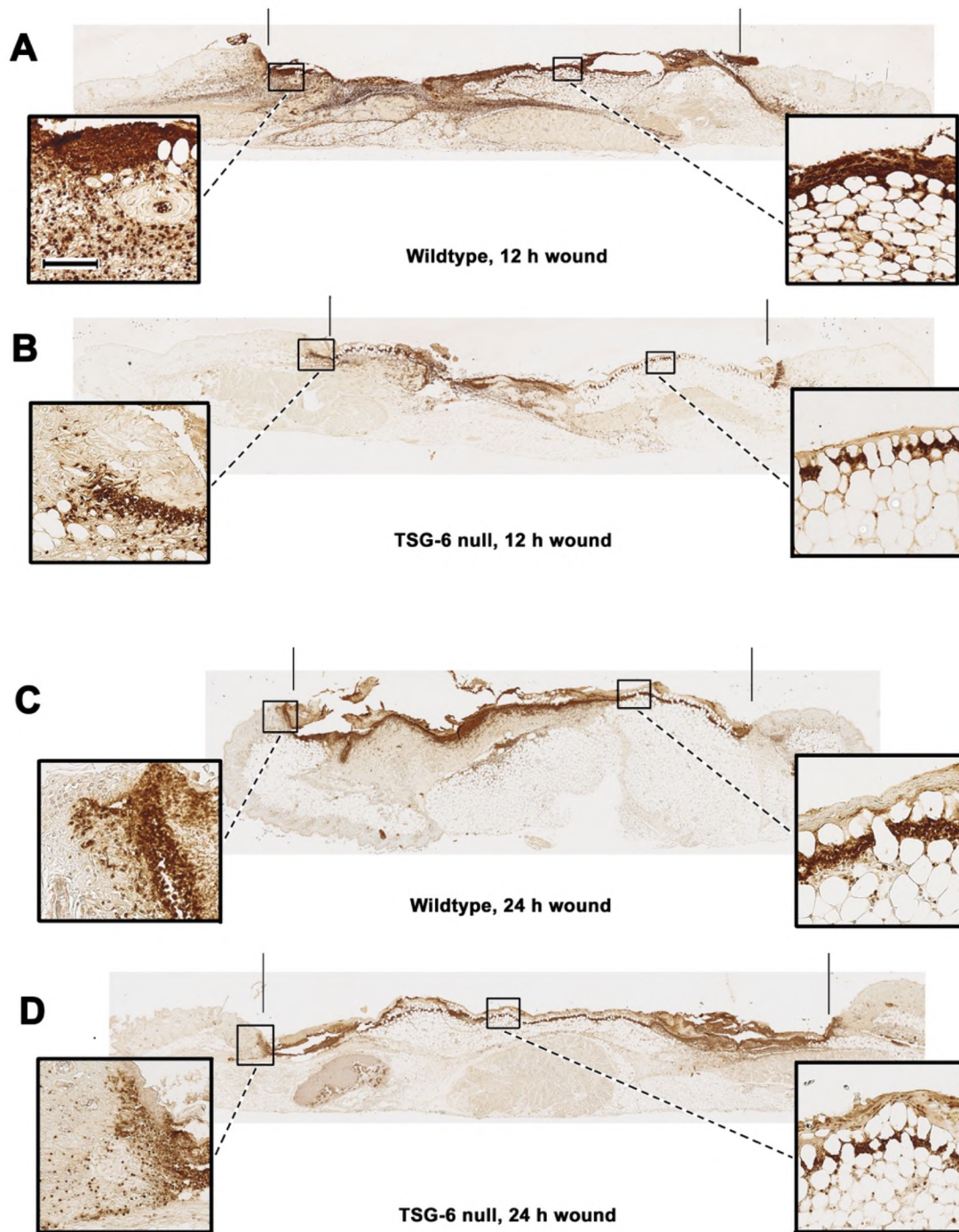


Figure 3-5. Loss of TSG-6 results in an abnormal inflammatory response.

Neutrophil staining of WT and TSG-6 null wounds. Representative images for **(a, b)** 12 h wounds, **(c-d)** 24 h wounds. The black lines above the full scans denote wound edges. The black boxes in the full scans show where the position of the zoomed view provided in the insets. The insets on the left show respective wound edges, while the insets on the right show the middle of the wound bed. Scale bar (in the first inset) = 100 μm

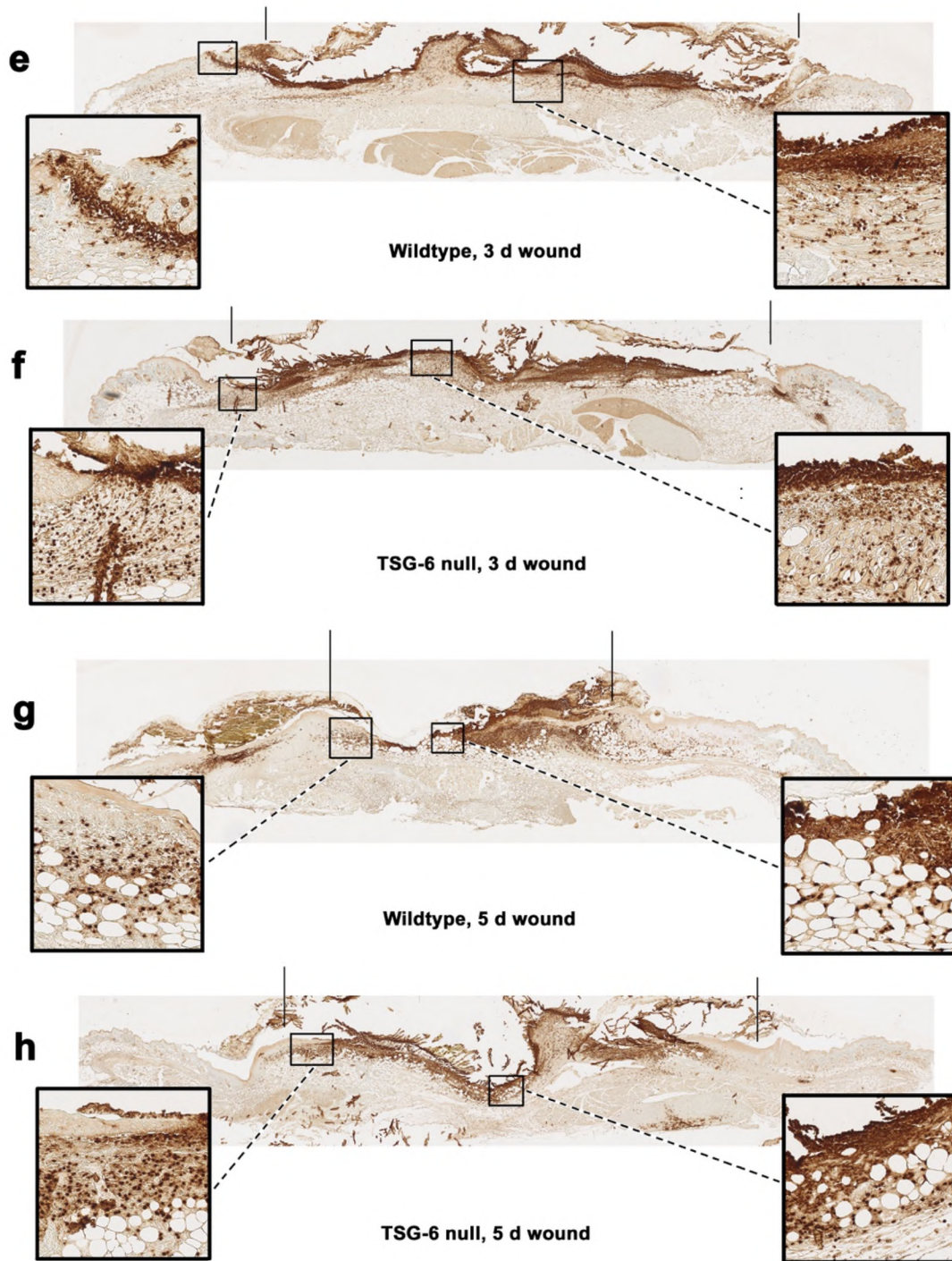


Figure 3-5. (Continued) Neutrophil staining of WT and TSG-6 null wounds. Representative images for **(e, f)** 3-day wounds, **(g-h)** 5-day wounds. The black lines above the full scans denote wound edges. The black boxes in the full scans show where the position of the zoomed view provided in the insets. The insets on the left show respective wound edges, while the insets on the right show the middle of the wound bed.

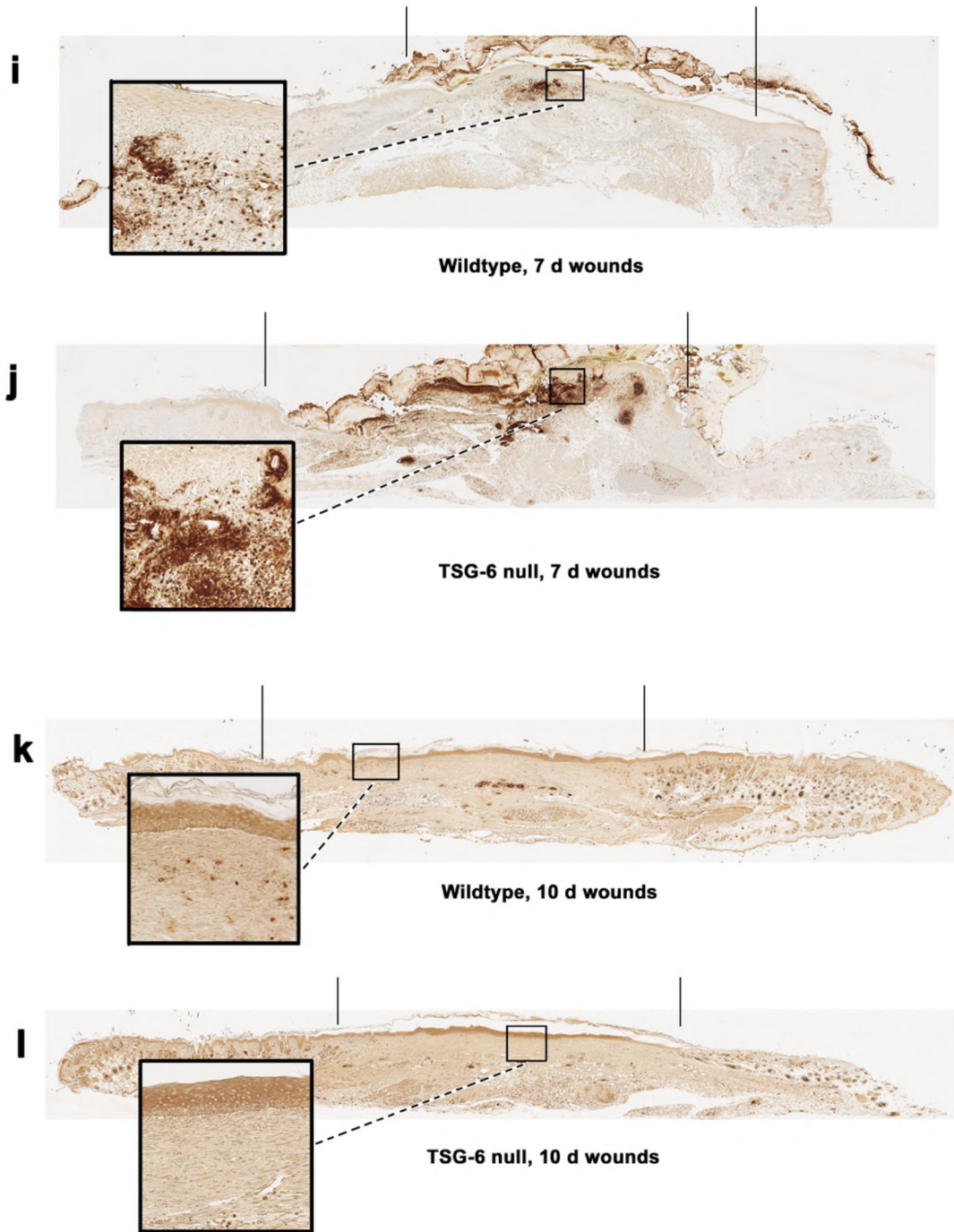


Figure 3-5. (Continued) Neutrophil staining of WT and TSG-6 null wounds. Representative images for (i, j) 7-day wounds, and (k-l) 10-day wounds. The black lines above the full scans denote wound edges. The black boxes in the full scans show where the position of the zoomed view provided in the insets. The insets on the left show respective wound edges, while the insets on the right show the middle of the wound bed.

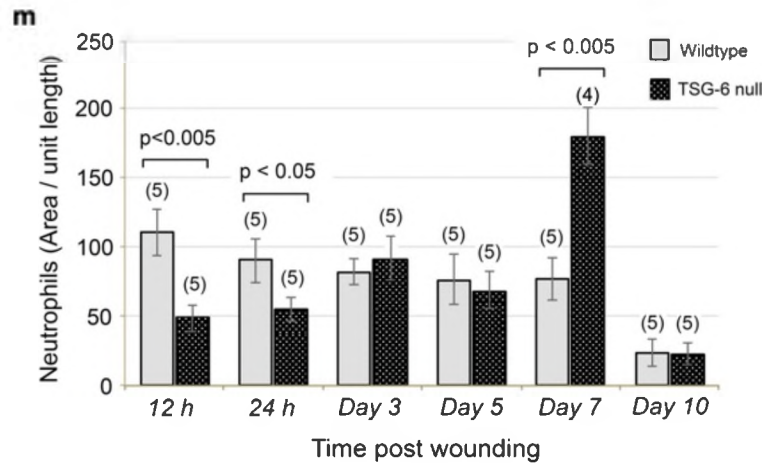


Figure 3-5. (Continued) (m) Neutrophil density was determined using IPLab. Neutrophil recruitment is delayed in early wounds (12 hours and 24 hours), while an exacerbated recruitment is seen at Day 7. Statistical analysis was performed using either Student's *t*-test or Mann-Whitney Rank Sum test. (n), number of animals.

3.3.6 TSG-6 null mice develop an abnormally pro-inflammatory wound milieu

TSG-6 is known to have anti-inflammatory effects in other systems (Day and Milner 2018). To assess the overall inflammatory status of wounds in TSG-6 null versus WT mice, we evaluated levels of TNF α protein in whole wound tissue at different time points after injury, using Western analysis (Figure 3-6a). Consistently higher levels of TNF α expression were found in TSG-6 null wounds than in WT wounds at all time points including unwounded skin at baseline (Figure 3-6b). Thus, TSG-6 null wounds constitute a more pro-inflammatory environment than WT wounds.

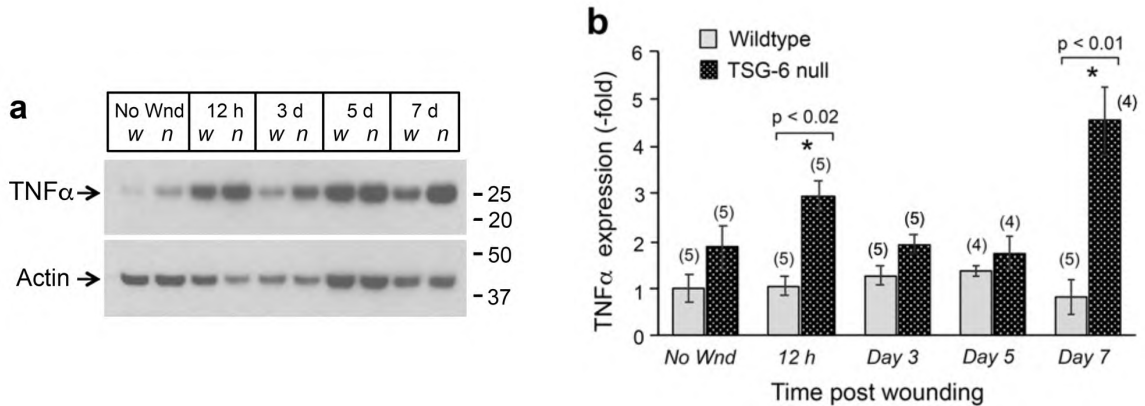


Figure 3-6. Absence of TSG-6 results to a more pro-inflammatory wound milieu. (a) Harvested WT and TSG-6 null unwounded and wound skin samples were analyzed using Western blot analysis with Actin as the loading control. (b) TNF α expression is relatively higher in TSG-6 null wounds at all time points including in unwounded skin. The difference is significant at 12 hours and 7 days post-wounding. Statistical analysis was performed using either Student's *t*-test or Mann-Whitney Rank Sum test. (n), number of animals.

3.3.7 No difference in absolute macrophage number in TSG-6 null wounds compared to WT wounds

To evaluate macrophages, we stained wound sections using the pan macrophage marker F4/80. No significant differences in the relative number of macrophages were observed between WT and TSG-6 null wounds, suggesting that the absence of TSG-6 and HC-HA had no significant effect upon total macrophage recruitment (Figure 3-7a and b).

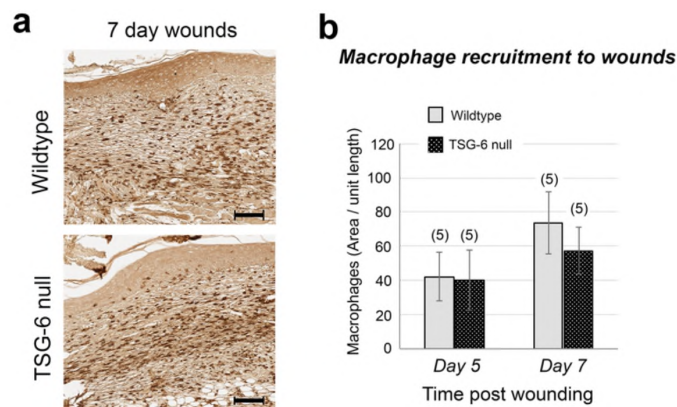


Figure 3-7. No difference in macrophage recruitment observed in TSG-6 null wounds compared to WT. (a) Macrophage staining of WT and TSG-6 null wounds. (b) Macrophage density was not significantly different in TSG-6 null wounds compared to WT for Days 5 and 7 post wounding.

Statistical analysis was performed using either Student's t-test or Mann-Whitney Rank Sum test (n), number of animals. Bar = 100 μ m.

3.3.8 TSG-6 null mice wound macrophages are polarized towards the pro-inflammatory M1 phenotype at Day 7 post wounding.

TSG-6 has been shown to play an important role in polarization of macrophages from a pro-inflammatory M1 to anti-inflammatory M2 phenotype. To determine whether macrophages in TSG-6 null wounds might be relatively more polarized toward an M1 phenotype compared to WT macrophages, we stained Day 7 wound sections for CD38 (an M1 marker), along with F4/80, in adjacent serial sections. Evaluation of these immunostains revealed that TSG-6 null wounds contain significantly more CD38-expressing macrophages than in WT wounds (Figure 3-8a). Next, we assessed the level of Arginase-1 (Arg1, an M2 marker) in whole wounds (Figure 3-8c), both by immunostaining (Figure 3-8b) and by western analysis (Figure 3-8e). We found that Arg1 is lower in TSG-6 null wounds at all time points evaluated, again suggesting a more pro-inflammatory M1 macrophages in TSG-6 null wounds. To focus more closely upon the expression of M1/M2 phenotypic markers in the macrophages themselves, single cells were isolated from Day 5 wounds by dispase/collagenase digestion, followed by flow cytometric analysis of macrophages. We found that in TSG-6 null mice, a higher proportion of F4/80 positive macrophages expressed TNF α (a well-established M1 marker), while the proportion of macrophages expressing Arg1 was lower, relative to WT wounds (Figure 3-8d and e). Thus, the absence of TSG-6 in null wounds results in polarization of the overall macrophage population to a more proinflammatory phenotype.

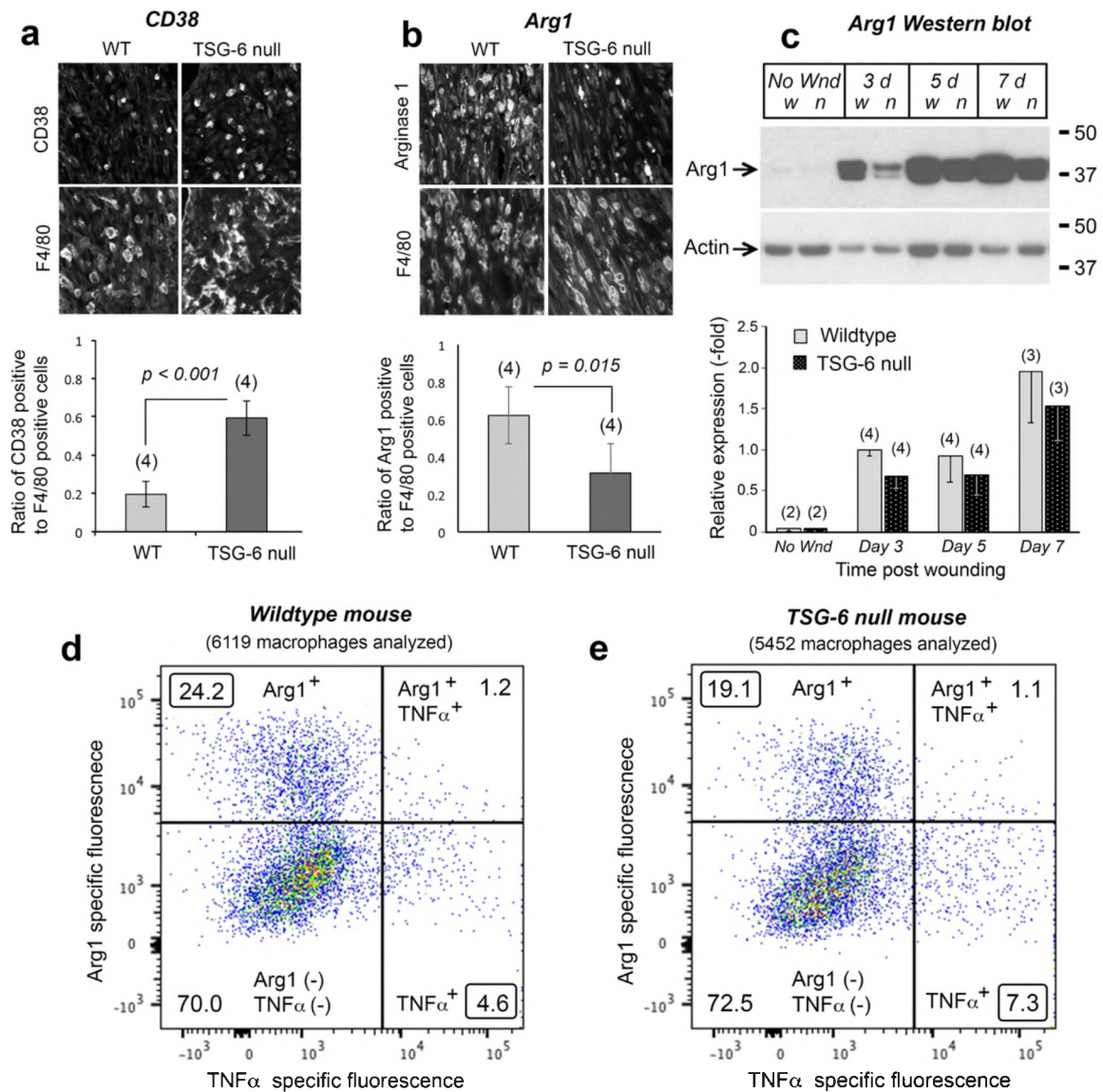


Figure 3-8. Loss of TSG-6 polarizes cutaneous macrophages to more pro-inflammatory and less anti-inflammatory phenotype.

Day 7 wounds were fixed, and paraffin embedded for immunostaining. **(a)** Parallel sections from WT and TSG-6 null wounds were stained for an M1 macrophage (CD38) marker and a pan macrophage marker (F4/80). The ratio of CD38 to F4/80 positive cells was significantly higher in TSG-6 null wounds, indicating prevalence of more pro-inflammatory macrophages. **(b)** Parallel sections from WT and TSG-6 null wounds were stained for an M2 (Arg1) macrophage marker and a pan macrophage marker (F4/80). The ratio of Arg1 to F4/80 positive cells was significantly lower in TSG-6 null wounds, suggesting less abundant anti-inflammatory macrophages in null wounds. **(c)** Western blot analysis of Arg1 protein reaffirms our finding in immunostaining. For each time point observed, the Arg1 protein expression is lower in TSG-6 null wounds compared to WT wounds. A preliminary flow cytometric analysis of single cell suspension from Day 5 **(d)** WT and **(e)** TSG-6 null wounds also showed that CD45⁺F4/80⁺ double positive macrophages are more frequently TNF α positive /M1 type and less frequently

Arg1 positive/M2 type in TSG-6 null wounds. *Statistical analysis was performed using either Student's t-test or Mann-Whitney Rank Sum test. (n), number of wounds.*

3.3.9 Reintroduction of recombinant TSG-6 into TSG-6 knockout wounds restores normal healing

To confirm that the difference in wound closure observed in WT versus TSG-6 null wounds was due to the loss of TSG-6, a protein rescue experiment was performed. Recombinant TSG-6 protein (rTSG-6) was reintroduced at two time points, i.e., immediately after wounding (Day 0) and at 4 days post-wounding (Figure 3-9a). In TSG-6 null mice, wound sizes trended slightly lower at Days 1-5 in wounds receiving the rTSG-6 injections, and became significantly smaller (and equal to control WT wounds) at Day 7 (Figure 3-9b and c). Interestingly, injection of rTSG-6 into WT wounds worsened wound closure compared to the WT vehicle control. These findings suggested that the delay in wound closure in TSG-6 null wounds is attributable to loss of TSG-6.

To confirm that differences in neutrophil recruitment between WT and TSG-6 null wounds were also due to loss of TSG-6, a similar TSG-6 reintroduction experiment was performed. The experimental scheme was essentially the same as Figure 3-9a, but now wounds were harvested (either at 12 h or Day 7). Sections were immunostained for Ly6G. The number of neutrophils at the wound site at 12 h post wounding, which was reduced in TSG-6 null mice relative to WT, was significantly increased after one injection of rTSG-6 becoming similar to WT (however, WT wounds receiving rTSG-6 showed some delay in neutrophil recruitment) (Figure 3-9d). Likewise, the number of neutrophils observed in Day 7 wounds, ordinarily much higher in TSG-6 null wounds, was completely normalized

to WT levels in mice receiving two rTSG-6 injections (Figure 3-9e). Thus, the differential neutrophil recruitment observed in TSG-6 null wounds is reversible when TSG-6 is restored in the skin.

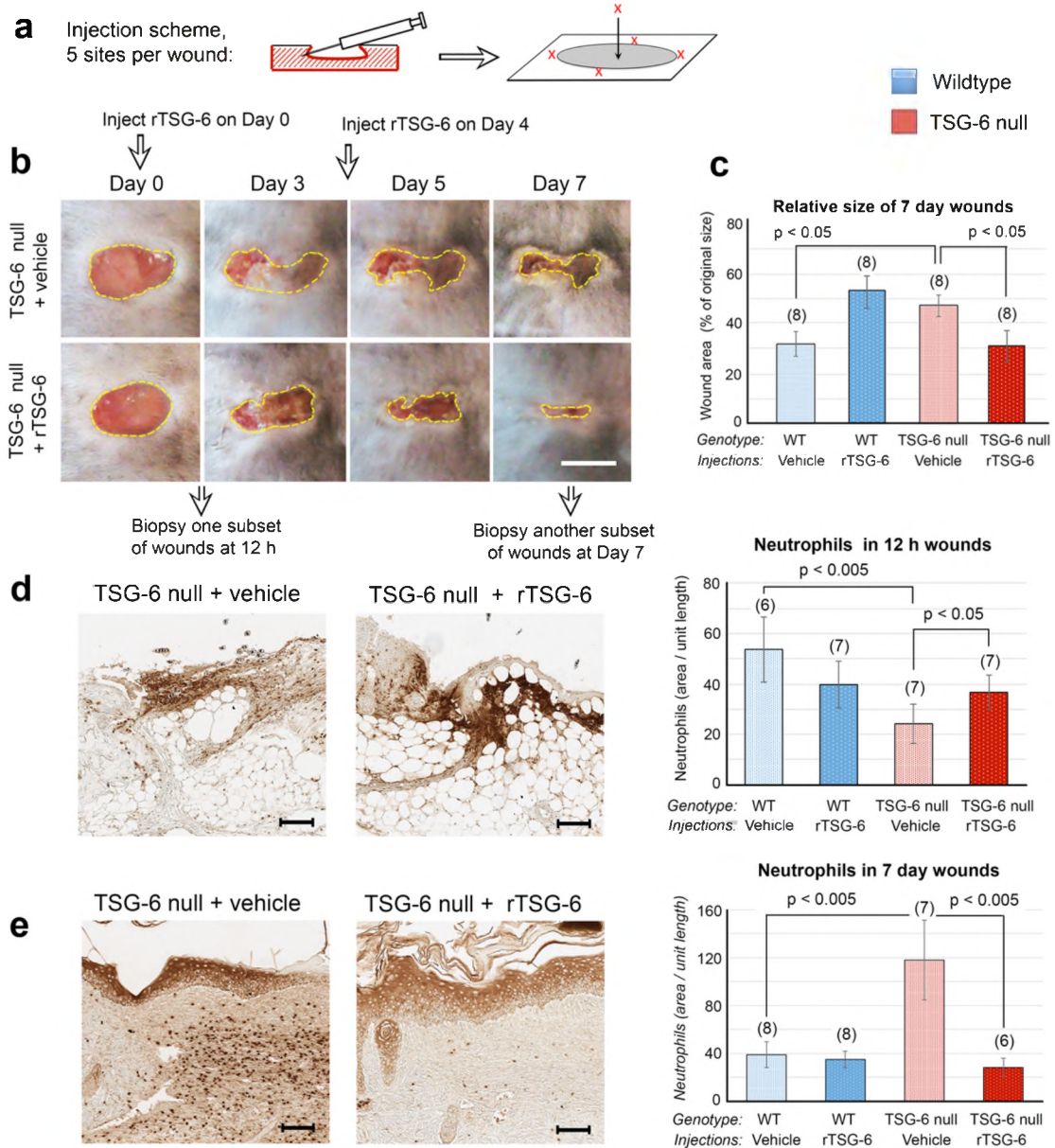


Figure 3-9. Introduction of rTSG-6 into TSG-6 null wounds rescues the delayed closure and abnormal neutrophil recruitment.

(a) Schematics showing a time course and location of injections in WT and TSG-6 null wounds. The black arrows indicate direction of injections. Wounds were injected with PBS only (vehicle) or PBS with recombinant TSG-6 protein (rTSG-6) for both WT and TSG-6 null animals. (b) Wounds were photographed and measured using IPLab imaging software to determine the

open wound area, wound edge indicated by yellow dotted lines. **(c)** Wound sizes are represented as the percentage of Day 0 area. Wound areas were significantly smaller for TSG-6 null wounds receiving rTSG-6 compared to TSG-6 null vehicle wounds. **(d)** Neutrophil staining of TSG-6 null vehicle control and TSG-6 null + rTSG-6 wounds at 12 hours post wounding showed that the delay in recruitment was significantly rescued in null wounds receiving rTSG-6 injections. **(e)** The exacerbated inflammatory response in TSG-6 null wounds at Day 7 was significantly abrogated after rTSG-6 treatment. *Statistical analysis was performed using either Two Way ANOVA with Bonferroni correction or Kruskal-Wallis ANOVA on ranks. (n), number of wounds; Scalebar= 100 μ m.*

3.4 Discussion

This study describes abnormal wound healing responses in mice lacking TSG-6, the enzyme that catalyzes cross-linking of heavy chain proteins to hyaluronan. Our overall findings show that relative to WT controls, TSG-6 null wounds display (i) delayed wound closure, (ii) delayed neutrophil recruitment in early wounds, (iii) exacerbated neutrophil recruitment in late wounds, and (iv) polarization of wound macrophages toward a pro-inflammatory (“M1”) phenotype. Reintroduction of recombinant TSG-6 can reverse both the delayed wound closure and the abnormal neutrophil recruitment.

Our study was motivated by previous literature suggesting an important role for TSG-6 in regulation of inflammation. In many cell and tissue types, TSG-6 expression is low or absent under normal conditions, but stimulated by pro-inflammatory factors such as $\text{TNF}\alpha$, interleukin-1 (IL-1), and LPS (Milner and Day 2003). Here we show that TSG-6 is constitutively expressed at low levels in unwounded mouse skin, in agreement with earlier findings in human skin (Tan et al. 2011). However, TSG-6 expression is greatly increased after wounding. Similarly, HC-HA complexes are detectable in low amounts in normal skin and become significantly elevated after wounding. HC-HA is completely absent in the skin of TSG-6 null mice. Therefore, levels of TSG-6 appear to correlate with levels

of its enzymatic product, HC-HA. Regarding wound inflammation, results reported after injection of rTSG-6 or MSCs (which produce TSG-6 along with many other factors) in other inflammatory models such as murine experimental arthritis (Bardos et al. 2001), myocardial infarction (Lee et al. 2009), DSS-induced colitis (Sala et al. 2015), and rabbit ear wounds (Wang et al. 2015), indicated that TSG-6 might have an anti-inflammatory role, resulting in decreased disease activity and/or improved recovery. In accordance with these studies, we found that absence of endogenous TSG-6 is deleterious to wound healing whereas restoration of the protein through direct dermal injection of rTSG-6 into TSG-6 null mouse wounds restored normal wound healing, at least in terms of the parameters evaluated here.

Beyond identifying a new wound-delay phenotype, our study provides several insights about inflammation and TSG-6 in wounds. Total loss of TSG-6 results in exacerbated pro-inflammatory effects in healing wounds. As a brief review, wounding initiates the release of multiple proinflammatory factors that stimulate local recruitment of neutrophils and monocytes into the wound bed (Martin and Leibovich 2005; Singer and Clark 1999; Wang 2018). Neutrophil recruitment starts as early as 4 h post-wounding and plateaus around 3 days (Kim et al. 2008). Studies in other models in which rTSG-6 protein was injected into inflamed tissue revealed a decreased inflammatory response, including reductions in pro-inflammatory cytokines and neutrophil infiltration (Beltran et al. 2015; Kim et al. 2014a; Oh et al. 2010); absence of TSG-6 on the other hand led to increased neutrophil infiltration (Szanto et al. 2004).

Interestingly, in our TSG-6 null wound model the neutrophil recruitment response appears to be biphasic. At early timepoints (12 and 24 h post-wounding), neutrophils are significantly lower in TSG-6 null wounds than in WT wounds. To explain this, we postulate an interaction between neutrophils and HC-HA on the endothelial glycocalyx. It is known that the luminal side (endothelium) of blood vessels is lined with an HA rich glycocalyx (Reitsma et al. 2007; Shakya et al. 2015), which we hypothesize under wound conditions becomes decorated with HC, forming HC-HA complexes. Because leukocytes bind more avidly to HC-HA complexes than to non-complexed HA (Lauer et al. 2014; Zhuo et al. 2006), HC-HA should facilitate neutrophil attachment within small vessels in the wound bed in WT wounds. Thus, the absence of HC-HA in TSG-6 null wounds should delay neutrophil recruitment in early wounds. However, in later wounds, mechanisms of neutrophil recruitment appear to be different since there is a relatively higher number of neutrophils in TSG-6 null wounds as compared to WT. The excessive levels of pro-inflammatory $TNF\alpha$ in TSG-6 null wounds may be one contributor to neutrophil overabundance especially at Day 7 where levels of $TNF\alpha$ and neutrophils are significantly higher in TSG-6 null wounds. $TNF\alpha$ elevation in TSG-6 deficient mice might occur via several mechanisms, e.g. through feedback inhibition pathways that become de-repressed upon loss of TSG-6, or via the action of cytokines released by incoming macrophages that stimulate cells in the wound bed to synthesize $TNF\alpha$. Regardless of the recruitment mechanism, excessive neutrophil activity has been tied to delayed wound healing (Kim et al.

2008; Wilgus et al. 2013), and is therefore a likely contributor to the aberrant wound healing observed in TSG-6 null mice.

Macrophages, the other major inflammatory cell type in wounds, remove apoptotic neutrophil debris and also secrete pro-inflammatory and anti-inflammatory cytokines, depending upon the particular macrophage phenotype (Koh and DiPietro 2011; Larouche et al. 2018; Wilgus et al. 2013). Although we found no significant difference in the absolute number of macrophages in TSG-6 null versus WT wounds, we did determine that macrophages in TSG-6 null wounds were skewed towards an M1 phenotype. This is in agreement with previous studies showing that TSG-6 and immobilized HC-HA complexes can drive macrophages to a more anti-inflammatory phenotype (Ferrer et al. 2017; He et al. 2013; Mittal et al. 2016), and that TSG-6-producing MSCs can lower proinflammatory marker expression and increase anti-inflammatory M2 macrophages in a colitis model (Song et al. 2017). From several lines of evidence, including the fact that M2 macrophages are known to promote tissue repair, and that M1 macrophages are greatly increased in chronic wounds such as diabetic ulcers, it is becoming clear that controlled regulation of macrophage phenotype is critical for proper wound healing (Hesketh et al. 2017a; Khanna et al. 2010; Krzyszczyk et al. 2018). Thus, we conclude that TSG-6 plays a crucial role in regulating macrophage phenotypes during cutaneous wound healing and this dysregulation in M1/M2 ratio in null wounds could be contributing to aberrant healing.

An additional factor to mention, because it could potentially contribute to the observed phenotypes, is an ability of TSG-6 to regulate chemokine function. As

shown by Dyer et al., TSG-6 can regulate chemokine availability by competitive binding to various chemokines and/or sulfated GAGs in the ECM (Dyer et al. 2016; Dyer et al. 2014). Absence of TSG-6 might interrupt some of these interactions and depending upon which cytokines are affected, could influence neutrophil migration. This possible mechanism would make an interesting subject for future investigation.

A strength of the current study is that TSG-6 restoration (rTSG-6 injection into TSG-6 deficient wounds) was shown to normalize wound closure and neutrophil recruitment. These results unambiguously establish that the defects observed in TSG-6 null mice result from loss of TSG-6 protein. Interestingly, while reintroduction of rTSG-6 into TSG-6 null wounds reversed the wound delay and neutrophil recruitment defects, addition of rTSG-6 into normal WT wounds worsened both of these phenomena. Apparently, tight regulation of TSG-6 is critical for proper wound healing, and either excessive or insufficient amounts are deleterious.

In summary, loss of TSG-6 leads to abnormal pro-inflammatory changes and is detrimental to wound healing, whereas a regulated amount of TSG-6 is crucial for a normal inflammatory response and proper wound closure. While more studies are needed to fully elucidate the mechanisms behind the phenotypes observed, our study provides important groundwork for understanding the role of endogenous TSG-6 in cutaneous wound healing.

3.5 Limitations

Following are some limitations of the methodologies involved in this study.

- The wound protocol described required sacrificing of the mice after each time-point post wounding for wound collection, making it impossible to perform linear study. An alternative could be developing neutrophil specific GFP tagged WT and TSG-6 null mice and follow neutrophil recruitment post-wounding in-vivo using an appropriate imaging system.
- The mouse wound closure study performed may have been affected by the contraction due to mouse skin mobility, resulting in uneven closure pattern. To avoid this, splints could be used to prevent the contraction due to skin mobility and thus avoid the effect of this variable in wound closure result.
- All the attempts to double stain the wound sections for pan macrophage marker, F4/80, and any of the M1 or M2 markers, were unsuccessful. Since this could provide a more conclusive result about differences in macrophage phenotype polarization between WT vs TSG-6 null wounds, additional effort to find combinations of pan-marker and M1/M2 markers that could be double stained could be made. Alternatively, different immunohistochemistry conditions that will make this happen with the available markers could be tried.
- For flow cytometric analysis of macrophage phenotype more than one M1/M2 marker each is desirable. However, this could not be attained here because of the cell number constraint. To include more M1/M2 markers, the amount of starting tissue material could be increased, which means more than 8 wounds (> 2 animals) per sample.

CHAPTER IV

ISOLATION OF SINGLE CELLS FROM CUTANEOUS WOUNDS FOR FLOW SORTING AND FLOW CYTOMETRIC ASSESSMENT OF MACROPHAGES

4.1 Introduction

The intricate process of skin wound healing is broadly divided into three overlapping phases— a) inflammation, b) tissue formation, and c) tissue remodeling (Singer and Clark 1999). Each of these phases constitutes multiple events coordinated by various cells, cytokines, chemokines, growth factors, and enzymes. Macrophages are an important inflammatory cell type regulating wound healing. These cells are known to regulate neutrophil recruitment and clearance during the early stage of inflammation, as well as the activation of fibroblasts and endothelial cells during the later phases of tissue formation and remodeling (Eming et al. 2007; Koh and DiPietro 2011). Macrophages fulfill their roles through controlled production of pro- and anti-inflammatory cytokines such as tumor necrosis factor (TNF)- α , interleukin 1 (IL-1), and interleukin 10 (IL-10), and growth factors such as the transforming growth factors TGF- α and TGF- β , platelet-derived growth factor (PDGF), and vascular endothelial growth factor (VEGF). Based upon the cytokines that they produce and the functions they perform, macrophages have been

categorized into two main phenotypes, classically activated/pro-inflammatory (M1) and alternatively activated/ anti-inflammatory (M2) (Hesketh et al. 2017b; Martinez and Gordon 2014). Studies show that controlled regulation of the M1/M2 ratio is critical for the proper and timely healing of wounds. For example, in chronic wounds such as diabetic ulcers, more macrophages are of the M1 kind than in normal wounds (Hesketh et al. 2017b; Krzyszczyk et al. 2018). In order to devise new therapies to enhance wound repair, a greater understanding of the dynamics of macrophage phenotype transition in normal vs. poorly healing/chronic wounds will be critical. However, a major challenge to achieving that goal is the isolation of intact macrophages (or other pure populations of cells such as neutrophils or lymphocytes) from wounds for their subsequent analysis.

Here, we present an optimized version of a method described by Wilson et al. (Wilson, Fathke and Isik, 2001) to prepare single cell suspensions from murine skin wounds for flow cytometry. As flow cytometric analysis and fluorescence-assisted cell sorting (FACS) are sensitive and well-known techniques to analyze specific cell population, we employed these methods for further characterization of macrophages. As per our experience, even the smallest details, such as the type and size of tubes used for centrifugation, and the centrifugation speed, are important and can influence the number and quality of viable cells obtained for analysis, sorting, and downstream applications. The current protocol has been developed by compiling information from across many sources and optimizing the protocol for our purpose. The four major points identified and were optimized, that were found to be critical for success, have been highlighted in blue boxes within

the protocol. Our methodological description provides a well-defined protocol to isolate cells from full-thickness cutaneous wounds, stain these cells for the hematopoietic cell marker CD45 and the macrophage pan-marker F4/80, and to analyze the cells by two different approaches, namely FACS for RNA analysis (A) and flow cytometric analysis (B).

The method is described in three steps. Steps 1 and 2 are mostly similar for the two analytical approaches (Analytic Method A and Analytic Method B) with occasional differences which have been emphasized. Flow cytometric analysis requires additional steps relative to cell sorting, so Step 3 has been divided into two sections.

4.2 Method details

4.2.1 Step 1: Wounding and wound collection

Materials and reagents

- Dulbecco's Phosphate Buffered Saline (PBS, 1X) (Thermo Fisher Scientific, Cat# 14190250, Waltham, MA, USA)
- Ethanol, 70%
- Ketamine and xylazine for anesthesia. (This will vary, depending upon your institution's animal protocol. We use Ketamine (100 mg/kg) and Xylazine (10-15 mg/kg) delivered intraperitoneally.
- Forceps (Roboz, Cat# RS-5130, Gaithersburg, MD, USA)
- Hair clipper (Wahl Clipper Corp., Model# 9962, Sterling, IL, USA)

- Skin biopsy punch, disposable 5mm (Acuderm Inc., Cat# P550, Fort Lauderdale, FL, USA)
- Heat lamp or Slide warmer

Procedure for Step 1

Notes:

- a) C57BL/6J mice were obtained from JAX Laboratories (Bar Harbor, ME). Mice were maintained per guidelines of the American Association for the Accreditation of Laboratory Animal Care. All procedures were approved by our hospital's Institutional Animal Care and Use Committee (IACUC).
- b) Male and female mice, 8-10 weeks of age, were used for wounding.

Shaving:

1-1. Put mice under light anesthesia and shave the fur from two-thirds of the dorsal skin, from below ear-level to the mid-back. Allow the mice to recover from anesthesia in a warm environment.

Wounding:

1-2. Inject an approved dose of anesthetic and disinfect the shaved skin area with 70% ethanol.

1-3. To make full thickness excisional wounds, pinch the dorsal shaved skin at midline to make a large fold. Lay the mouse down on the surgical table laterally, with the right side (right ear of the mouse) facing up, and the folded skin pulled far away from the body. Press the skin biopsy punch through the folded skin to create two clean wounds, located about a centimeter (1 cm) below the head and 1 cm

apart. Similarly, using a new biopsy punch, make a second set of wounds 1 cm caudal to the first set (Figure 4-1).



Figure 4-1. Wounds on the shaved back of a mouse.
Using 2 punch biopsies, make 4 wounds per mouse.

1-4. Let the mice recover in a warm environment (under a heat lamp or on a slide warmer in a cage). After wounding, each mouse should be housed individually and monitored until collection day.

Wound collection:

1-5. At Day 7 post-wounding (or at a different timepoint as needed), under deep general anesthesia, harvest the entire wound area plus ~2 mm rim of unwounded skin. Store the collected tissue on wet ice during this process, in a labeled container such as the lid of a 60 mm tissue culture plate.

1.6. Once all the wounds are collected, euthanize the mice.

4.2.2 Step 2: Tissue Digestion and single cell preparation

Materials and reagents

- Collagenase, Type 1 (Worthington, Cat# LS004196, Lakewood, NJ, USA)
- Dispase II (Roche Diagnostics, Cat# 04942078001, Indianapolis, IN, USA)
- DNase I (Worthington, Cat# LS002060)

- Dulbecco's Phosphate Buffered Saline (PBS, 1X) (Thermo Fisher Scientific, Cat# 14190250)
- EDTA disodium salt (Thermo Fisher Scientific, Cat# BP120)
- Fetal Bovine Serum (FBS), Heat-inactivated (Gibco™, Thermo Fisher Scientific, Cat# 10082139)
- Fixation/Permeabilization Solution Kit with BD GolgiPlug™ (BD Biosciences Cat# 555028, San Jose, CA, USA); This is NOT REQUIRED if doing FACS sorting only
- Flow Buffer (3% FBS and 0.1 mM EDTA in PBS)
- G418 Sulfate antibiotic (Corning, Cat# 61-234-RG, Corning, NY, USA)
- Hank's buffered salt solution (HBSS, 1X) (Thermo Fisher Scientific, Cat# 14175079)
- Trypan Blue solution (Lonza, Cat# 17-942E, Walkersville, MD, USA)
- Falcon® 40-µm cell strainer (Corning, Cat# 352340)
- Falcon® 15 ml polypropylene conical tube (Corning, Cat# 352097)
- Falcon® 50 ml polypropylene conical tube (Corning, Cat# 352098)
- Forceps (Roboz, Cat# RS-5130)
- Hemacytometer (Bright-Line™, Sigma-Aldrich, Cat# Z359629, St. Louis, MO, USA)
- Kimwipes™ (Kimberly-Clark, Cat# 34120, Milsons Point, NSW, Australia)
- Scissors (V. Mueller® Iris scissors, CareFusion, Cat# OP5526, McGaw Park, IL, USA)

- Syringe filter, Fisherbrand® 25 mm, 0.2-µm (Thermo Fisher Scientific, Cat# 09-719C)
- Syringe, BD 60 ml (Becton Dickinson, Cat# 309653, Franklin Lakes, NJ, USA)
- Centrifuge (5810 R, Eppendorf, Hauppauge, NY, USA)
- Heat lamp or Slide warmer
- Incubator shaker (C24, New Brunswick Scientific, Edison, NJ, USA)

Procedure for Step 2

Notes:

- a) To have enough cells to process samples for flow cytometric analysis or FACS sorting, wounds from 2 mice are pooled for each sample (total of 8 wounds per sample).

Optimization 1:

Here, we define the number of wounds and the amount of wound tissue required per sample to have enough cells for flow cytometric analysis (as outlined) or flow sorted macrophages to investigate M1/M2 polarization. Initially two wounds were made per mouse, however, cell yields were sub-optimal. For optimum use of available animals, 4 wounds per mice were made instead of 2 wounds (Figure 1). Eight wounds from 2 mice were pooled to have enough starting tissue per sample.

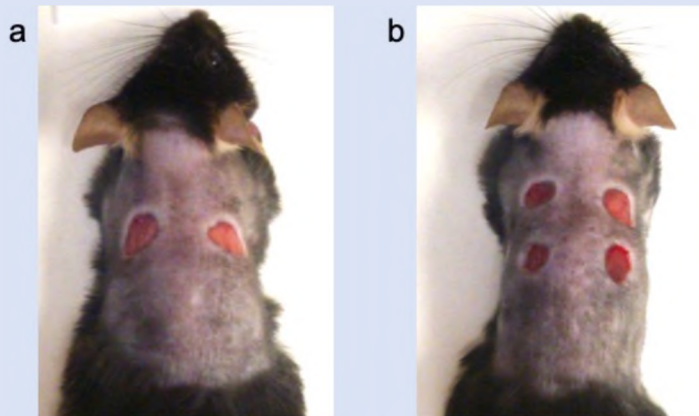


Figure 1. Instead of two wounds per animal (a), four wounds were made per animal (b) for flow cytometry purposes.

- b)** Keep the tissue pieces and the cells on wet ice (or at 4 °C) at all times, unless otherwise stated.
- c)** Prepare 500 ml of Flow Buffer and store it at 4 °C (or on ice) at all times. This buffer will be used for all washing and incubation steps unless otherwise mentioned.

Dispase digestion:

2-1. Weigh wound tissue, then rinse one time in 70% ethanol and one time in 1X PBS. Dab tissue with a Kim-wipe to remove remnant PBS. On average, four 7-day wounds from one mouse weighs about 175 mg.

2-2. Prepare dispase digestion buffer in HBSS by adding Dispase II at 1 mg/ml, G418 at 10 mg/ml, and 3% FBS. Filter using a 0.2- μ m syringe filter and a 60 ml syringe. A Stericup vacuum filtration system with a 0.22 μ m pore size (Millipore, Cat# S2GPU02RE, Burlington, MA, USA) can be used in processing a bigger volume. Prepare this buffer fresh every time.

2-3. Each milligram of wound tissue will require 20 μ l of the dispase digestion buffer. For each sample (8 wounds), aliquot the required amount of the dispase digestion buffer into a 50 ml polypropylene conical tube on wet ice. Two points to note:

- It is important to use polypropylene conical tube (and not polystyrene dishes) to avoid the released cells from adhering to the container.
- We use 50 ml conical tubes, even though the total volume is generally less than 10 ml because it makes it easier to remove tissue pieces for the next step.

2-4. Using forceps and scalpel, cut tissues into 2-3 mm² pieces and put them in the tubes with dispase buffer. Do this on wet ice. Incubate at 4 °C overnight (No shaking required).

2-5. The following step is only for flow cytometric analysis. For the last two hours of dispase digestion, add BD GolgiPlug™ from the Fixation/Permeabilization solution kit to each sample, at a concentration of 1 μ l/ml of digestion buffer.

Optimization 2:

Here, we modified the addition of GolgiPlug™ to 2 hours before stopping the dispase digestion step for flow cytometric analysis. This helped in retaining the secretory cytokine (for example, TNF α in this case) inside the Golgi body in cells while also preventing cell death from long term exposure to GolgiPlug™.

Collagenase digestion:

2-6. Prepare collagenase digestion buffer in HBSS by adding Collagenase I at 1 mg/ml, G418 at 5 mg/ml and DNase I at 75 U/ml. Filter using a 0.2- μ m syringe filter and a 60 ml syringe. Again, a Stericup vacuum filtration system with a 0.22 μ m pore size, can be used in processing a bigger volume. Prepare this buffer fresh every time; this can, however, be prepared a day earlier and stored at 4 °C.

2-7. If doing flow cytometry analysis, add BD GolgiPlug™ from the Fixation/Permeabilization solution kit at 1 μ l/ml to the filtered collagenase digestion buffer mix above.

2-8. Each milligram of wound tissue requires 80 μ l of the collagenase digestion buffer. For each sample, aliquot the required amount of the collagenase digestion buffer into a labeled 50 ml conical tube at room temperature. Using forceps, transfer tissue pieces from the dispase to the collagenase digestion buffer. Incubate for 2 h at 37 °C with shaking at 95 rpm in an incubator shaker. Save the remaining dispase buffer, which will contain a population of cells released from the first digestion step, on ice.

2-9. After incubation, combine cell suspensions from the dispase and collagenase digestions and filter through a 40 μ m cell strainer into a new 50 ml

conical tube. Use 4-5 ml of Flow Buffer to rinse both tubes and pass this through the cell strainer.

2-10. For centrifugation, divide the filtered cell suspension into several 15 ml Falcon tubes, about 10-12 ml in each (Figure 4-2). Each sample may require 5 or more tubes. The rationale here is that under the centrifugation conditions required (see below), cells fail to form nice pellets in 50 ml tubes when large volumes are used, and many cells are lost in the process. If you still prefer to use 50 ml tubes instead of 15 ml ones, limit the volume in each tube to 10 ml.

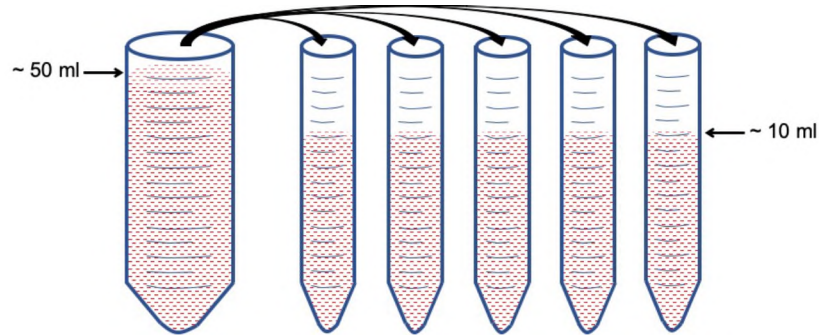


Figure 4-2. Schematic for step 2-10.

Schematic showing the transfer of filtered cell suspension from one 50 ml conical tube to multiple 15 ml conical tubes for centrifugation, as described in Step 2-10.

Optimization 3:

Single cell suspensions obtained after dispase and collagenase digestions were transferred to 15 ml tubes for better centrifugation. As shown in the figure below, the cells did not form a proper pellet when centrifuged with large volumes in 50 ml conical tubes (Figure 2a). When centrifuged in 15 ml tubes, the cells formed a nice pellet as desired (Figure 2b).

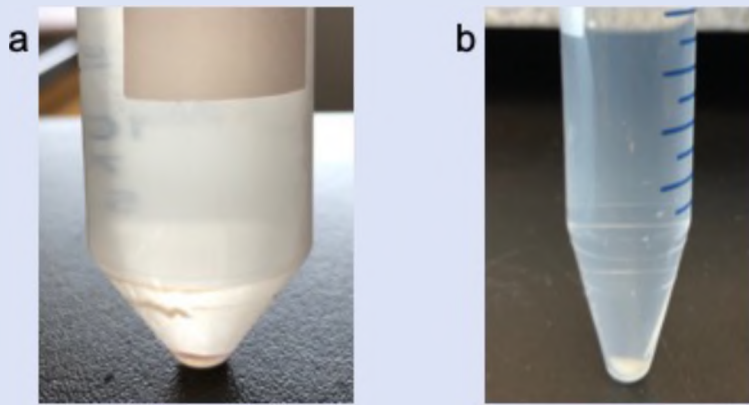


Figure 2. Use of appropriate tube sizes was found to be critical during centrifugation to keep the cells intact and form a proper cell pellet.

Shown on the left is a 50 ml conical tube with a poorly formed pellet (a), while shown on the right is a 15 ml conical tube with a clean, properly formed cell pellet (b).

2-11. Centrifuge at 350 x g for 10 min at 4 °C.

2-12. Being careful not to disturb the cell pellet, remove the supernatant using a vacuum aspirator or pipettor, leaving about 1 ml.

2-13. Add 3 ml of Flow Buffer to the cell pellet and resuspend using a 10 ml pipet.

Centrifuge at 350 x g for 10 min at 4 °C.

2-14. Again, remove the supernatant with a vacuum aspirator, leaving about 500 µl of supernatant.

2-15. Resuspend cell pellets in 1 ml of Flow Buffer per tube, then combine the cell suspensions into a single 15 ml conical tube and pipet to mix well. Count live cells under hemacytometer.

Assessment of viability of the single cell suspension: Combine 10 μ l of well-mixed cell suspension and 10 μ l of Trypan Blue solution. Pipette 10 μ l of this mix onto a hemacytometer. Incubate for 2 min and count the unstained (viable) cells. We typically obtain an average of 10 million live cells per sample (8 wounds) with >97% viability.

Note: It is normal to see some debris along with single cells in the mixture under the microscope.

4.2.3 Step 3: Cell staining with fluorophore markers for FACS sorting or flow cytometric analysis

For analysis of cells by flow sorting (where cells are collected), or by cytometric analysis (in which cells are analyzed but ultimately discarded), the initial steps are the same. Thus, Steps 3-1 to 3-13 below are the same for both approaches. After that, the procedures diverge. Section A (Steps 3-14 to 3-22) contains procedures unique to FACS sorting of macrophages, while Section B (Steps 3-23 to 3-39) contains instructions designed for flow cytometric analysis.

Materials and reagents

The following four antibodies, fluorophore-tagged:

⇒ FITC anti-mouse CD45 antibody (BioLegend, Cat# 103107, San Diego, CA)

- ⇒ PE/Cy5 anti-mouse F4/80 antibody (BioLegend, Cat# 123111)
- ⇒ Brilliant Violet 650™ anti-mouse TNF α antibody (BioLegend, Cat# 506333)
- ⇒ PE anti-mouse Arginase-1 antibody (Novus, Cat# IC5868P, Centennial, CO, USA)

Reagents and materials, as follows:

- AbC™ Total Antibody Compensation Bead Kit (Thermo Fisher Scientific, Cat# A10497)
- Fixation/Permeabilization Solution Kit with BD GolgiPlug™ (BD Biosciences Cat# 555028); NOT REQUIRED if only doing FACS sorting
- LIVE/DEAD™ Fixable Blue Dead Cell Stain Kit (Thermo Fisher Scientific, Cat# L23105)
- Mouse BD Fc Block™, Purified Rat Anti-Mouse CD16/CD32 (BD Biosciences, Cat# 553141)
- TRIzol™ Reagent (Thermo Fisher Scientific, Cat# 15596018)
- 1.7 ml microcentrifuge tubes (Denville, Cat# C2170, Saint-Laurent, QC, Canada)
- 2 ml microcentrifuge tubes (USA Scientific, Cat# 1620-2700, Ocala, FL, USA)
- CellTrics® filters, 30 μ m (Sysmex Partec GMBH, Cat# 04-004-2326, Görlitz, Germany)
- Fisherbrand® serological pipets (Thermo Fisher Scientific, 5 ml, Cat# 13-678-11D, and 10 ml, Cat# 13-678-11E)
- Centrifuge 5415 D (Eppendorf) [store in a cold-room, at 4 °C, for cold centrifugation]

Procedure for Step 3

Notes:

a) Treat the live cells as gently as possible. Use 5- or 10- ml serological pipets to mix cells in centrifuge tubes or careful pipetting using 1 ml pipette in microcentrifuge tubes. Do not vortex live cells.

b) The working concentrations for all antibodies used in this protocol are based on optimization done for our tissue/cell type. Optimization is done by testing for at least 6 serial dilutions starting with a concentration recommended in the antibody datasheet and tested by flow cytometry. The working concentrations for the antibodies are as follows: anti-CD45 at 1:200, anti- F4/80 at 1:80, anti-Arginase-1 antibody at 1:10 and anti-TNF α antibody at 1:40.

c) Having a proper set of controls is critical for successful flow cytometric analysis as well as for FACS sorting. Control tubes and experimental tubes should be treated in the same way, with the same number of washes and centrifugations. To prepare control tubes with cells, mix aliquots of cell suspension from each sample to achieve 1 million cells for each type of control. For example, if you have 4 samples resuspended at 1 million cells/ml, take 250 μ l from each sample tube and put in a 1.7 ml microcentrifuge tube (Figure 4-3).

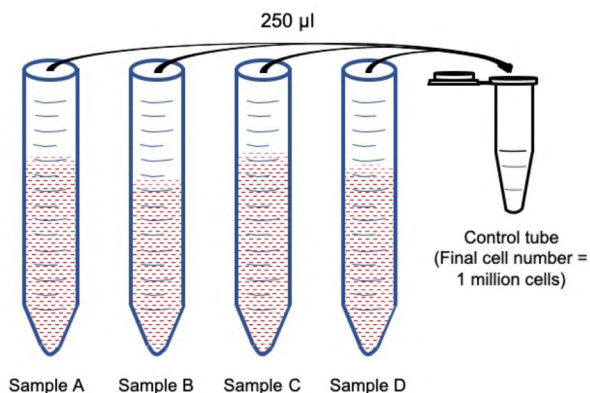


Figure 4-3. Schematic showing preparation of control tube with cells.

To prepare each control tube with cells, mix aliquots of cell suspension from all samples into a 1.7 ml tube.

d) **Table 4-1** (below) gives a list of controls required for the FACS sorting of macrophages. **Table 4-2** gives a list of controls required for flow cytometric analysis of M1/M2 macrophages. Note that the AbC™ Compensation beads were used for antibody compensation controls for both techniques, except for Arginase-1 antibody. Our Arginase-1 is a sheep-primary antibody and is not compatible with the AbC™ beads kit, so cells were used instead.

Table 4-1. List of controls required for FACS sorting of macrophages (Analytical Method A)

(For further explanation of controls refer to Note c)

Tube #	Fluorophore tagged markers			Label
	Live/Dead™ blue	CD45	F4/80	
1	x	x	x	Unstained
2	✓	x	x	Live/Dead only
3	✓	✓	x	L/D + CD45
4*	x	✓	x	CD45 Comp.
5*	x	x	✓	F4/80 Comp.

✓ = Marker added into tube

x = Marker not added

* = Compensation control with AbC™ compensation beads

**Table 4-2. List of controls required for Flow cytometric analysis (Analytical Method B)
(For further explanation of controls, refer to Note c)**

Tube#	Fluorophore tagged markers					Label
	Live/Dead™ blue	CD45	F4/80	Arg-1	TNF α	
1	x	x	x	x	x	Unstained
2	✓	x	x	x	x	Live/Dead only
3	✓	✓	x	x	x	L/D + CD45
4	✓	✓	✓	x	x	L/D + CD45 + F4/80
5	✓	✓	✓	✓	x	FMO TNF α
6	✓	✓	✓	x	✓	FMO Arg-1
7**	x	x	x	✓	x	Arg-1 Comp.
8*	x	✓	x	x	x	CD45 Comp.
9*	x	x	✓	x	x	F4/80 Comp.
10*	x	x	x	x	✓	TNF α Comp.

✓ = Marker added into tube

x = Marker not added

* = Compensation control with AbC™ compensation beads

** = Compensation control with cells (unique to Arg-1)

FMO = Fluorescence minus one

e) Compensation beads were stained as outlined in the kit manual.

f) Centrifugation conditions for preparation of controls and samples: For 1.7 ml microcentrifuge tubes, 400 x g for 5.5 min at 4 °C. For 15 ml conical tubes, 350 x g for 10 min at 4 °C.

Optimization 4:

Limiting the number of centrifugations to twice instead of 3-times between steps at the above-mentioned speed and duration throughout the protocol helped limit the loss of cells during washing and subsequent pipetting.

SHARED STEPS (common to FACS sorting and to Flow cytometry)

Staining with Live/Dead™ blue:

3-1. For each sample from Step 2 (in 15 ml tubes), add Flow Buffer to adjust the cell count to 1 million cells/ml.

3-2. Prepare a 1 ml aliquot for unstained control (Tube# 1) into a labeled 1.7 ml microcentrifuge tube (as outlined in Note c) and treat this tube similarly to the rest of the cells. Remember to centrifuge/wash control tubes the same number of times as the other tubes for the entire procedure. If doing flow cytometry analysis, separate an additional aliquot for Arginase-1 compensation control (Tube# 7 in Table 4-2).

3-3. Stain cell samples in 15 ml tubes for dead cells using LIVE/DEAD™ Fixable Blue Dead Cell Stain Kit as recommended in the user guide. Remember to bring the vial of DMSO and a tube of reactive dye from the kit to room temperature before using. Add 1 μ l of reconstituted fluorescent reactive dye per 1 mL of cell suspension.

3-4. Mix well using a 10 ml pipet and incubate on ice for 30 minutes in the dark.

3-5. After incubation, add 5 mL of Flow Buffer to each sample and centrifuge. Remember to centrifuge control Tube# 1 (and Tube# 7 for flow cytometry analysis) as well.

3-6. Remove supernatant as before, leaving about 500 μ l. Resuspend the pellet in 6 ml of Flow Buffer (and control pellet in 1 ml of Flow Buffer) and then centrifuge one more time.

3-7. Remove supernatants from 15 ml tubes as before, leaving about 250 μ l. (Resuspend control pellets in 1 ml Flow Buffer and place on ice).

Blocking Fc receptors and staining for fluorophore-tagged (extracellular) antibody markers:

3-8. Resuspend cell pellets in the 15 ml tubes at a concentration of 1 million cells per 50 μ l of Flow Buffer.

3-9. Separate out a 50 μ l total aliquot of cells for Live/Dead only control (Tube# 2) into a labeled 1.7 ml microcentrifuge tube. As explained in Note (c) above, the control is prepared by mixing aliquots of cell suspension from all samples [that is, if you have 4 samples, take 12.5 μ l from each sample to prepare a control tube]. Add 50 μ l of Flow Buffer to bring the volume to a total of 100 μ l.

3-10. To the remaining cells in the 15 ml tubes, add 1 μ g (= 2 μ l) of Mouse BD Fc Block™ per 50 μ l of cell suspension and incubate for 5 min on ice in the dark.

3-11. During this incubation, prepare cell surface antibody mix as follows:

- For Live/Dead + CD45 control (control Tube# 3), prepare 50 μ l of anti-CD45 antibody at 1:100 in Flow Buffer.
- For the remaining cells in 15 ml tubes, prepare a cocktail of anti-CD45 antibody at 1:100 and anti-F4/80 antibody at 1:40 in Flow Buffer. Prepare 50 μ l of this mix per 1 million cells. Calculate the volume of the antibody cocktail required as follows:

For example, if Sample A has 5 million cells and Sample B has 8 million cells, the total volume of antibody cocktail required is: $50 \times (5+8) = 650 \mu$ l.

3-12. After incubation with Fc Block, separate an aliquot of 50 μ l cell suspension for Live/Dead + CD45 control (Tube# 3) into a labeled 1.7 ml microcentrifuge tube by again mixing aliquots from all samples (as outlined in Note c).

3-13. Add antibody mix prepared in step 3-11 into the control Tube# 3 and the 15 ml tubes and incubate for 20 minutes on ice in the dark.

*** *If you are doing Flow Cytometric Analysis, go to Section B (step 3-23).*

Otherwise, continue to step 3-14 to perform FACS sorting of macrophages.

Optimization:

The effect of the major optimizations highlighted thus far is shown in the figure below. Figure 3a represents the total number of cells before optimization whereas Figure 3b shows the total number of cells after optimization. In the latter, the number of cells were much higher which subsequently resulted in obtaining higher number of macrophages for flow cytometric analysis or sorting.

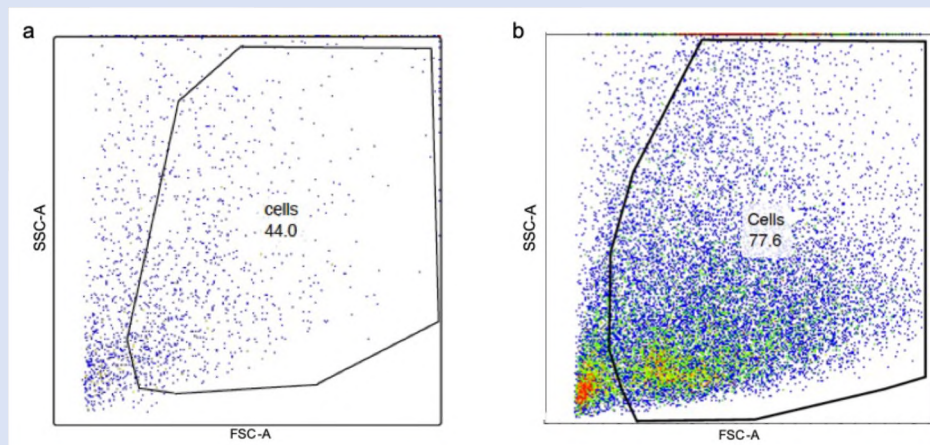


Figure 3. After all the described optimizations, the percentage of cells retained at the endpoint of flow cytometry was much higher (b) than before (a). The gate was applied as shown to filter out the debris during analysis.

Analytical Method A: FACS sorting for macrophages

Tube:	Control Tube# 1	Control Tube# 2	Control Tube# 3	Control Tube# 4	Control Tube# 5	Experimental Tube# A	Experimental Tube# B ...
Contains:	Cells	Cells	Cells	Compensation beads	Compensation beads	Cells	Cells
Antibody mix:	No Antibody	No Antibody	CD45	CD45	F4/80	CD45 F4/80	CD45 F4/80
Live/Dead Blue	No	Yes	Yes	No	No	Yes	Yes

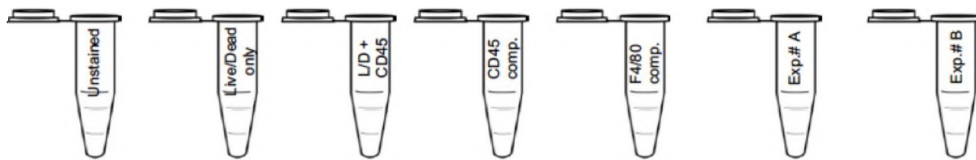


Figure 4-4. Control and experimental tubes for FACS sorting.

3-14. During the incubation, transfer the remaining sample from 15 ml tubes into as many (1.7 ml or 2 ml) microcentrifuge tubes for experimental samples, irrespective of the cell number per sample tube.

3-15. After incubation, add 500 µl Flow Buffer to all microcentrifuge tubes, and spin.

3-16. Remove supernatant using a 1 ml pipette, leaving about 50 µl. Resuspend in 1 ml of Flow Buffer and centrifuge once more.

3-17. Remove supernatant carefully using a 1 ml pipette leaving about 50 µl. Resuspend at 1 million cells per 100 µl of Flow Buffer and store in cold for FACS sorting. Plan to sort these cells as soon as possible after staining.

Figure 4-4 depicts the tubes we need to have with all the applicable conditions by the end of this process.

FACS sorted cell collection:

Flow sorting was done using a BD FACSAria II sorter and BD FACSDiva software (BD Biosciences) with assistance from personnel at Cleveland Clinic LRI Flow Cytometry Core. Cells were sorted using a 100 µm nozzle size at a low sheath pressure of 20 psi.

3-18. Label 2 ml microcentrifuge tubes or 15 ml conical tubes as required to collect the desired cell populations. For each experimental sample, we collected two subsets of cell populations for RNA isolation, as follows:

- CD45⁺ (CD45 only positive) cells for control.
- CD45⁺ F4/80⁺ (CD45 and F4/80 double positive) macrophages.

3-19. Add 500 µl of TRIzol™ reagent into the labeled collection tubes before loading them onto the sorter.

3-20. Right before sorting, filter the cell samples (controls and experimental's) through CellTrics® 30 µm filters to remove any clumps.

3-21. After sorting, calculate the volume of cell suspension sorted into each tube using a 1 ml pipette and add more TRIzol to bring the ratio of sort volume and TRIzol to at least 1:3. Pipette up and down multiple times to lyse the cells and homogenize well.

3-22. Store the homogenized sample on ice. When ready to isolate RNA, incubate the homogenized sample for 5 minutes at room temperature and proceed with RNA isolation following standard protocol.

- Note: The samples in TRizol can be frozen at -20 °C if necessary, for later RNA isolation. However, it is discouraged for this protocol as the number of sorted cells is limited. See Method validation section below for further details.

Analytical Method B: Flow cytometric analysis of M1/M2 macrophages

Tube:	Control Tube# 1	Control Tube# 2	Control Tube# 3	Control Tube# 4	Control Tube# 5	Control Tube# 6	Control Tube# 7	Control Tube# 8	Control Tube# 9	Control Tube# 10	Experimental Tube# A	Experimental Tube# B
Contains:	Cells	Cells	Cells	Cells	Cells	Cells	Cells	Compensation beads	Compensation beads	Compensation beads	Cells	Cells
Antibody mix:	No Antibody	No Antibody	CD45	CD45 F4/80	CD45 F4/80 Arg-1	CD45 F4/80 TNF α	Arg-1	CD45	F4/80	TNF α	CD45 F4/80 Arg-1 TNF α	CD45 F4/80 Arg-1 TNF α
Live/Dead Blue:	No	Yes	Yes	Yes	Yes	Yes	No	No	No	Yes	Yes	Yes

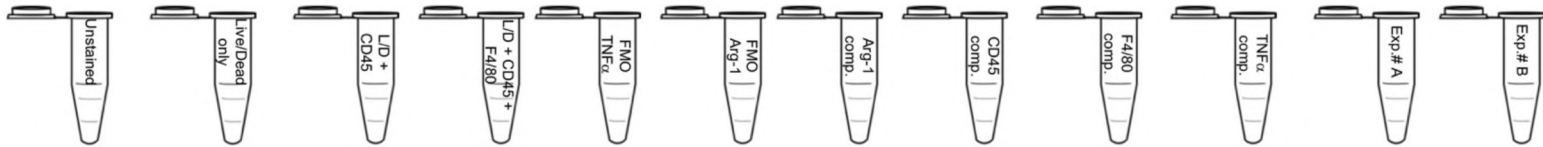


Figure 4-5. Control and experimental tubes for flow cytometric analysis.

Fixation/Permeabilization:

3-23. After incubation with cell surface antibody mix in Step 3-13 above, add 2 ml buffer to 15 ml tubes and centrifuge.

3-24. Remove supernatant carefully using a 1 ml pipette, leaving about 100 μ l. Resuspend in 3 ml buffer and centrifuge again.

3-25. Remove supernatant and resuspend cells at a concentration of 1 million cells per 100 μ l of Flow Buffer.

3-26. Add 250 μ l of Fixation/Permeabilization solution per 1 million cells, mix by pipetting, and incubate for 20 minutes on ice in the dark.

3-27. During the incubation, prepare 1 X Perm/Wash buffer from the 10X BD Perm/Wash buffer in the Fixation/Permeabilization Solution Kit as recommended. After incubation with the fixation/permeabilization buffer, add 500 μ l of 1 X Perm/Wash buffer per 1 million cells, mix and centrifuge.

3-29. Remove supernatant using 1 ml pipette, resuspend in 1 mL BD Perm/Wash buffer and centrifuge again.

3-30. Remove supernatant and resuspend the cell pellets at 1 million cells per 50 μ l of Flow Buffer.

3-31. Prepare an aliquot of 50 μ l cell suspension for Live/Dead + CD45 + F4/80 control (Tube# 4) as before in Step 3-9.

3-32. To the remaining sample tubes, add 1 μ g (= 2 μ l) of Mouse BD Fc Block™ per 50 μ l of cell suspension and incubate for 5 minutes in the dark at room temperature.

3-33. During this incubation, prepare the intracellular antibodies as follows:

- For FMO TNF α control (Tube# 5), prepare 50 μ l of anti-Arginase-1 antibody at 1:5 in Flow Buffer.
- For FMO Arg-1 control (Tube# 6), prepare 50 μ l of anti-TNF α antibody at 1:20 in Flow Buffer.
- For Arg-1 comp. control (Tube# 7), prepare 50 μ l of anti-Arginase-1 antibody at 1:5 in Flow Buffer.
- For the experimental tubes, prepare a cocktail containing anti-Arginase-1 antibody at 1:5, and anti-F4/80 antibody at 1:40 in Flow Buffer. Prepare 50 μ l of this mix for as many experimental samples as required. This can be simply calculated as: (Number of samples) x 50 μ l.

Refer to Table 4-2 and/or Figure 4-5 for more information about the controls.

3-34. After incubation with Fc Block, prepare aliquots of 50 μ l cell suspension (~1 million cells ideally) for FMO control tubes (Tube# 5-6) into labeled 1.7 ml microcentrifuge tube as before in Step 3-9.

3-35. From the remaining cells, prepare experimental samples. Transfer one 50 μ l aliquot (1 million cells) from one 15 ml tube to one 1.7 ml microcentrifuge tube.

Note: It is important to have an equal number of cells in each experimental sample.

Staining for intracellular markers for M1 and M2:

3-36. Add 50 μ l of intracellular antibody mix prepared in step 3-33 to respective control tubes and experimental tubes. Incubate for 25 minutes in the dark at room temperature

3-37. During this incubation, prepare the compensation controls with beads (Tube# 8, 9 and 10). Stain the beads as outlined in the kit manual.

3-38. After the incubation, add 500 μ l of Flow Buffer to all tubes and centrifuge @ 900 x g for 5.5 minutes at room temperature. Resuspend cell pellet in 1 mL buffer and centrifuge once more.

3-39. Resuspend cell pellet in 100 μ l of Flow Buffer and store in dark until ready for flow cytometry analysis.

4.3 Method validation

4.3.1 Validation of FACS sorting

Single cells were isolated from wounds as described. After staining, the cells were FACS sorted. The gates for cell sorting were determined by evaluating events from the control tubes and experimental samples as depicted in Figure 4-6a-f. Also shown are representative dot plots for different controls and an experimental sample. During sorting, two groups of cells were collected directly in TRIzol reagent. For n= 10 samples (8 wounds/ sample), approximately, an average of the following number of cells were obtained:

- 55,400 CD45⁺ F4/80⁺ double positive macrophages
- 85,900 CD45⁺ only positive cells

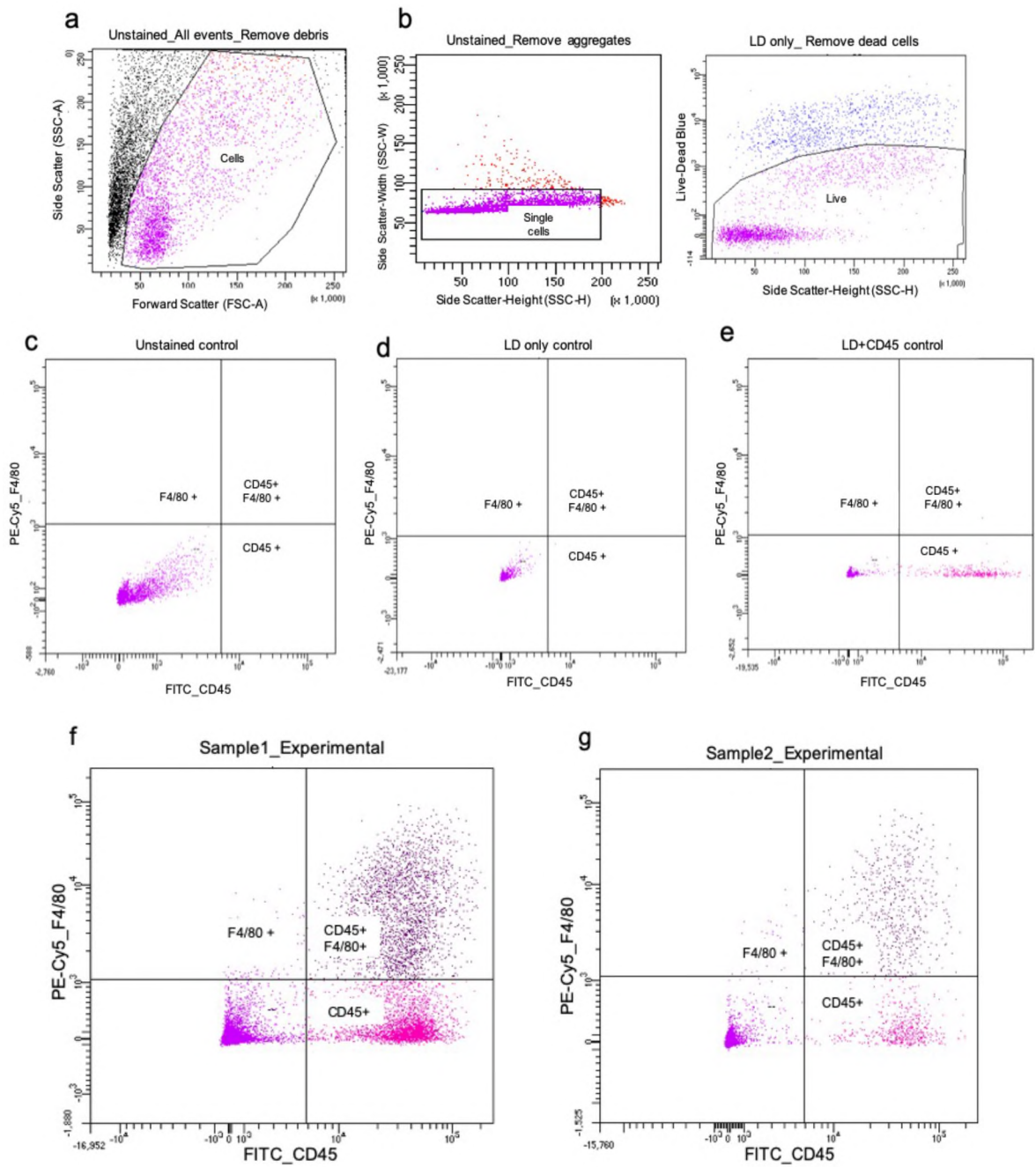


Figure 4-6. Representative dot plots for FACS sorting.

(a) Cell debris were excluded using the forward- and side-scatter gates from unstained control (Tube# 1); (b) Unstained (Tube# 1) and Live/Dead only (Tube# 2) controls were used to filter out dead cells.

Representative dot plots for (c) Unstained control (Tube# 1), (d) Live/Dead only control (Tube# 2), (e) Live/Dead+CD45 control (Tube# 3) and (f) and (g) Experimental samples.

Control tubes #4 and #5 were used to remove any spillover between the fluorescence channels (Image not shown)

When ready for RNA isolation, the homogenized samples stored in ice (or thawed in ice for frozen samples) were incubated at room temperature for 5 min. RNA was isolated as per the standard TRIzol RNA isolation protocol using chloroform. To enhance the amount of RNA obtained, the Phase Lock Gel™ Heavy tubes (VWR, Cat# 10847-802, Radnor, PA, USA) were used for better separation of the aqueous layer from the interphase and organic phase during centrifugation. The RNA pellets obtained after isopropanol separation were washed twice with 75% ethanol and resuspended in RNase free water. Quantification was done using a NanoDrop 2000 spectrophotometer (Thermo Fisher Scientific) and complementary DNA (cDNA) were prepared using 200 ng of RNA each.

To validate the specificity of the sort, we performed quantitative PCR (qPCR) assay for the *Adgre1* (adhesion G protein-coupled receptor E1) gene that encodes for the F4/80 protein. TaqMan primers for *Adgre1* (Thermo Fisher Scientific, Cat# 4331182) along with 18S (Cat# 4333760F) as the endogenous control were used for this purpose. We evaluated 10 samples for the CD45⁺ only positive group, among which half the samples had C_t (cycle threshold) value undetermined indicating that the target gene was too low in these samples to be detectable. The C_t values for the remaining 5 samples were analyzed in comparison to C_t values for the CD45⁺ F4/80⁺ double positive samples (n= 6) to calculate the relative expression of *Adgre1* gene in the two groups. Using delta-delta C_t ($\Delta\Delta C_t$) method, we found that *Adgre1* gene expression was more than 94

-fold higher (p-value $\ll 0.0001$) in the double positive macrophage group, thus indicating a successful sort (Figure 4-7).

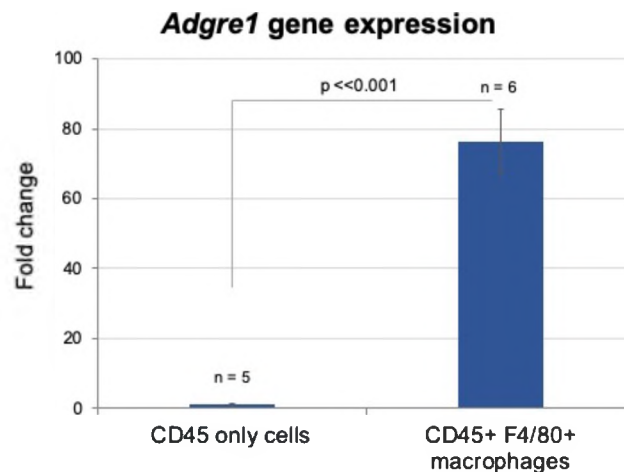


Figure 4-7. Evaluation of Adgre1 expression for the two FACS sorted cell populations. The gene encoding macrophage specific marker protein F4/80 is expressed at least 75 -fold higher in the double positive macrophage cell population than the CD45 only positive control cell population. *Statistical analysis was performed using Student's t-test. n, number of samples.*

4.3.2 Validation of flow cytometric analysis

Single cells were isolated from full thickness skin wounds and stained for cell surface markers followed by intracellular markers after fixation, as described. Flow cytometry assay was done using BD LSR Fortessa cell analyzer and BD FACSDiva software (BD Biosciences) at the Cleveland Clinic LRI Flow Cytometry Core with assistance from the core personnel. Gating hierarchy was determined as per standard flow analysis using the unstained, live-dead blue, and fluorescence minus one (FMO) controls. Analysis was performed using Flow Jo. The gating hierarchy for flow analysis is shown in Figure 4-8a - d. Using gating, dead cells and debris were excluded along with cell clumps. For further analysis,

only cells expressing high intensity of CD45⁺ F4/80⁺ signals, which should be macrophages, were selected as shown by the gate in Figure 4-8d.

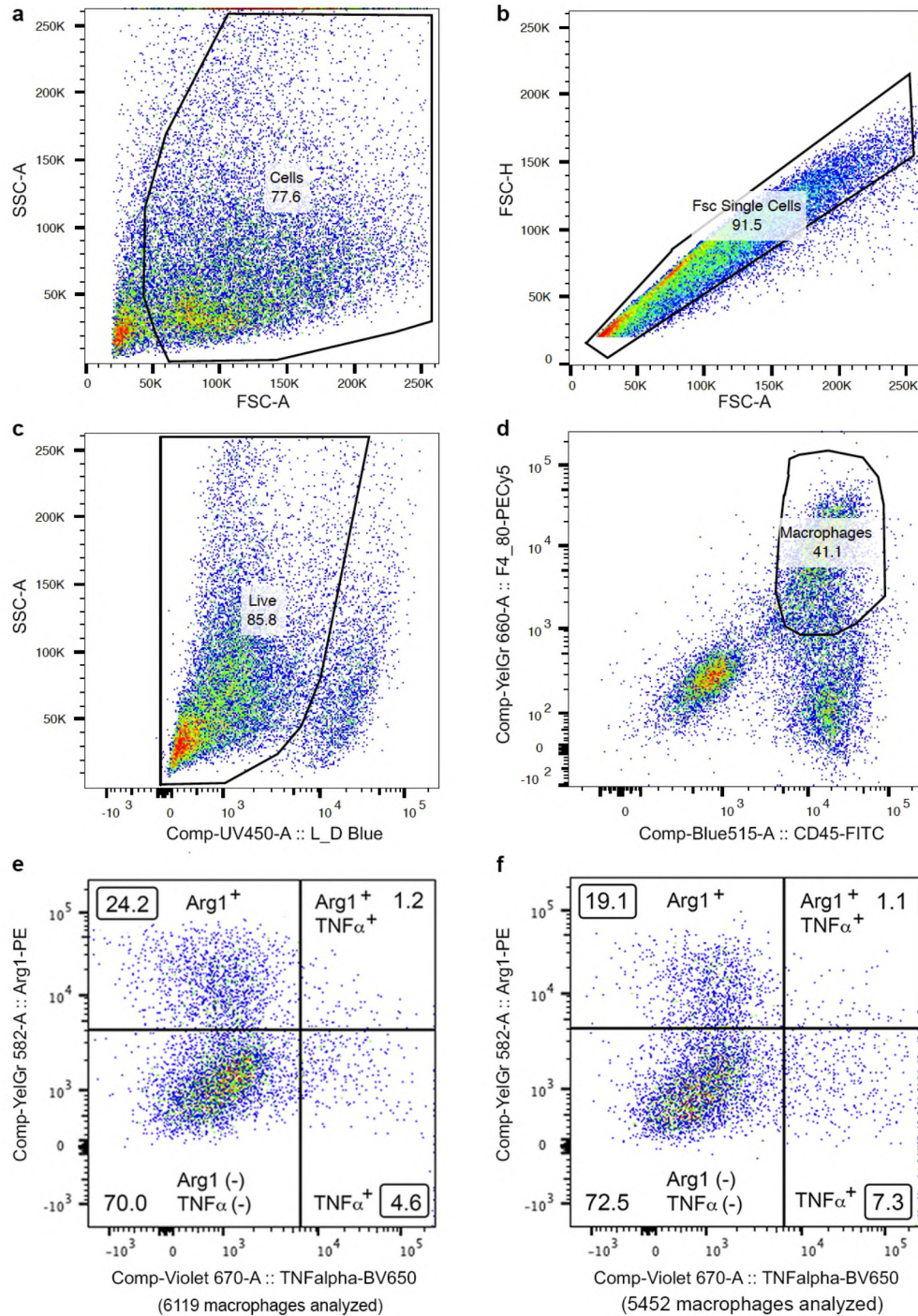


Figure 4-8. Gating strategy for flow cytometric analysis and representative dot plots for experimental samples.

Macrophages analyzed from wounds at 5 days post wounding. **(a)** The smaller cell fragments and debris are dropped from analysis using FSC/SSC **(b)** All non-single cells or cells clumps

are gated out using FSC-A/FSC-H **(c)** The live gate removes the Live/Dead blue positive dead cells and only live cells are considered for further analysis **(d)** Cells double positive for CD45 and F4/80 are gated as macrophages for M1/M2 phenotype characterization **(e and f)** Representative dot plot quadrants from 2 separate experiments with the percentage of cells in each quadrant outlined.

Figure 4-8e and f depict two representative dot plots for the experimental samples after all the gating. Each dot in either of these plots represents a macrophage which was further analyzed for the expression of the chosen M1 marker, $\text{TNF}\alpha$, and the M2 marker, Arg-1. Preliminary analysis of macrophage phenotype in our experiment show that most of the macrophages at the 5-day time point analyzed here are either high positive for Arg-1 (Arg-1^+) or double negative/low positive for both Arg-1 and $\text{TNF}\alpha$ ($\text{Arg-1}^- \text{TNF}\alpha^-$). Only a small fraction of the cells is high positive for $\text{TNF}\alpha$ ($\text{TNF}\alpha^+$), and a negligible portion of the cells are high double positive ($\text{Arg-1}^+ \text{TNF}\alpha^+$). Hence, many of the cells have not undergone polarization at this time point after wounding although a higher percentage of cells are of the M1 phenotype.

4.4 Summary

Here, we have provided a detailed protocol for the isolation of single cells from cutaneous wounds with an emphasis on analysis of macrophages in particular using FACS sorting and flow cytometric analysis. These should prove to be very helpful techniques for the identification and functional assessment of specific cell populations and even of individual cells. This method could be extended to isolate other, different cell populations from wounds (such as neutrophils or lymphocytes), and to assess their characteristics by employing markers specific to the cell type of interest.

4.5 Limitations

Following are some limitations of the methodologies involved in this study.

- For flow cytometric analysis, due to cell number constraint, only one marker each for M1 and M2 macrophage phenotypes could be used. However, as M1/M2 is not an absolute phenomenon and the expression of these markers is more transitional, a combination of 2 or more markers for each phenotype is preferred. Thus, for a more conclusive result to determine any differences in wound macrophage phenotype more markers could be included. This indicates that an additional amount of wound tissue will be required for flow cytometric analysis.
- Here, since whole wounds are used that consists of a substantial amount of extracellular matrix, the protocol required rigorous digestion steps as described. In the process, it is expected to have a lot of debris in the single cell suspension used for antibody staining and further analysis. To avoid this, an additional filtration step could be included to remove the debris as much as possible from the cell suspension.

CHAPTER V

IN-VIVO ASSESSMENT OF LEUKOCYTE ROLLING AND ADHESION UPON
CHEMICAL INJURY IN THE PRESENCE OR ABSENCE OF TUMOR
NECROSIS FACTOR-STIMULATED GENE-6 USING INTRAVITAL
MICROSCOPY

5.1 Introduction

The tumor necrosis factor-stimulated gene-6 (TSG-6), a 30-35 kDa protein encoded by the *TSG-6* gene, is stimulated upon exposure to pro-inflammatory cytokines such as $\text{TNF}\alpha$ and IL-1, or lipopolysaccharide (LPS) (Lee et al. 1990; Mittal et al. 2016; Wisniewski et al. 1996). The TSG-6 protein is predominantly known to play an anti-inflammatory role through its ability to bind to different ligands. TSG-6 is known to bind to matrix molecules such as sulfated and non-sulfated glycosaminoglycans (GAGs), matrix proteins such as heavy chains (HC) from inter-alpha-trypsin inhibitor ($\text{I}\alpha\text{I}$), fibronectin, pentraxin-3, and thrombospondin-1, as well as immune regulating chemokines such as CXCL-8. Binding to most of these molecules has been demonstrated to involve the Link domain of TSG-6, while a few require the CUB domain (Day and Milner 2018).

Neutrophils are known to be the first inflammatory cell type to reach sites of inflammation (Rosales et al. 2017), and multiple studies have shown that TSG-6 is involved in neutrophil recruitment. In an arthritic mouse model, mice lacking TSG-6 (TSG-6 null) displayed an early and increased infiltration of neutrophils resulting in a significantly greater rate of disease progression and severity compared to wildtype (WT) mice (Lesley et al. 2004; Szanto et al. 2004). Conversely, addition of recombinant TSG-6 (rTSG-6) into the inflammatory site has been demonstrated to have a therapeutic effect in many disease conditions by modulation of neutrophil recruitment. In a murine air pouch model of acute inflammation, injection of rTSG-6 along with the inflammatory stimulus lead to a significant reduction in the number of cells infiltrating the air pouch 4 hours after injection (Wisniewski et al. 1996). Similarly, injection of rTSG-6 in a rodent model of gingival wounds resulted in less inflammation and reduced expression of the neutrophil-related inflammatory marker, myeloperoxidase (MPO), followed by early wound healing (Beltran et al. 2015). Moreover, studies in corneal injury models showed a decrease in neutrophil infiltration after treatment with rTSG-6 compared to vehicle-only controls, along with a reduction in corneal damage (Kim et al. 2014b; Oh et al. 2010).

Additionally, studies have shown that TSG-6 is produced by activated mesenchymal stem cells (MSCs) under inflammatory conditions, providing an anti-inflammatory effect. In a peritonitis model, the infusion of MSCs caused a reduction in the number of neutrophils reaching the inflammation site. This was attributed partially to the effect of TSG-6 produced by activated MSCs on the resident

macrophages, resulting in reduced CD44-dependent TLR2 and NF- κ B signaling (Choi et al. 2011).

Although TSG-6 is mostly demonstrated to have an anti-inflammatory effect, a study by Swaidani et al. in a murine model of asthma provides a different viewpoint. In the study, bronchoalveolar lavage fluid obtained from TSG-6 null mice after induction of pulmonary inflammation contained significantly fewer inflammatory cells, including a reduced number of neutrophils, compared to WT littermates (Swaidani et al. 2013). This was accompanied by a decrease in the quantity of the non-sulfated GAG, hyaluronan (HA), in the lavage fluid as well as the lung tissue, indicating a role of pathological HA in creating the higher level of inflammation in WT mice. This effect was also attributed to the absence of HC-HA complexes (the product of HC and HA crosslinking mediated by the enzymatic action of TSG-6), in TSG-6 null mice.

While all the above studies show that TSG-6 plays a role in inflammation and recruitment of neutrophils into sites of injury or inflammation, there is still no direct evidence to indicate that loss of TSG-6 affects the rolling and adhesion behavior of neutrophils nor their rate of extravasation from blood vessels. Therefore, in this chapter we attempted to address this question by employing intravital microscopy for direct visualization of leukocyte rolling, adhesion, and transmigration in-vivo, using a murine ear model of acute skin inflammation. The model involved application of croton oil, a chemical irritant. Our main purpose was to determine whether the absence of TSG-6 affects any of the component steps in

the extravasation of neutrophils (rolling, adhesion/arrest, and transmigration) as the neutrophils transition from the circulation into the chemically injured tissue.

5.2 Materials and Methods

5.2.1 Animals

C57BL/6J wild-type (WT) mice were obtained from JAX Laboratories (Bar Harbor, ME). TSG-6 null mice, whose generation was described by Fülöp et al. (Fulop 2003), in C57BL/6 background was generously provided by Dr. Mark Aronica in our institute. All mice were maintained per guidelines of the American Association for the Accreditation of Laboratory Animal Care. All procedures were approved by the Cleveland Clinic Institutional Animal Care and Use Committee.

5.2.2 Croton oil-induced ear inflammation

Mice (WT, or TSG-6 KO, age-matched male and female) were anesthetized with isoflurane and chemical inflammation was induced as described by Coruzzi et al. (Coruzzi et al. 2012) with some modification. Croton oil (Sigma-Aldrich, St. Louis, MO) (2% in acetone) was topically applied on the inner surface of the left ear (50 μ l per ear) with a micropipette and cotton swab. An equal amount of acetone was applied on the right ear as vehicle control. After the applications, the mice were allowed to recover from the anesthesia and housed under optimum conditions before proceeding to the next step. Croton oil application was staggered by 1.5 hours between any two mice, to allow enough time to perform intravital microscopy of both ears of each mouse.

5.2.3 Validation of croton oil-induced inflammation

To validate the induction of inflammation, 4 hours after croton oil application, a set of mice were euthanized by ketamine-xylazine anesthesia, followed by cervical dislocation, and both the left and right ears were cut at the base and fixed in Histochoice (Amresco, Solon, OH), followed by paraffin embedding. Using a microtome, 5-micron thick sections were cut and stained for the neutrophil granulocyte marker, myeloperoxidase (MPO). The sections were rehydrated and incubated overnight at 4 °C with rabbit polyclonal anti-MPO antibody (Thermo Fisher Scientific, Waltham, MA) at 1:100 dilution. Sections were then incubated with Donkey anti-rabbit Rhodamine Red-X-conjugated secondary antibody (Jackson ImmunoResearch, West Grove, PA) at 1:500 dilution, for 1.5 hour, and mounted in VECTASHIELD mounting medium (Vector Laboratories, Burlingame, CA). Images were captured using a Leica DM upright microscope (Leica Biosystems).

5.2.4 Intravital microscopy

In-vivo labeling of leukocytes by intravenous injection of dyes

For visualization of leukocytes, the dye *Rhodamine 6G* (Sigma-Aldrich) was used at 0.5 mg/kg body weight as described previously (Ichioka et al. 2007). Rhodamine 6G is a membrane-permeable DNA fluorescent dye that stains nucleated cells (Gál et al. 2005). Contrast enhancement of the intravascular space was achieved by using Qtracker® 655 Vascular Label (Thermo Fisher Scientific, Waltham, MA), which binds intravascular serum proteins such as albumin. At 4 hours after croton oil application, the mice were anesthetized with an

intraperitoneal injection of Ketamine-Xylazine. A single injection containing Rhodamine 6G (0.5 mg/kg body weight) and Qtracker® 655 (20 μ l) in normal saline, in a maximum total volume of 120 μ l, was administered retro-orbitally (RO). Intravital microscopy was started within 5 minutes of the RO injection.

Positioning of mice for microscopy

After the retro-orbital injection, the anesthetized mouse was placed on a heated stage for microscopy as shown in Figure 5-1. The ear was positioned to lie flat against a glass cover slip on the stage, and secured with tape.



Figure 5-1. Positioning of the mice for microscopy.

Mouse, lying on its side, was placed on a heated stage of the inverted microscope. The ear was taped flat to a glass cover slip that sits above the objective lens. (The objective, located beneath the stage, cannot be seen here).

Microscopy and video recording

A Leica DMI8 inverted microscope connected to a Leica TCS SP8 confocal system (Leica Microsystems, Wetzlar, Germany) was used to record videos of leukocyte behavior in vivo. A combination of lasers at 514 nm and 488 nm was used for excitation of Rhodamine 6G and Qtracker 655, respectively. Wavelength ranges of 526-600 nm for Rhodamine 6G, and 620-752 nm for Qtracker 655, were

used for collection of the emitted light. Video recordings of 30 second duration, from each of 2-4 vessels per mouse, were made using a 40X oil immersion lens. Leica Application Suite X (LASX) (Leica Microsystems), running on the computer connected to the confocal system, was used to control this process.

5.2.5 Analysis of leukocyte behavior

The recorded videos were analyzed offline using LASX. Leukocyte behaviors of rolling or adhesion were defined as described in previous studies (Ichioka et al. 2007; Jbeily et al. 2014). Briefly, a *rolling* leukocyte was defined as a cell moving along the endothelial wall at a velocity much less than that of the surrounding blood flow, and which interacted with the endothelial lining for only a few seconds during the 30 second recording. An *adherent* leukocyte (or *arrested* leukocyte) was defined as a cell that remained stuck to the vessel wall for the entire duration of the 30 second video.

The number of rolling and adherent leukocytes was determined by observing cell behavior within 100- μm vessel segments, in small-caliber vessels of a diameter between 10 to 50 μm . Calculations of rolling and adhesion were done as discussed by Gál et al. (Gál et al. 2005). Briefly, *rolling cells* were quantified by counting the number of rolling cells in the 100 μm vessel length during 30 s, and expressing this as the number of rolling cells per minute per $10^3 \mu\text{m}$ of vessel perimeter. *Adherent* cells were quantified by counting the number of adhered cells in the 100 μm vessel length, and expressing this as the number of adherent cells per $10^5 \mu\text{m}^2$ of vessel area.

5.2.6 Statistical analysis

Numerical data were expressed as Mean \pm SEM. All statistical analyses were performed using SigmaPlot 12 (Systat Software Inc., San Jose, CA). Normality of the data was tested using the Shapiro-Wilk Normality test after which statistical analyses were performed using the Kruskal-Wallis ANOVA on ranks. P-value \leq 0.05 was considered statistically significant. (See Appendix for full analysis.)

5.3 Results

5.3.1 Croton oil induces inflammation at 4 hours after application

Multiple studies have previously used croton oil application as a model of acute inflammation. However, to validate croton oil-induced ear inflammation as a successful model of acute inflammation in our hands, paraffin-embedded ear sections of ears that had been exposed for 4 h exposure to croton oil or to inert vehicle were stained with an anti-MPO antibody. In absence of croton oil, no neutrophils were seen in the ear tissue (Figure 5-2a), while in response to the application of croton oil, numerous MPO positive neutrophils that had extravasated out of blood vessels and into the tissue were observed (Figure 5-2b). This verifies that croton oil is a good inducer of neutrophil inflammation, thus making it a nice model to study leukocyte behavior in acute inflammation.

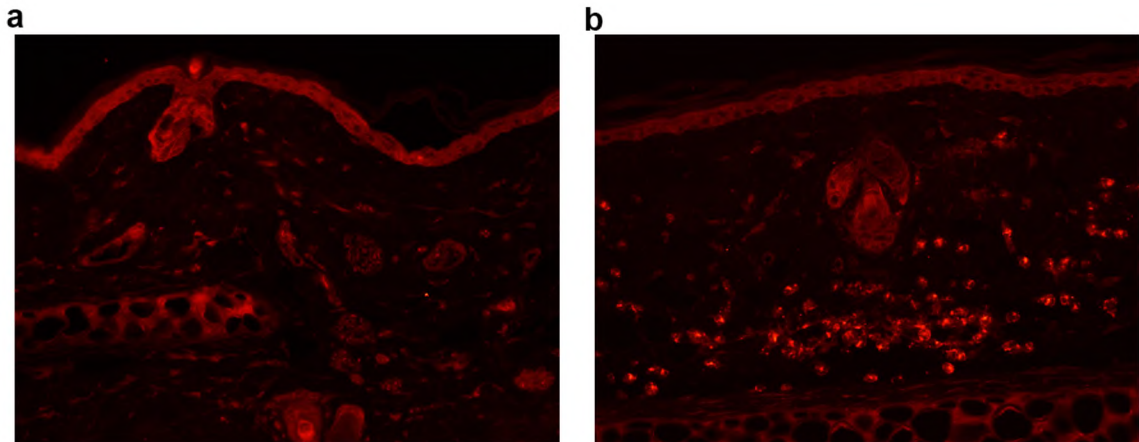


Figure 5-2. Croton oil induces neutrophil recruitment after 4 hours of application. (a) Acetone only treated control ear had no MPO positive cell, while (b) Croton oil application substantially increases the number of extravasated cells into the ear tissue.

5.3.2 The number of rolling cells induced by chemical injury is lower in TSG-6 null ears compared to WT ears.

The number of rolling leukocytes (cells that move slowly along the endothelial lining for a few seconds, before “popping off”) was determined in WT control mice, and in TSG-6 null mice to observe the effect that an absence of TSG-6 might have upon the rolling behavior of leukocytes. By calculating the rolling cell numbers per minute normalized by the vessel perimeter, it was observed that application of croton oil significantly increased the overall rolling behavior in WT vessels at 4 hours post injury. However, rolling cells in the TSG-6 null vessels were much less increased by croton oil application. Additionally, a comparison of leukocyte rolling behavior in WT mice vs TSG-6 null, although not statistically significant in this pilot experiment, suggested a relative decrease in injury-induced rolling in TSG-6 null ears relative to WT ears (Figure 5-3, 5-5a -d). Table 5-1 gives a detailed information on the number of rolling cells counted.

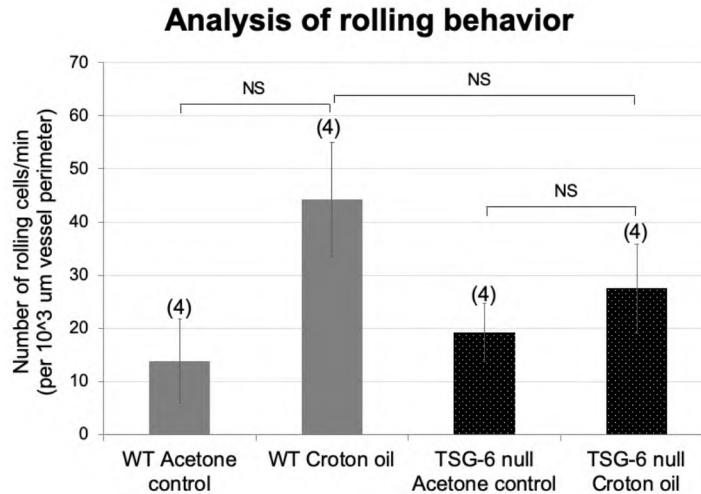


Figure 5-3. Rolling behavior of leukocytes.

Our analysis suggests that the rolling of leukocytes per minute at 4 hours after application of croton oil is lower in TSG-6 null mice compared to WT. *Statistical analysis was performed using either the Kruskal-Wallis ANOVA on ranks. (n), number of mice analyzed; NS, Not significant.*

5.3.3 The number of adherent cells induced by chemical injury appears to be higher in TSG-6 null ears than in WT ears.

Adherent leukocytes (cells that had stopped rolling and become tightly adherent to the blood vessel wall), were analyzed as described in section 5.2.5, in both WT mice and in TSG-6 null mice in order to observe any potential differences in adhesion behavior due to the loss of TSG-6. Calculations of the number of adherent leukocytes per unit vessel area present at 4 h after application showed that application of croton oil significantly increases the number of adherent leukocytes relative to vehicle control, in both WT and TSG-6 null mice. Leukocyte adhesion is increased more in the TSG-6 null croton oil group, relative to WT group (Figure 5-4, Table 5-1). While not statistically significant given the small sample size, this latter difference suggests a very interesting trend.

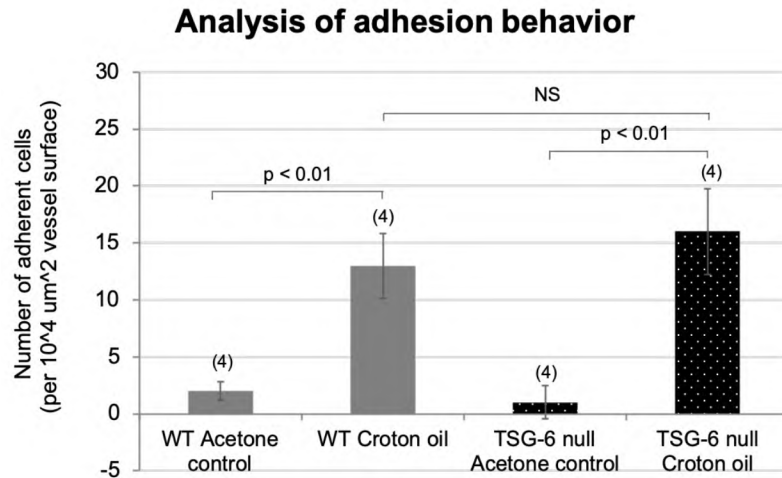


Figure 5-4. Adhesion behavior of leukocytes.

Croton oil significantly increases the number of adherent neutrophils in both WT and TSG-6 null groups. The number of these adherent neutrophils in croton oil-treated ears is higher in TSG-6 null ears than that in WT ears, although the difference is not significant. *Statistical analysis was performed using either the Kruskal-Wallis ANOVA on ranks. (n), number of mice analyzed; NS= Not significant*

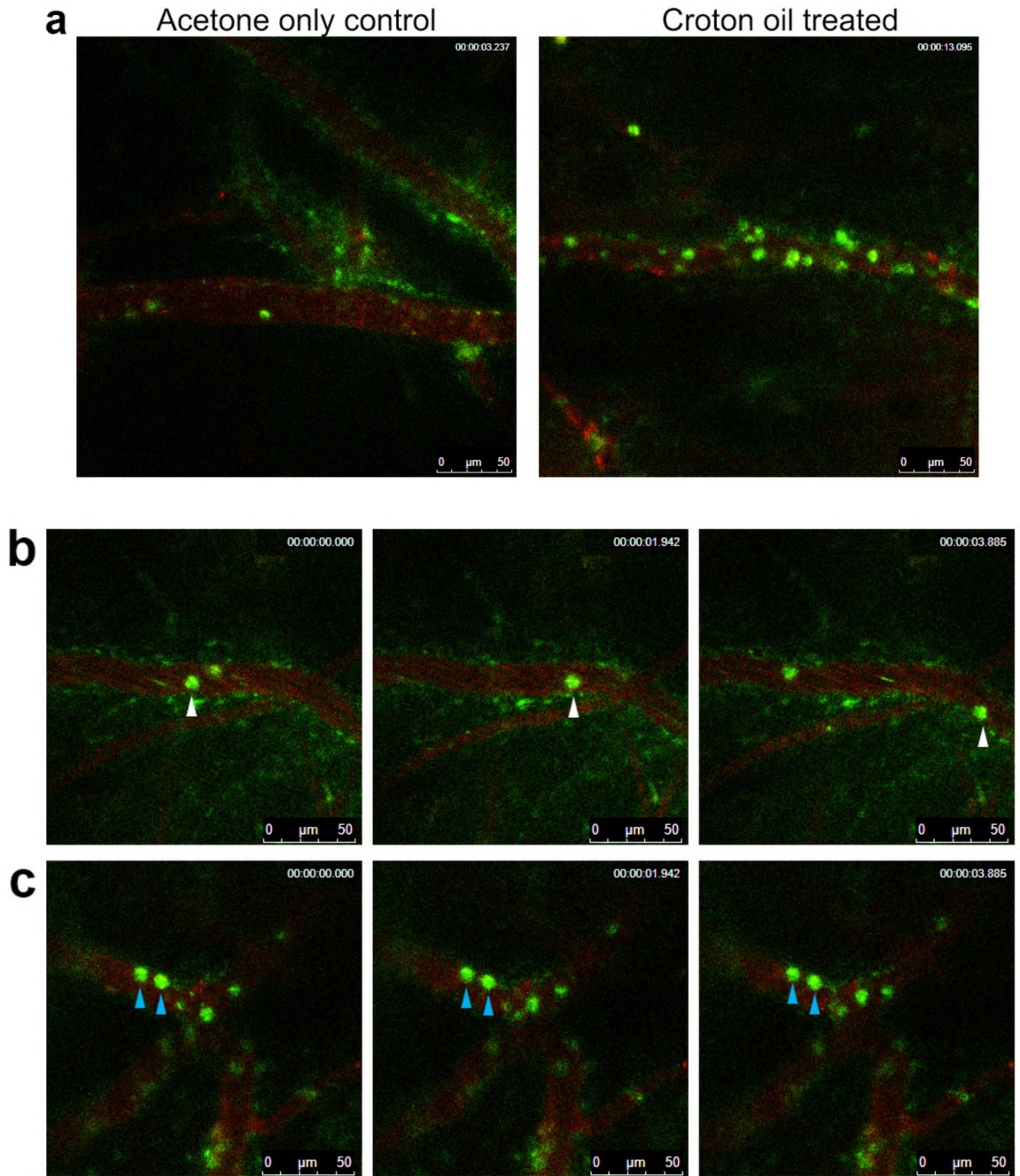


Figure 5-5. Representative images for intravital microscopy of croton oil or acetone treated ear vessels.

(a) Application of croton oil results in an increase in the population of both rolling and adherent cells. (b) and (c) Series of images to represent rolling (white arrowhead) vs adherent cells (blue arrowheads). In green= rhodamine labeled leukocytes; red= vessels labeled with Qtracker dye; time-stamp, upper right corner; scalebar (50 μm), lower right corner.

Table 5-1. Table detailing the different measurements and calculations for each group

Group	Animal #	Vessel Diameter (um)	# of leukocytes observed in 30 s		Vessel Perimeter (um)	Vessel surface (um^2)	# of rolling cells/min (per 10^3 um vessel perimeter)	# of adherent cells (per 10^4 um^2 vessel surface)
			Rolling	Adherent				
WT Acetone Control	WT (1)	15.50	5	1	231.0	1550.0	43	6
		20.00	0	0	240.0	2000.0	0	0
		21.50	0	0	243.0	2150.0	0	0
	WT (2)	23.33	0	0	246.7	2333.3	0	0
		22.67	0	0	245.3	2266.7	0	0
	WT (3)	27.00	0	1	254.0	2700.0	0	4
		23.33	3	0	246.7	2333.3	24	0
		16.33	0	0	232.7	1633.3	0	0
		18.00	0	1	236.0	1800.0	0	6
	WT (4)	27.00	9	1	254.0	2700.0	71	4
				Average # cells	14	2		
				SEM		7.87	0.83	
WT Croton Oil	WT (1)	22.00	11	2	244	2200	90	9
		18.50	7	5	237	1850	59	27
		19.50	9	4	239	1950	75	21
	WT (2)	17.00	8	0	234	1700	68	0
		16.00	9	2	232	1600	78	13
	WT (3)	53.00	6	3	306	5300	39	6
		18.33	1	0	236.67	1833.33	8	0
		16.33	2	3	232.67	1633.33	17	18
		41.00	0	7	282	4100	0	17
	WT (4)	39.00	1	7	278	3900	7	18
				Average # cells	44	13		
				SEM		10.73	2.85	
TSG-6 null Acetone Control	TSG-6 null (1)	26.00	6	0	252	2600	48	0
		33.00	4	0	266	3300	30	0
		11.50	0	0	223	1150	0	0
	TSG-6 null (2)	21.00	0	0	242	2100	0	0
		28.00	0	0	256	2800	0	0
	TSG-6 null (3)	18.67	3	3	237.33	1866.67	25	16
		25.33	5	0	250.67	2533.33	40	0
		20.67	1	0	241.33	2066.67	8	0
		17.67	3	0	235.33	1766.67	25	0
	TSG-6 null (4)	14.00	4	0	228	1400	35	0
25.67		0	0	251.33	2566.67	0	0	
				Average # cells	19	1		
				SEM		5.46	1.46	
TSG-6 null Croton oil	TSG-6 null (1)	15	0	6	230	1500	0	40
		28.33	3	5	256.67	2833.33	23	18
		16.00	1	4	232	1600	9	25
	TSG-6 null (2)	44.33	0	0	288.67	4433.33	0	0
		13.00	2	1	226	1300	18	8
	TSG-6 null (3)	12	8	1	224	1200	71	8
		11.50	2	1	223	1150	18	9
		13.67	9	4	227.33	1366.67	79	29
		14.33	1	3	228.67	1433.33	9	21
	TSG-6 null (4)	40.33	7	0	280.67	4033.33	50	0
17.00		3	3	234	1700	26	18	
				Average # cells	28	16		
				SEM		8.27	3.76	

Vessel length= 100 μm; Vessel perimeter = 2 * (Vessel length + Vessel diameter);
 Vessel surface= Vessel length * Vessel diameter;
 SEM= S.D./√(number of vessel sections quantified)

5.4 Discussion

This is a preliminary study to determine the effects of loss of TSG-6, a protein generally known to be anti-inflammatory and a modifier of hyaluronan, in the rolling and adhesion behavior of leukocytes during inflammation. Using a model of acute cutaneous inflammation in which a chemical irritant is applied to the ears of mice and the dynamic behavior of leukocytes (mainly neutrophils in this model) are observed by intravital confocal microscopy. In a complete experimental set of 8 mice (4 WT and 4 TSG-6 null mice, each with one ear serving as a bilateral vehicle-only control), we observed that the number of rolling leukocytes at 4 hours after application was relatively less in TSG-6 null mice than in WT mice. Conversely, the number of adherent leukocytes was relatively higher in TSG-6 null mice than in WT mice. These numbers, although not statistically significant given the pilot nature of the experiment, are suggestive of possible differences in leukocyte behavior between the two genotypes and fit with predictions that can be inferred from the literature (as discussed below).

Previous literature as well as our own findings provide evidence that TSG-6 plays an important role in regulating inflammation, by influencing neutrophil recruitment (Day and Milner 2018). However, the previous lack of any direct evidence evaluating the effect of TSG-6 upon the individual steps in leukocyte extravasation motivated us to conduct this study. TSG-6, as discussed in the chapter Introduction, has mostly been shown to inhibit neutrophil recruitment into inflamed sites. At the same time, we note that a few studies contradict the notion that TSG-6 is always anti-inflammatory (Lauer et al. 2013; Swaidani et al. 2013),

an suggest instead that the effects could be tissue-specific and/or dependent upon the time point of inflammation observed.

A study by Cao et al. showed that addition of TSG-6 Link module (Link_TSG-6) in an IL-1 β induced peritonitis model causes all three phases of extravasation (rolling, adhesion and transmigration) to slow down within 2 hours of IL-1 β application. Fewer cells were rolling or adhering in the mesenteric microcirculation, and fewer cells were recruited into the tissue (Cao et al. 2004). As the Link_TSG-6 domain consists of the HA binding portion of TSG-6, one can expect that the observed decrease in neutrophil migration could be accompanied by modification of HA in the vessel lumen, although this remains to be determined. Another study investigating the effect of rTSG-6 in an inflammatory air pouch model showed significant reduction in the number of recruited cells; the authors postulated that this was due to the ability of TSG-6 to modulate the interaction between HA and the cell-surface CD44 receptor, thus modulating CD44-dependent rolling of leukocytes and ultimately the extravasation of leukocytes (Wisniewski et al. 1996). Yet another study showed that Link_TSG-6 is sufficient to inhibit neutrophil migration, independent of its HA or α 1 dependent functionality (Getting et al. 2002). In line with these reports, we observed that in the absence of TSG-6 in our null mice, the number of adherent leukocytes at 4 h after croton oil application was higher. This suggests a possibly quicker rolling and stronger adhesion of leukocytes onto the endothelium in the absence of the inhibitory TSG-6 molecule, resulting in fewer rolling leukocytes by 4 h of inflammation, while the number of adherent leukocytes is increased.

Moreover, TSG-6 has been described to perform anti-inflammatory role by interrupting the interaction of the glycosaminoglycan (GAG) molecules with various chemokines. (Chemokines are small protein mediators that are chemotactic for leukocytes, affecting their activation and migratory behavior). TSG-6 has been shown to be able to bind to many chemokines as well as to sulfated GAGs such as chondroitin sulfate, thus competing with the binding of pro-inflammatory chemokines to GAGs, and to binding of specific chemokines to neutrophils (Dyer et al. 2016; Dyer et al. 2014). This could also possibly explain the presence of more adherent neutrophils on the luminal (endothelial) surface in the absence of TSG-6 in null mice, if in fact they are regulated by cytokines on the GAG-rich luminal glycocalyx. Since adhesion is the step immediately before transmigration of leukocytes out of the vessel and into the injury site, a stronger adhesion could promote more transmigration.

On the other hand, HA is an important part of the glycocalyx of the luminal side of endothelium (Reitsma et al. 2007). In the study by Swaidani et al., upon induction of pulmonary inflammation, the bronchoalveolar lavage fluid from TSG-6 null mice contained fewer neutrophils, relative to WT (Swaidani et al. 2013). As HC-HA complexes are reportedly more leukocyte-adhesive as well as more stable than HA alone (Day and de la Motte 2005; Lauer et al. 2015b), absence of HC-HA could lead to a reduction in inflammatory cell invasion into the inflamed lung tissue in TSG-6 null mice in this study. This could also explain our finding of reduced neutrophil rolling in TSG-6 null mice, if HA in the glycocalyx cannot be decorated with HC's (due to the absence of TSG-6 enzyme) and therefore become less

sticky. HA has been shown to play roles in leukocyte binding and adhesion to endothelial surfaces during different inflammatory conditions, such as in diabetes (Shakya et al. 2015), suggesting that reduced rolling could in fact be due to loss of HC-HA in the vessel lumen.

In summary, in this Chapter we have presented preliminary findings suggesting that the absence of TSG-6 affects leukocyte rolling and adhesion. This question is one that we believe has not been addressed anywhere in the literature to date. Considering the large number of inflammatory and disease condition in which TSG-6 has been implicated, we regard these findings as very interesting, and highly supportive of the need for future experiments. For a more conclusive result, more animals, ears, and vessels will need to be analyzed, and that is indeed the future plan for our laboratory.

5.5 Limitations

Following are some limitations of the methodologies involved in this study.

- The aim of the study was to investigate the difference in neutrophil recruitment in WT vs TSG-6 null mice. Rhodamine-6G, however, labels all leukocytes in the blood flow without discrimination. So, the labeled cells we observed could also be other category of leukocytes and not just neutrophils. An alternative could be deriving a neutrophil specific GFP labeled TSG-6 null mouse line that could then be compared with neutrophil specific GFP labeled WT mice.
- Croton oil ear application is an acute ear inflammation model suitable to study the early neutrophil recruitment phenotype observed in our TSG-6 null wounds. But this is inadequate to study the late neutrophil recruitment phenotype

observed in our earlier study. A possible solution to this could be a full-thickness ear wound model using ear punches to create puncture wounds. The ear skin around the wounds could then be observed under confocal microscope at various time points post wounding.

CHAPTER VI

CONCLUSIONS AND RECOMMENDATIONS

6.1 Introduction

As discussed in the earlier chapters, understanding the wound microenvironment is a crucial step towards devising any new treatment methodology. Earlier studies have investigated tumor necrosis factor-stimulated gene-6 (TSG-6) in many disease conditions and found that in most situations, it offers an anti-inflammatory effect. TSG-6 is also known to modify the ubiquitous extracellular matrix molecule, hyaluronan (HA), by forming complexes between HA and heavy chains (HC) from the serum; HA and HC-HA have also been shown to regulate inflammation. In our current work, we found that TSG-6 expression is increased post-wounding, suggesting that there is much more to understand regarding how TSG-6 affects the cutaneous wound environment and its probable therapeutic potential. In this study we sought to explore how loss of endogenous TSG-6 changes the cutaneous wound environment, including wound closure rates and the program of inflammation within wounds, by using a mouse model with a genetic deletion of TSG-6 (TSG-6 null). Experiments in Chapter 3 established that loss of TSG-6 leads to significant delays in wound closure, and increases the

expression of pro-inflammatory cytokines in the wounds. Chapters 4 and 5 pioneered methods that will be needed to further investigate the mechanisms of the abnormal inflammation observed in Chapter 4. Thus, to examine how macrophage polarization is regulated in TSG-6 null wounds versus wildtype (WT) wounds, we tested and compile a detailed protocol to isolate single cells (leukocytes) from wound tissue and perform macrophage population analysis by flow cytometry. We also developed a method to determine whether loss of TSG-6 affects leukocyte migration behavior in small cutaneous vessels, using intravital confocal microscopy. The primary research questions pursued in this thesis were:

1. Does loss of TSG-6 affect cutaneous wound closure and inflammation?
2. Can we isolate viable macrophages from skin wounds to investigate differences in macrophage polarization in TSG-6 null versus WT wounds?
3. Does loss of TSG-6 affect leukocyte rolling and adhesion behavior?

6.2 Findings

The main findings from each chapter are detailed within the text of each respective chapter. Table 6-1 provides a summary of the outcomes of this work.

Table 6-1. Summary of the specific aims and the results from the hypotheses explored in the thesis

Aim	Outcomes
<p>Aim 1: Determine how loss of TSG-6 affects wound closure and recruitment of inflammatory cells</p>	<ul style="list-style-type: none"> - TSG-6 protein and HC-HA complexes are present in unwounded murine skin, and increase post wounding. - There are no redundant enzymes that transfer HC to HA in the skin - The absence of TSG-6 results in delayed wound closure. - The absence of TSG-6 results in differential regulation of neutrophil infiltration into wound bed. While delayed neutrophil recruitment was observed in early wounds, exacerbated inflammation was observed in later wounds - TSG-6 null mice develop an abnormal pro-inflammatory wound environment. - Absence of TSG-6 does not affect macrophage recruitment but affects the polarization of macrophages. Wound macrophages are polarized towards the pro-inflammatory M1 phenotype TSG-6 null mice. - Reintroduction of recombinant TSG-6 into TSG-6 null wounds rescues the delayed wound closure and differential neutrophil recruitment.
<p>Aim 2: Develop a viable protocol to isolate single cells from cutaneous wounds for flow sorting and flow cytometric assessment of leukocytes in WT and TSG-6 null wounds, with a particular emphasis on macrophages</p>	<ul style="list-style-type: none"> - Validated the isolation of viable single cells from cutaneous wounds. - After antibody staining of the isolated viable single cells, the macrophage-specific population was successfully sorted for RNA analysis. - Isolated viable single cells were successfully stained for M1/M2 phenotype specific markers and flow cytometric analysis was performed.

<p>Aim 3: Determine how the absence of TSG-6 affects rolling and adhesion behavior of leukocytes <i>in vivo</i> after chemical injury using intravital microscopy</p>	<ul style="list-style-type: none"> - Croton oil application was shown to be an efficient model of inflammation, by inducing the recruitment of leukocytes at sites of chemical injury. - Preliminary findings showed that the number of rolling cells (leukocytes) induced by chemical injury is lower in TSG-6 null ears than in WT ears. - The number of adherent cells induced by chemical injury appears to be higher in TSG-6 null ears than in WT ears.
---	--

6.3 Recommendation for future research

There were a number of limitations of this study, and some research ideas beyond the scope of this study. What follows are recommendations for some future experiments to extend and apply the results of this thesis work.

1. It is known that HA is present in the endothelial glycocalyx of small blood vessels and plays a role in regulating adhesion of leukocytes to the endothelium in different inflammatory conditions such as atherosclerosis and diabetes. TSG-6 modifies HA forming HC-HA which is also upregulated in skin wounds along with TSG-6 and there is no compensatory molecule for this enzymatic action in TSG-6 null wounds. Therefore, it will be interesting to investigate whether the HA in the glycocalyx is complexed to HC under normal wounding conditions, and whether HC-HA regulates leukocyte rolling and/or adhesion during inflammation.
2. Angiogenesis is an important factor in normal wound healing. This aspect has not been directly investigated in this study, but is highly recommended as a topic of future investigation.

3. An important aspect of wound healing, beyond the scope of this study, is fibroblast proliferation and fibrosis. The extent of fibrosis (scarring) is well known to be dependent upon inflammation in the wound. Therefore, It will be informative to evaluate the later stages of wound healing in the TSG-6 null mice to see whether there are any differences in the tissue formation phase or the tissue reparative phase.
4. Immunohistological staining of the Day 7 wound sections suggested differences (increases) in the M1/M2 ratio in TSG-6 null vs WT wounds (Chapter 3). In our study we only explored Day 7 wounds for this purpose. However, M1/M2 is not a discrete phenomenon but rather a continuous one. Thus, in the future, it will be important to determine how macrophage polarization progresses at different time point post-wounding. Adding more markers, in addition to CD38 (M1) and Arginase-1 (M2), will be helpful in this regard.
5. Flow cytometric analysis is known to be a reliable technique to characterize single cells within cell populations. Chapter 4 of this thesis developed a detailed protocol to isolate viable, single leukocytes from wounds. Future studies, using these flow cytometric procedures, could be very helpful in determining the expression levels of M1/M2 specific marker proteins at different time points after wounding, thereby revealing possible changes in macrophage polarization related to the absence of TSG-6.

In this thesis, we performed a preliminary investigation of the rolling and adhesion steps during leukocyte extravasation in TSG-6 null and WT mice. A

recommended next step is to observe the transmigration step, which following adhesion, directly. Although differences in rolling and/or adhesion behaviors may be indicative of differential recruitment of leukocytes, having additional information about transmigration through the endothelium would be helpful in explaining neutrophil recruitment phenotypes observed in the wounding experiments.

6.4 Conclusion

This thesis work highlighted the role of TSG-6 in the regulation of wound healing, with a special focus on inflammation. One of the strongest aspects of the study is the confirmation of a rescue effect observed after addition of recombinant TSG-6; this experiment verified that the phenotypes we observe in TSG-6 null wounds are specifically due to loss of TSG-6. Another important contribution of this study is the creation of a detailed methodology to isolate single, viable leukocytes from the wound bed and to process them for staining and/or RNA analysis. We believe that the details of this procedure, which have rarely been previously attempted, will be helpful in future investigations.

BIBLIOGRAPHY

- Ather S, Harding KG, Tate SJ. Wound management and dressings. Adv. Text. Wound Care. Elsevier; 2019 [cited 2019 Aug 18]. p. 1–22 Available from: <https://linkinghub.elsevier.com/retrieve/pii/B9780081021927000011>
- Aya KL, Stern R. Hyaluronan in wound healing: Rediscovering a major player: Hyaluronan in wound healing. *Wound Repair Regen.* 2014;22(5):579–93
- Back SA, Tuohy TM, Chen H, Wallingford N, Craig A, Struve J, et al. Hyaluronan accumulates in demyelinated lesions and inhibits oligodendrocyte progenitor maturation. *Nat. Med.* 2005;11(9):966–72
- Bannon P, Wood S, Restivo T, Campbell L, Hardman MJ, Mace KA. Diabetes induces stable intrinsic changes to myeloid cells that contribute to chronic inflammation during wound healing in mice. *Dis. Model. Mech.* 2013;6(6):1434–47
- Baranova NS, Nileback E, Haller FM, Briggs DC, Svedhem S, Day AJ, et al. The inflammation-associated protein TSG-6 cross-links hyaluronan via hyaluronan-induced TSG-6 oligomers. *J. Biol. Chem.* 2011;286(29):25675–86
- Bardos T, Kamath RV, Mikecz K, Glant TT. Anti-inflammatory and chondroprotective effect of TSG-6 (tumor necrosis factor-alpha-stimulated gene-6) in murine models of experimental arthritis. *Am. J. Pathol.* 2001;159(5):1711–21

Barrientos S, Stojadinovic O, Golinko MS, Brem H, Tomic-Canic M.

PERSPECTIVE ARTICLE: Growth factors and cytokines in wound healing: Growth factors and cytokines in wound healing. *Wound Repair Regen.* 2008;16(5):585–601

Beltran SR, Svoboda KK, Kerns DG, Sheth A, Prockop DJ. Anti-inflammatory protein tumor necrosis factor-alpha-stimulated protein 6 (TSG-6) promotes early gingival wound healing: an in vivo study. *J. Periodontol.* 2015;86(1):62–71

Brancato SK, Albina JE. Wound Macrophages as Key Regulators of Repair. *Am. J. Pathol.* 2011;178(1):19–25

Broughton G, Janis JE, Attinger CE. The Basic Science of Wound Healing: *Plast. Reconstr. Surg.* 2006;117(SUPPLEMENT):12S-34S

Camenisch TD, Spicer AP, Brehm-Gibson T, Biesterfeldt J, Augustine ML, Calabro A Jr, et al. Disruption of hyaluronan synthase-2 abrogates normal cardiac morphogenesis and hyaluronan-mediated transformation of epithelium to mesenchyme. *J. Clin. Invest.* 2000;106(3):349–60

Cao TV, La* M, Getting* SJ, Day AJ, Perretti* M. Inhibitory Effects of TSG-6 Link Module on Leukocyte–Endothelial Cell Interactions *In Vitro* and *In Vivo*. *Microcirculation.* 2004;11(7):615–24

Chhabra S, Chhabra N, Kaur A, Gupta N. Wound Healing Concepts in Clinical Practice of OMFS. *J. Maxillofac. Oral Surg.* 2017;16(4):403–23

- Choi H, Lee RH, Bazhanov N, Oh JY, Prockop DJ. Anti-inflammatory protein TSG-6 secreted by activated MSCs attenuates zymosan-induced mouse peritonitis by decreasing TLR2/NF- κ B signaling in resident macrophages. *Blood*. 2011;118(2):330–8
- Clark RA. Fibrin and wound healing. *Ann. N. Y. Acad. Sci.* 2001;936(Journal Article):355–67
- Colon E, Shytuhina A, Cowman MK, Band PA, Sanggaard KW, Enghild JJ, et al. Transfer of inter-alpha-inhibitor heavy chains to hyaluronan by surface-linked hyaluronan-TSG-6 complexes. *J. Biol. Chem.* 2009;284(4):2320–31
- Coruzzi G, Pozzoli C, Adami M, Grandi D, Guido N, Smits R, et al. Strain-dependent effects of the histamine H4 receptor antagonist JNJ7777120 in a murine model of acute skin inflammation: Histamine H4 receptors and mouse ear inflammation. *Exp. Dermatol.* 2012;21(1):32–7
- Coulson-Thomas VJ, Lauer ME, Soleman S, Zhao C, Hascall VC, Day AJ, et al. Tumor Necrosis Factor-stimulated Gene-6 (TSG-6) Is Constitutively Expressed in Adult Central Nervous System (CNS) and Associated with Astrocyte-mediated Glial Scar Formation following Spinal Cord Injury. *J. Biol. Chem.* 2016;291(38):19939–52
- Day AJ, Milner CM. TSG-6: A multifunctional protein with anti-inflammatory and tissue-protective properties. *Matrix Biol.* 2018; Available from: <https://linkinghub.elsevier.com/retrieve/pii/S0945053X17304730>

- Day AJ, de la Motte CA. Hyaluronan cross-linking: a protective mechanism in inflammation? *Trends Immunol.* 2005;26(12):637–43
- Dhivya S, Padma VV, Santhini E. Wound dressings – a review. *BioMedicine.* 2015;5(4) Available from:
<http://www.globalsciencejournals.com/article/10.7603/s40681-015-0022-9>
- Di G, Du X, Qi X, Zhao X, Duan H, Li S, et al. Mesenchymal Stem Cells Promote Diabetic Corneal Epithelial Wound Healing Through TSG-6–Dependent Stem Cell Activation and Macrophage Switch. *Investig. Ophthalmology Vis. Sci.* 2017;58(10):4344
- Diegelmann RF, Evans MC. Wound healing: an overview of acute, fibrotic and delayed healing. *Front. Biosci. J. Virtual Libr.* 2004;9(Journal Article):283–9
- Dyer DP, Salanga CL, Johns SC, Valdambrini E, Fuster MM, Milner CM, et al. The Anti-inflammatory Protein TSG-6 Regulates Chemokine Function by Inhibiting Chemokine/Glycosaminoglycan Interactions. *J. Biol. Chem.* 2016;291(24):12627–40
- Dyer DP, Thomson JM, Hermant A, Jowitt TA, Handel TM, Proudfoot AE, et al. TSG-6 inhibits neutrophil migration via direct interaction with the chemokine CXCL8. *J. Immunol. Baltim. Md 1950.* 2014;192(5):2177–85
- Eming SA, Hammerschmidt M, Krieg T, Roers A. Interrelation of immunity and tissue repair or regeneration. *Semin. Cell Dev. Biol.* 2009;20(5):517–27

Eming SA, Krieg T, Davidson JM. Inflammation in Wound Repair: Molecular and Cellular Mechanisms. *J. Invest. Dermatol.* 2007;127(3):514–25

Engelhardt E, Toksoy A, Goebeler M, Debus S, Bröcker E-B, Gillitzer R. Chemokines IL-8, GRO α , MCP-1, IP-10, and Mig Are Sequentially and Differentially Expressed During Phase-Specific Infiltration of Leukocyte Subsets in Human Wound Healing. *Am. J. Pathol.* 1998;153(6):1849–60

Ferrer RA, Saalbach A, Grünwedel M, Lohmann N, Forstreuter I, Saupe S, et al. Dermal Fibroblasts Promote Alternative Macrophage Activation Improving Impaired Wound Healing. *J. Invest. Dermatol.* 2017;137(4):941–50

Fraser JR, Laurent TC. Turnover and metabolism of hyaluronan. *Ciba Found. Symp.* 1989;143(Journal Article):41–53; discussion 53-9, 281–5

Fulop C. Impaired cumulus mucification and female sterility in tumor necrosis factor-induced protein-6 deficient mice. *Development.* 2003;130(10):2253–61

Fulop C, Kamath RV, Li Y, Otto JM, Salustri A, Olsen BR, et al. Coding sequence, exon-intron structure and chromosomal localization of murine TNF-stimulated gene 6 that is specifically expressed by expanding cumulus cell-oocyte complexes. *Gene.* 1997a;202(1–2):95–102

Fulop C, Kamath RV, Li Y, Otto JM, Salustri A, Olsen BR, et al. Coding sequence, exon-intron structure and chromosomal localization of murine

TNF-stimulated gene 6 that is specifically expressed by expanding cumulus cell-oocyte complexes. *Gene*. 1997b;202(1–2):95–102

Gál I, Bajnok É, Szántó S, Sarraj B, Glant TT, Mikecz K. Visualization and in situ analysis of leukocyte trafficking into the ankle joint in a systemic murine model of rheumatoid arthritis. *Arthritis Rheum*. 2005;52(10):3269–78

Getting SJ, Mahoney DJ, Cao T, Rugg MS, Fries E, Milner CM, et al. The Link Module from Human TSG-6 Inhibits Neutrophil Migration in a Hyaluronan- and Inter- α -inhibitor-independent Manner. *J. Biol. Chem*. 2002;277(52):51068–76

Glant TT, Kamath RV, Bárdos T, Gál I, Szántó S, Murad YM, et al. Cartilage-specific constitutive expression of TSG-6 protein (product of tumor necrosis factor α -stimulated gene 6) provides a chondroprotective, but not antiinflammatory, effect in antigen-induced arthritis: Chondroprotective Effect of TSG-6 in Transgenic Mice. *Arthritis Rheum*. 2002;46(8):2207–18

Guest JF, Ayoub N, McIlwraith T, Uchegbu I, Gerrish A, Weidlich D, et al. Health economic burden that wounds impose on the National Health Service in the UK. *BMJ Open*. 2015;5(12):e009283

Gurtner GC, Werner S, Barrandon Y, Longaker MT. Wound repair and regeneration. *Nature*. 2008;453(7193):314–21

- Hampton MB, Kettle AJ, Winterbourn CC. Inside the neutrophil phagosome: oxidants, myeloperoxidase, and bacterial killing. *Blood*. 1998;92(9):3007–17
- Hascall V, Esko JD. Hyaluronan. In: Varki A, Cummings RD, Esko JD, Freeze HH, Stanley P, Bertozzi CR, et al., editors. *Essent. Glycobiol.* 2nd ed. Cold Spring Harbor (NY): The Consortium of Glycobiology Editors, La Jolla, California; 2009.
- He H, Zhang S, Tighe S, Son J, Tseng SCG. Immobilized Heavy Chain-Hyaluronic Acid Polarizes Lipopolysaccharide-activated Macrophages toward M2 Phenotype. *J. Biol. Chem.* 2013;288(36):25792–803
- Hertsenberg AJ, Shojaati G, Funderburgh ML, Mann MM, Du Y, Funderburgh JL. Corneal stromal stem cells reduce corneal scarring by mediating neutrophil infiltration after wounding. Connon CJ, editor. *PLOS ONE*. 2017;12(3):e0171712
- Hesketh M, Sahin KB, West ZE, Murray RZ. Macrophage Phenotypes Regulate Scar Formation and Chronic Wound Healing. *Int. J. Mol. Sci.* 2017a;18(7):1545
- Hesketh M, Sahin KB, West ZE, Murray RZ. Macrophage Phenotypes Regulate Scar Formation and Chronic Wound Healing. *Int. J. Mol. Sci.* 2017b;18(7):1545

Hull RL, Johnson PY, Braun KR, Day AJ, Wight TN. Hyaluronan and hyaluronan binding proteins are normal components of mouse pancreatic islets and are differentially expressed by islet endocrine cell types. *J. Histochem. Cytochem. Off. J. Histochem. Soc.* 2012;60(10):749–60

Ichioka S, Sekiya N, Shibata M, Nakatsuka T. AlphaV beta3 ($\alpha_v\beta_3$) integrin inhibition reduces leukocyte-endothelium interaction in a pressure-induced reperfusion model. *Wound Repair Regen.* 2007;15(4):572–6

Iozzo RV, Murdoch AD. Proteoglycans of the extracellular environment: clues from the gene and protein side offer novel perspectives in molecular diversity and function. *FASEB J. Off. Publ. Fed. Am. Soc. Exp. Biol.* 1996;10(5):598–614

Itano N, Kimata K. Mammalian hyaluronan synthases. *IUBMB Life.* 2002;54(4):195–9

Jbeily N, Claus RA, Dahlke K, Neugebauer U, Bauer M, Gonnert FA. Comparative suitability of CFDA-SE and rhodamine 6G for *in vivo* assessment of leukocyte-endothelium interactions: Leukocyte labelling for intravital microscopy. *J. Biophotonics.* 2014;7(6):369–75

Jessen TE, Ødum L. Role of tumour necrosis factor stimulated gene 6 (TSG-6) in the coupling of inter-alpha-trypsin inhibitor to hyaluronan in human follicular fluid. *Reprod. Camb. Engl.* 2003;125(1):27–31

- Kessler SP, Obery DR, de la Motte C. Hyaluronan Synthase 3 Null Mice Exhibit Decreased Intestinal Inflammation and Tissue Damage in the DSS-Induced Colitis Model. *Int. J. Cell Biol.* 2015;2015(Journal Article):745237
- Khanna S, Biswas S, Shang Y, Collard E, Azad A, Kauh C, et al. Macrophage Dysfunction Impairs Resolution of Inflammation in the Wounds of Diabetic Mice. *Vij N, editor. PLoS ONE.* 2010;5(3):e9539
- Kim J-A, Ko JH, Ko AY, Lee HJ, Kim MK, Wee WR, et al. TSG-6 Protects Corneal Endothelium From Transcorneal Cryoinjury in Rabbits. *Investig. Ophthalmology Vis. Sci.* 2014a;55(8):4905
- Kim J-T, Lee DY, Kim E-J, Jang J-W, Cho N-I. Tissue response to implants of hyaluronic acid hydrogel prepared by microbeads. *Tissue Eng. Regen. Med.* 2014b;11(1):32–8
- Kim M-H, Liu W, Borjesson DL, Curry F-RE, Miller LS, Cheung AL, et al. Dynamics of Neutrophil Infiltration during Cutaneous Wound Healing and Infection Using Fluorescence Imaging. *J. Invest. Dermatol.* 2008;128(7):1812–20
- Kirsner RS, Eaglstein WH. The wound healing process. *Dermatol. Clin.* 1993;11(4):629–40
- Kishimoto TK, Kahn J, Migaki G, Mainolfi E, Shirley F, Ingraham R, et al. Regulation of L-selectin expression by membrane proximal proteolysis. *Agents ActionsSupplements.* 1995;47(Journal Article):121–34

- Koh TJ, DiPietro LA. Inflammation and wound healing: the role of the macrophage. *Expert Rev. Mol. Med.* 2011;13 Available from: http://www.journals.cambridge.org/abstract_S1462399411001943
- Krzyszczczyk P, Schloss R, Palmer A, Berthiaume F. The Role of Macrophages in Acute and Chronic Wound Healing and Interventions to Promote Pro-wound Healing Phenotypes. *Front. Physiol.* 2018;9 Available from: <http://journal.frontiersin.org/article/10.3389/fphys.2018.00419/full>
- Larouche J, Sheoran S, Maruyama K, Martino MM. Immune Regulation of Skin Wound Healing: Mechanisms and Novel Therapeutic Targets. *Adv. Wound Care.* 2018;7(7):209–31
- Lauer ME, Aytekin M, Comhair SA, Loftis J, Tian L, Farver CF, et al. Modification of Hyaluronan by Heavy Chains of Inter- α -Inhibitor in Idiopathic Pulmonary Arterial Hypertension. *J. Biol. Chem.* 2014;289(10):6791–8
- Lauer ME, Cheng G, Swaidani S, Aronica MA, Weigel PH, Hascall VC. Tumor necrosis factor-stimulated gene-6 (TSG-6) amplifies hyaluronan synthesis by airway smooth muscle cells. *J. Biol. Chem.* 2013;288(1):423–31
- Lauer ME, Loftis J, de la Motte C, Hascall VC. Analysis of the heavy-chain modification and TSG-6 activity in pathological hyaluronan matrices. *Methods Mol. Biol. Clifton NJ.* 2015a;1229(Journal Article):543–8
- Lauer ME, Majors AK, Comhair S, Ruple LM, Matuska B, Subramanian A, et al. Hyaluronan and Its Heavy Chain Modification in Asthma Severity and

Experimental Asthma Exacerbation. *J. Biol. Chem.* 2015b;290(38):23124–34

Lawrence MB, Springer TA. Leukocytes roll on a selectin at physiologic flow rates: distinction from and prerequisite for adhesion through integrins. *Cell.* 1991;65(5):859–73

Lee DE, Ayoub N, Agrawal DK. Mesenchymal stem cells and cutaneous wound healing: novel methods to increase cell delivery and therapeutic efficacy. *Stem Cell Res. Ther.* 2016;7(1) Available from: <http://stemcellres.com/content/7/1/37>

Lee MJ, Kim DH, Ryu JS, Ko AY, Ko JH, Kim MK, et al. Topical TSG-6 Administration Protects the Ocular Surface in Two Mouse Models of Inflammation-Related Dry Eye. *Investig. Ophthalmology Vis. Sci.* 2015;56(9):5175

Lee TH, Lee GW, Ziff EB, Vilcek J. Isolation and characterization of eight tumor necrosis factor-induced gene sequences from human fibroblasts. *Mol. Cell. Biol.* 1990;10(5):1982–8

Lee RH, Pulin AA, Seo MJ, Kota DJ, Ylostalo J, Larson BL, et al. Intravenous hMSCs Improve Myocardial Infarction in Mice because Cells Embolized in Lung Are Activated to Secrete the Anti-inflammatory Protein TSG-6. *Cell Stem Cell.* 2009;5(1):54–63

- Lee TH, Wisniewski HG, Vilcek J. A novel secretory tumor necrosis factor-inducible protein (TSG-6) is a member of the family of hyaluronate binding proteins, closely related to the adhesion receptor CD44. *J. Cell Biol.* 1992;116(2):545–57
- Lennon FE, Singleton PA. Hyaluronan regulation of vascular integrity. *Am. J. Cardiovasc. Dis.* 2011;1(3):200–13
- Lesley J, Gál I, Mahoney DJ, Cordell MR, Rugg MS, Hyman R, et al. TSG-6 Modulates the Interaction between Hyaluronan and Cell Surface CD44. *J. Biol. Chem.* 2004;279(24):25745–54
- Ley K, Laudanna C, Cybulsky MI, Nourshargh S. Getting to the site of inflammation: the leukocyte adhesion cascade updated. *Nat. Rev.* 2007;7(9):678–89
- Lindholm C, Searle R. Wound management for the 21st century: combining effectiveness and efficiency: Wound management for the 21st century. *Int. Wound J.* 2016;13:5–15
- Mack JA, Abramson SR, Ben Y, Coffin JC, Rothrock JK, Maytin EV, et al. Hoxb13 knockout adult skin exhibits high levels of hyaluronan and enhanced wound healing. *FASEB J. Off. Publ. Fed. Am. Soc. Exp. Biol.* 2003;17(10):1352–4
- Mack JA, Feldman RJ, Itano N, Kimata K, Lauer M, Hascall VC, et al. Enhanced inflammation and accelerated wound closure following tetraphorbol ester

application or full-thickness wounding in mice lacking hyaluronan synthases Has1 and Has3. *J. Invest. Dermatol.* 2012;132(1):198–207

Martin P. Wound Healing--Aiming for Perfect Skin Regeneration. *Science.* 1997;276(5309):75–81

Martin P, Leibovich SJ. Inflammatory cells during wound repair: the good, the bad and the ugly. *Trends Cell Biol.* 2005;15(11):599–607

Martinez FO, Gordon S. The M1 and M2 paradigm of macrophage activation: time for reassessment. *F1000prime Rep.* 2014;6(Journal Article):13-13. eCollection 2014

Maytin EV. Hyaluronan: More than just a wrinkle filler. *Glycobiology.* 2016;26(6):553–9

McLafferty E, Hendry C, Farley A. The integumentary system: anatomy, physiology and function of skin. *Nurs. Stand.* 2013. 2012;27(3):35

Milner CM, Day AJ. TSG-6: a multifunctional protein associated with inflammation. *J. Cell Sci.* 2003;116(Pt 10):1863–73

Mittal M, Tiruppathi C, Nepal S, Zhao Y-Y, Grzych D, Soni D, et al. TNF α -stimulated gene-6 (TSG6) activates macrophage phenotype transition to prevent inflammatory lung injury. *Proc. Natl. Acad. Sci.* 2016;113(50):E8151–8

- Mukhopadhyay D, Asari A, Rugg MS, Day AJ, Fülöp C. Specificity of the tumor necrosis factor-induced protein 6-mediated heavy chain transfer from inter-alpha-trypsin inhibitor to hyaluronan: implications for the assembly of the cumulus extracellular matrix. *J. Biol. Chem.* 2004;279(12):11119–28
- Muller WA, Weigl SA, Deng X, Phillips DM. PECAM-1 is required for transendothelial migration of leukocytes. *J. Exp. Med.* 1993;178(2):449–60
- Nagy N, Freudenberger T, Melchior-Becker A, Rock K, Ter Braak M, Jastrow H, et al. Inhibition of hyaluronan synthesis accelerates murine atherosclerosis: novel insights into the role of hyaluronan synthesis. *Circulation.* 2010;122(22):2313–22
- Neame PJ, Christner JE, Baker JR. Cartilage proteoglycan aggregates. The link protein and proteoglycan amino-terminal globular domains have similar structures. *J. Biol. Chem.* 1987;262(36):17768–78
- Neudecker BA, Stern R, Connolly MK. Aberrant serum hyaluronan and hyaluronidase levels in scleroderma. *Br. J. Dermatol.* 2004;150(3):469–76
- Nishio N, Okawa Y, Sakurai H, Isobe K. Neutrophil depletion delays wound repair in aged mice. *AGE.* 2008;30(1):11–9
- Noble PW. Hyaluronan and its catabolic products in tissue injury and repair. *Matrix Biol. J. Int. Soc. Matrix Biol.* 2002;21(1):25–9

Nussbaum SR, Carter MJ, Fife CE, DaVanzo J, Haught R, Nusgart M, et al. An Economic Evaluation of the Impact, Cost, and Medicare Policy Implications of Chronic Nonhealing Wounds. *Value Health*. 2018;21(1):27–32

Odland G, Goldsmith I. Physiology, biochemistry and molecular biology of the skin. V. 1991;1:3–62

Oh JY, Roddy GW, Choi H, Lee RH, Ylostalo JH, Rosa RH, et al. Anti-inflammatory protein TSG-6 reduces inflammatory damage to the cornea following chemical and mechanical injury. *Proc. Natl. Acad. Sci*. 2010;107(39):16875–80

Olczyk P, Mencner Ł, Komosinska-Vassev K. The Role of the Extracellular Matrix Components in Cutaneous Wound Healing. *BioMed Res. Int*. 2014;2014:1–8

de Oliveira S, Rosowski EE, Huttenlocher A. Neutrophil migration in infection and wound repair: going forward in reverse. *Nat. Rev. Immunol*. 2016;16(6):378–91

Pardue EL, Ibrahim S, Ramamurthi A. Role of hyaluronan in angiogenesis and its utility to angiogenic tissue engineering. *Organogenesis*. 2008;4(4):203–14

Prockop DJ, Youn Oh J. Mesenchymal Stem/Stromal Cells (MSCs): Role as Guardians of Inflammation. *Mol. Ther*. 2012;20(1):14–20

- Proksch E, Brandner JM, Jensen J-M. The skin: an indispensable barrier. *Exp. Dermatol.* 2008;17(12):1063–72
- Qi Y, Jiang D, Sindrilaru A, Stegemann A, Schatz S, Treiber N, et al. TSG-6 released from intradermally injected mesenchymal stem cells accelerates wound healing and reduces tissue fibrosis in murine full-thickness skin wounds. *J. Invest. Dermatol.* 2014;134(2):526–37
- Rayahin JE, Buhrman JS, Zhang Y, Koh TJ, Gemeinhart RA. High and low molecular weight hyaluronic acid differentially influence macrophage activation. *ACS Biomater. Sci. Eng.* 2015;1(7):481–93
- Rehfeld A, Nylander M, Karnov K. The Integumentary System. In: Rehfeld A, Nylander M, Karnov K, editors. *Compend. Histol. Theor. Pract. Guide.* Cham: Springer International Publishing; 2017. p. 411–32 Available from: https://doi.org/10.1007/978-3-319-41873-5_20
- Reinhardt PH, Elliott JF, Kubes P. Neutrophils can adhere via alpha4beta1-integrin under flow conditions. *Blood.* 1997;89(10):3837–46
- Reitsma S, Slaaf DW, Vink H, van Zandvoort MAMJ, oude Egbrink MGA. The endothelial glycocalyx: composition, functions, and visualization. *Pflüg. Arch. - Eur. J. Physiol.* 2007;454(3):345–59
- Rosales C, Lowell CA, Schnoor M, Uribe-Querol E. Neutrophils: Their Role in Innate and Adaptive Immunity 2017. *J. Immunol. Res.* 2017;2017:1–2

- Rugg MS, Willis AC, Mukhopadhyay D, Hascall VC, Fries E, Fülöp C, et al. Characterization of Complexes Formed between TSG-6 and Inter- α -inhibitor That Act as Intermediates in the Covalent Transfer of Heavy Chains onto Hyaluronan. *J. Biol. Chem.* 2005;280(27):25674–86
- Sadik CD, Kim ND, Luster AD. Neutrophils cascading their way to inflammation. *Trends Immunol.* 2011;32(10):452–60
- Sala E, Genua M, Petti L, Anselmo A, Arena V, Cibella J, et al. Mesenchymal Stem Cells Reduce Colitis in Mice via Release of TSG6, Independently of Their Localization to the Intestine. *Gastroenterology.* 2015;149(1):163-176.e20
- Salustri A, Camaioni A, Di Giacomo M, Fulop C, Hascall VC. Hyaluronan and proteoglycans in ovarian follicles. *Hum. Reprod. Update.* 1999;5(4):293–301
- Salustri A, Fülöp C. Role of hyaluronan during ovulation and fertilisation. 1998; Available from:
<http://glycoforum.gr.jp/science/hyaluronan/HA03/HA03E.html>
- Schafer M, Werner S. Cancer as an overhealing wound: an old hypothesis revisited. *Nat. Rev. Cell Biol.* 2008;9(8):628–38
- Sebag J. Age-related changes in human vitreous structure. *Graefes Arch. Clin. Exp. Ophthalmol. Albrecht Von Graefes Arch. Klin. Exp. Ophthalmol.* 1987;225(2):89–93

- Sen CK. Human Wounds and Its Burden: An Updated Compendium of Estimates. *Adv. Wound Care*. 2019;8(2):39–48
- Sen CK, Gordillo GM, Roy S, Kirsner R, Lambert L, Hunt TK, et al. Human skin wounds: A major and snowballing threat to public health and the economy. *Wound Repair Regen*. 2009;17(6):763–71
- Shakya S, Wang Y, Mack JA, Maytin EV. Hyperglycemia-Induced Changes in Hyaluronan Contribute to Impaired Skin Wound Healing in Diabetes: Review and Perspective. *Int. J. Cell Biol*. 2015;2015:1–11
- Siiskonen H, Oikari S, Pasonen-Seppanen S, Rilla K. Hyaluronan synthase 1: a mysterious enzyme with unexpected functions. *Front. Immunol*. 2015;6(Journal Article):43
- Singer AJ, Clark RA. Cutaneous wound healing. *N. Engl. J. Med*. 1999;341(10):738–46
- Slevin M, Krupinski J, Gaffney J, Matou S, West D, Delisser H, et al. Hyaluronan-mediated angiogenesis in vascular disease: uncovering RHAMM and CD44 receptor signaling pathways. *Matrix Biol. J. Int. Soc. Matrix Biol*. 2007;26(1):58–68
- Smith JA. Neutrophils, host defense, and inflammation: a double-edged sword. *J. Leukoc. Biol*. 1994;56(6):672–86

Song W-J, Li Q, Ryu M-O, Ahn J-O, Ha Bhang D, Chan Jung Y, et al. TSG-6 Secreted by Human Adipose Tissue-derived Mesenchymal Stem Cells Ameliorates DSS-induced colitis by Inducing M2 Macrophage Polarization in Mice. *Sci. Rep.* 2017;7(1) Available from: <http://www.nature.com/articles/s41598-017-04766-7>

Sotiropoulou PA, Blanpain C. Development and Homeostasis of the Skin Epidermis. *Cold Spring Harb. Perspect. Biol.* 2012;4(7):a008383–a008383

Stenson WF. Hyaluronic acid and intestinal inflammation. *Curr. Opin. Gastroenterol.* 2010;26(2):85–7

Stern R, Jedrzejewski MJ. Hyaluronidases: their genomics, structures, and mechanisms of action. *Chem. Rev.* 2006;106(3):818–39

Stone PC, Nash GB. Conditions under which immobilized platelets activate as well as capture flowing neutrophils. *Br. J. Haematol.* 1999;105(2):514–22

Swaidani S, Cheng G, Lauer ME, Sharma M, Mikecz K, Hascall VC, et al. TSG-6 protein is crucial for the development of pulmonary hyaluronan deposition, eosinophilia, and airway hyperresponsiveness in a murine model of asthma. *J. Biol. Chem.* 2013;288(1):412–22

Swann DA, Radin EL, Nazimiec M, Weisser PA, Curran N, Lewinnek G. Role of hyaluronic acid in joint lubrication. *Ann. Rheum. Dis.* 1974;33(4):318–26

- Szanto S, Bardos T, Gal I, Glant TT, Mikecz K. Enhanced neutrophil extravasation and rapid progression of proteoglycan-induced arthritis in TSG-6-knockout mice. *Arthritis Rheum.* 2004;50(9):3012–22
- Tammi MI, Day AJ, Turley EA. Hyaluronan and homeostasis: a balancing act. *J. Biol. Chem.* 2002;277(7):4581–4
- Tammi R, Ripellino JA, Margolis RU, Tammi M. Localization of epidermal hyaluronic acid using the hyaluronate binding region of cartilage proteoglycan as a specific probe. *J. Invest. Dermatol.* 1988;90(3):412–4
- Tan KT, McGrouther DA, Day AJ, Milner CM, Bayat A. Characterization of hyaluronan and TSG-6 in skin scarring: differential distribution in keloid scars, normal scars and unscarred skin. *J. Eur. Acad. Dermatol. Venereol. JEADV.* 2011;25(3):317–27
- Toole BP. Hyaluronan in morphogenesis. *Semin. Cell Dev. Biol.* 2001;12(2):79–87
- Toole BP, Wight TN, Tammi MI. Hyaluronan-cell interactions in cancer and vascular disease. *J. Biol. Chem.* 2002;277(7):4593–6
- Turley EA, Noble PW, Bourguignon LY. Signaling properties of hyaluronan receptors. *J. Biol. Chem.* 2002;277(7):4589–92
- Underhill C. CD44: the hyaluronan receptor. *J. Cell Sci.* 1992;103 (Pt 2)(Pt 2):293–8

- Von Andrian UH, Hansell P, Chambers JD, Berger EM, Torres Filho I, Butcher EC, et al. L-selectin function is required for beta 2-integrin-mediated neutrophil adhesion at physiological shear rates in vivo. *Am. J. Physiol.* 1992;263(4 Pt 2):H1034-44
- Wagner JG, Roth RA. Neutrophil migration mechanisms, with an emphasis on the pulmonary vasculature. *Pharmacol. Rev.* 2000;52(3):349–74
- Wang J. Neutrophils in tissue injury and repair. *Cell Tissue Res.* 2018;371(3):531–9
- Wang H, Chen Z, Li XJ, Ma L, Tang YL. Anti-inflammatory cytokine TSG-6 inhibits hypertrophic scar formation in a rabbit ear model. *Eur. J. Pharmacol.* 2015;751(Journal Article):42–9
- Wang A, Hascall VC. Hyaluronan structures synthesized by rat mesangial cells in response to hyperglycemia induce monocyte adhesion. *J. Biol. Chem.* 2004;279(11):10279–85
- Weigel PH, Fuller GM, LeBoeuf RD. A model for the role of hyaluronic acid and fibrin in the early events during the inflammatory response and wound healing. *J. Theor. Biol.* 1986;119(2):219–34
- Wight TN, Heinegård DK, Hascall VC. Proteoglycans: Structure and Function. In: Hay ED, editor. *Cell Biol. Extracell. Matrix. Second.* Springer Science & Business Media; 2013. p. 45

- Wilgus TA, Roy S, McDaniel JC. Neutrophils and Wound Repair: Positive Actions and Negative Reactions. *Adv. Wound Care*. 2013;2(7):379–88
- Wisniewski HG, Burgess WH, Oppenheim JD, Vilcek J. TSG-6, an arthritis-associated hyaluronan binding protein, forms a stable complex with the serum protein inter-alpha-inhibitor. *Biochemistry*. 1994;33(23):7423–9
- Wisniewski HG, Hua JC, Poppers DM, Naime D, Vilcek J, Cronstein BN. TNF/IL-1-inducible protein TSG-6 potentiates plasmin inhibition by inter-alpha-inhibitor and exerts a strong anti-inflammatory effect in vivo. *J. Immunol. Baltim. Md 1950*. 1996;156(4):1609–15
- Wisniewski HG, Maier R, Lotz M, Lee S, Klampfer L, Lee TH, et al. TSG-6: a TNF-, IL-1-, and LPS-inducible secreted glycoprotein associated with arthritis. *J. Immunol. Baltim. Md 1950*. 1993;151(11):6593–601
- Wisniewski HG, Vilcek J. TSG-6: an IL-1/TNF-inducible protein with anti-inflammatory activity. *Cytokine Growth Factor Rev*. 1997;8(2):143–56
- Yamakawa S, Hayashida K. Advances in surgical applications of growth factors for wound healing. *Burns Trauma*. 2019;7:10
- Zhang S, He H, Day AJ, Tseng SCG. Constitutive Expression of Inter- α -inhibitor (I α I) Family Proteins and Tumor Necrosis Factor-stimulated Gene-6 (TSG-6) by Human Amniotic Membrane Epithelial and Stromal Cells Supporting Formation of the Heavy Chain-Hyaluronan (HC-HA) Complex. *J. Biol. Chem*. 2012;287(15):12433–44

Zhuo L, Kanamori A, Kannagi R, Itano N, Wu J, Hamaguchi M, et al. SHAP Potentiates the CD44-mediated Leukocyte Adhesion to the Hyaluronan Substratum. *J. Biol. Chem.* 2006;281(29):20303–14

Zhuo L, Kimata K. Structure and function of inter-alpha-trypsin inhibitor heavy chains. *Connect. Tissue Res.* 2008;49(5):311–20

Zhuo L, Yoneda M, Zhao M, Yingsung W, Yoshida N, Kitagawa Y, et al. Defect in SHAP-Hyaluronan Complex Causes Severe Female Infertility: A STUDY BY INACTIVATION OF THE BIKUNIN GENE IN MICE. *J. Biol. Chem.* 2001;276(11):7693–6

APPENDIX

Figure 3-1b:

One Way Repeated Measures Analysis of Variance

Monday, September 23, 2019, 11:41:54 PM

Data source: Data 1 in TSG6protein_WT ExW 02-14-18

Normality Test (Shapiro-Wilk) Failed (P < 0.050)

Equal Variance Test: Passed (P = 0.364)

Treatment Name	N	Missing	Mean	Std Dev	SEM
uW	5	0	1.000	0.217	0.0971
12 h	5	0	4.497	1.569	0.701
Day1	4	0	4.568	1.312	0.656
Day 3	5	0	5.136	3.171	1.418
Day5	4	0	3.188	1.127	0.564
Day 7	5	0	2.178	0.593	0.265
Day 10	5	0	2.519	1.558	0.697

Source of Variation	DF	SS	MS	F	P
Between Subjects	4	15.045	3.761		
Between Treatments	6	63.930	10.655	4.240	0.006
Residual	22	55.290	2.513		
Total	32	136.592	4.269		

The differences in the mean values among the treatment groups are greater than would be expected by chance; there is a statistically significant difference (P = 0.006). To isolate the group or groups that differ from the others use a multiple comparison procedure.

Power of performed test with alpha = 0.050: 0.839

Expected Mean Squares:

Approximate DF Residual = 22.000

Expected MS(Subj) = var(res) + 6.500 var(Subj)

Expected MS(Treatment) = var(res) + var(Treatment)

Expected MS(Residual) = var(res)

Multiple Comparisons versus Control Group (Holm-Sidak method):

Overall significance level = 0.05

Comparisons for factor:

Comparison	Diff of Means	t	P	P<0.050
uW vs. Day 3	4.136	4.125	0.003	Yes
uW vs. 12 h	3.497	3.488	0.010	Yes
uW vs. Day1	3.296	3.066	0.022	Yes
uW vs. Day5	1.916	1.782	0.243	No
uW vs. Day 10	1.519	1.515	0.267	No
uW vs. Day 7	1.178	1.175	0.253	No

Figure 3-1b:

t-test

Monday, September 23, 2019, 11:49:07 PM

Data source: Data 1 in Figure 3-1d_HC-HA assay

Normality Test (Shapiro-Wilk) Passed (P = 0.516)

Equal Variance Test: Passed (P = 0.435)

Group Name	N	Missing	Mean	Std Dev	SEM
Fold change uW	3	0	1.000	0.300	0.173
Fold change ExW	3	0	2.697	0.0899	0.0519

Difference -1.697

t = -9.376 with 4 degrees of freedom. (P = <0.001)

95 percent confidence interval for difference of means: -2.199 to -1.194

The difference in the mean values of the two groups is greater than would be expected by chance; there is a statistically significant difference between the input groups (P = <0.001).

Power of performed test with alpha = 0.050: 1.000

Figure 3-3:

Day 3 Excisional wound

t-test

Monday, September 23, 2019, 11:54:02 PM

Data source: Data 1 in Figure 3-3_Wound closure WTvsTSG6null

Normality Test (Shapiro-Wilk) Failed (P < 0.050)

Test execution ended by user request, Rank Sum Test begun

Mann-Whitney Rank Sum Test

Monday, September 23, 2019, 11:54:02 PM

Data source: Data 1 in Figure 3-3_Wound closure WTvsTSG6null

Group	N	Missing	Median	25%	75%
WT Day 3	20	0	60.724	49.646	66.180
TSG-6 null Day 3	20	0	68.654	60.104	90.453

Mann-Whitney U Statistic= 124.000

T = 334.000 n(small)= 20 n(big)= 20 (P = 0.041)

The difference in the median values between the two groups is greater than would be expected by chance; there is a statistically significant difference (P = 0.041)

Day 5 Excisional wound

t-test

Monday, September 23, 2019, 11:54:17 PM

Data source: Data 1 in Figure 3-3_Wound closure WTvsTSG6null

Normality Test (Shapiro-Wilk) Failed (P < 0.050)

Test execution ended by user request, Rank Sum Test begun

Mann-Whitney Rank Sum Test

Monday, September 23, 2019, 11:54:17 PM

Data source: Data 1 in Figure 3-3_Wound closure WTvsTSG6null

Group	N	Missing	Median	25%	75%
WT Day 5	20	0	50.116	41.706	57.361
TSG-6 null Day 5	20	0	67.621	45.614	90.832

Mann-Whitney U Statistic= 121.000

T = 331.000 n(small)= 20 n(big)= 20 (P = 0.034)

The difference in the median values between the two groups is greater than would be expected by chance; there is a statistically significant difference (P = 0.034)

Day 7 Excisional wound

t-test

Monday, September 23, 2019, 11:54:37 PM

Data source: Data 1 in Figure 3-3_Wound closure WTvsTSG6null

Normality Test (Shapiro-Wilk) Passed (P = 0.333)

Equal Variance Test: Passed (P = 0.275)

Group Name	N	Missing	Mean	Std Dev	SEM
WT Day 7	20	0	32.445	17.590	3.933
TSG-6 null Day 7	20	0	50.693	27.283	6.101

Difference -18.247

t = -2.514 with 38 degrees of freedom (P = 0.016)

95 percent confidence interval for difference of means: -32.941 to -3.553

The difference in the mean values of the two groups is greater than would be expected by chance; there is a statistically significant difference between the input groups (P = 0.016).

Power of performed test with alpha = 0.050: 0.612

Day 10 Excisional wound

t-test

Monday, September 23, 2019, 11:54:58 PM

Data source: Data 1 in Figure 3-3_Wound closure WTvsTSG6null

Normality Test (Shapiro-Wilk) Passed (P = 0.426)

Equal Variance Test: Passed (P = 0.568)

Group Name	N	Missing	Mean	Std Dev	SEM
WT Day 10	10	0	13.092	4.855	1.535
TSG-6 null Day 10	10	0	19.310	5.352	1.692

Difference -6.218

t = -2.721 with 18 degrees of freedom (P = 0.014)

95 percent confidence interval for difference of means: -11.018 to -1.417

The difference in the mean values of the two groups is greater than would be expected by chance; there is a statistically significant difference between the input groups (P = 0.014).

Power of performed test with alpha = 0.050: 0.671

Figure 3-4:

Day 1 Excisional wound

t-test

Tuesday, September 24, 2019, 12:23:34 AM

Data source: Data 1 in Figure 3-4_Re-epithelialization

Normality Test (Shapiro-Wilk) Failed (P < 0.050)

Test execution ended by user request, Rank Sum Test begun

Mann-Whitney Rank Sum Test

Tuesday, September 24, 2019, 12:23:34 AM

Data source: Data 1 in Figure 3-4_Re-epithelialization

Group	N	Missing	Median	25%	75%
Day 1 WT	4	0	0.000	0.000	1.369
Day 1 TSG-6 null	4	0	0.000	0.000	0.648

Mann-Whitney U Statistic= 7.500

T = 18.500 n(small)= 4 n(big)= 4 P(est.)= 1.000 P(exact)= 0.886

The difference in the median values between the two groups is not great enough to exclude the possibility that the difference is due to random sampling variability; there is not a statistically significant difference (P = 0.886)

Day 3 Excisional wound

t-test

Tuesday, September 24, 2019, 12:23:46 AM

Data source: Data 1 in Figure 3-4_Re-epithelialization

Normality Test (Shapiro-Wilk) Failed (P < 0.050)

Test execution ended by user request, Rank Sum Test begun

Mann-Whitney Rank Sum Test

Tuesday, September 24, 2019, 12:23:46 AM

Data source: Data 1 in Figure 3-4_Re-epithelialization

Group	N	Missing	Median	25%	75%
Day 3 WT	7	0	11.569	6.686	15.399
Day 3 TSG-6 null	8	0	13.557	8.798	29.748

Mann-Whitney U Statistic= 21.000

T = 49.000 n(small)= 7 n(big)= 8 P(est.)= 0.452 P(exact)= 0.463

The difference in the median values between the two groups is not great enough to exclude the possibility that the difference is due to random sampling variability; there is not a statistically significant difference (P = 0.463)

Day 5 Excisional wound

t-test

Tuesday, September 24, 2019, 12:23:55 AM

Data source: Data 1 in Figure 3-4_Re-epithelialization

Normality Test (Shapiro-Wilk) Passed (P = 0.288)

Equal Variance Test: Passed (P = 0.341)

Group Name	N	Missing	Mean	Std Dev	SEM
Day 5 WT	8	0	84.379	22.447	7.936
Day 5 TSG-6 null	7	0	54.366	28.348	10.714

Difference 30.013

t = 2.288 with 13 degrees of freedom (P = 0.040)

95 percent confidence interval for difference of means: 1.679 to 58.348

The difference in the mean values of the two groups is greater than would be expected by chance; there is a statistically significant difference between the input groups (P = 0.040).

Power of performed test with alpha = 0.050: 0.470

Day 7 Excisional wound

t-test

Tuesday, September 24, 2019, 12:24:05 AM

Data source: Data 1 in Figure 3-4_Re-epithelialization

Normality Test (Shapiro-Wilk) Failed (P < 0.050)

Test execution ended by user request. Rank Sum Test begun

Mann-Whitney Rank Sum Test

Tuesday, September 24, 2019, 12:24:05 AM

Data source: Data 1 in Figure 3-4_Re-epithelialization

Group	N	Missing	Median	25%	75%
Day 7 WT	10	0	100.000	99.000	100.000
Day 7 TSG-6 null	9	0	60.899	25.225	100.000

Mann-Whitney U Statistic= 19.500

T = 64.500 n(small)= 9 n(big)= 10 (P = 0.027)

The difference in the median values between the two groups is greater than would be expected by chance; there is a statistically significant difference (P = 0.027)

Day 10 Excisional wound

t-test

Tuesday, September 24, 2019, 12:24:15 AM

Data source: Data 1 in Figure 3-4_Re-epithelialization

Normality Test (Shapiro-Wilk) Failed (P < 0.050)

Test execution ended by user request. Rank Sum Test begun

Mann-Whitney Rank Sum Test

Tuesday, September 24, 2019, 12:24:15 AM

Data source: Data 1 in Figure 3-4_Re-epithelialization

Group	N	Missing	Median	25%	75%
Day 10 WT	9	0	100.000	94.997	100.000
Day 10 TSG-6 null	10	0	100.000	86.348	100.000

Mann-Whitney U Statistic= 39.500

T = 95.500 n(small)= 9 n(big)= 10 (P = 0.637)

The difference in the median values between the two groups is not great enough to exclude the possibility that the difference is due to random sampling variability; there is not a statistically significant difference (P = 0.637)

Figure 3-5:

12h Excisional wound

t-test

Tuesday, September 24, 2019, 12:38:08 AM

Data source: Data 1 in Figure 3-5_Neutrophil Quantification_Breadloaf Method

Normality Test (Shapiro-Wilk) Passed (P = 0.560)

Equal Variance Test: Failed (P < 0.050)

Test execution ended by user request, Rank Sum Test begun

Mann-Whitney Rank Sum Test

Tuesday, September 24, 2019, 12:38:08 AM

Data source: Data 1 in Figure 3-5_Neutrophil Quantification_Breadloaf Method

Group	N	Missing	Median	25%	75%
12 h WT	23	0	114.898	40.542	165.081
12h TSG6 null	20	0	51.683	23.962	80.310

Mann-Whitney U Statistic= 122.000

T = 332.000 n(small)= 20 n(big)= 23 (P = 0.009)

The difference in the median values between the two groups is greater than would be expected by chance; there is a statistically significant difference (P = 0.009)

Day 1 Excisional wound

t-test

Tuesday, September 24, 2019, 12:38:18 AM

Data source: Data 1 in Figure 3-5_Neutrophil Quantification_Breadloaf Method

Normality Test (Shapiro-Wilk) Failed (P < 0.050)

Test execution ended by user request, Rank Sum Test begun

Mann-Whitney Rank Sum Test

Tuesday, September 24, 2019, 12:38:18 AM

Data source: Data 1 in Figure 3-5_Neutrophil Quantification_Breadloaf Method

Group	N	Missing	Median	25%	75%
Day1 WT	21	0	75.336	44.233	122.118
Day1 TSG-6 null	21	0	51.256	31.772	84.220

Mann-Whitney U Statistic= 153.000

T = 519.000 n(small)= 21 n(big)= 21 (P = 0.092)

The difference in the median values between the two groups is not great enough to exclude the possibility that the difference is due to random sampling variability; there is not a statistically significant difference (P = 0.092)

Day 3 Excisional wound

t-test

Tuesday, September 24, 2019, 12:38:32 AM

Data source: Data 1 in Figure 3-5_Neutrophil Quantification_Breadloaf Method

Normality Test (Shapiro-Wilk) Failed (P < 0.050)

Test execution ended by user request. Rank Sum Test begun

Mann-Whitney Rank Sum Test

Tuesday, September 24, 2019, 12:38:32 AM

Data source: Data 1 in Figure 3-5_Neutrophil Quantification_Breadloaf Method

Group	N	Missing	Median	25%	75%
Day3 WT	17	0	80.016	64.860	101.183
Day3 TSG-6 null	17	0	71.019	36.827	110.587

Mann-Whitney U Statistic= 140.000

T = 302.000 n(small)= 17 n(big)= 17 (P = 0.890)

The difference in the median values between the two groups is not great enough to exclude the possibility that the difference is due to random sampling variability; there is not a statistically significant difference (P = 0.890)

Day 5 Excisional wound

t-test

Tuesday, September 24, 2019, 12:38:41 AM

Data source: Data 1 in Figure 3-5_Neutrophil Quantification_Breadloaf Method

Normality Test (Shapiro-Wilk) Failed (P < 0.050)

Test execution ended by user request. Rank Sum Test begun

Mann-Whitney Rank Sum Test

Tuesday, September 24, 2019, 12:38:41 AM

Data source: Data 1 in Figure 3-5_Neutrophil Quantification_Breadloaf Method

Group	N	Missing	Median	25%	75%
Day5 WT	10	0	46.478	24.450	105.458
Day5 TSG-6 null	13	0	43.679	27.456	109.829

Mann-Whitney U Statistic= 61.000

T = 124.000 n(small)= 10 n(big)= 13 (P = 0.828)

The difference in the median values between the two groups is not great enough to exclude the possibility that the difference is due to random sampling variability; there is not a statistically significant difference (P = 0.828)

Day 7 Excisional wound

t-test

Tuesday, September 24, 2019, 12:39:02 AM

Data source: Data 1 in Figure 3-5_Neutrophil Quantification_Breadloaf Method

Normality Test (Shapiro-Wilk) Failed (P < 0.050)

Test execution ended by user request, Rank Sum Test begun

Mann-Whitney Rank Sum Test

Tuesday, September 24, 2019, 12:39:02 AM

Data source: Data 1 in Figure 3-5_Neutrophil Quantification_Breadloaf Method

Group	N	Missing	Median	25%	75%
Day7 WT	17	0	63.332	43.748	108.457
Day7 TSG-6 null	18	0	151.543	120.124	237.908

Mann-Whitney U Statistic= 35.000

T = 188.000 n(small)= 17 n(big)= 18 (P = <0.001)

The difference in the median values between the two groups is greater than would be expected by chance; there is a statistically significant difference (P = <0.001)

Day 10 Excisional wound

t-test

Tuesday, September 24, 2019, 12:39:14 AM

Data source: Data 1 in Figure 3-5_Neutrophil Quantification_Breadloaf Method

Normality Test (Shapiro-Wilk) Failed (P < 0.050)

Test execution ended by user request, Rank Sum Test begun

Mann-Whitney Rank Sum Test

Tuesday, September 24, 2019, 12:39:14 AM

Data source: Data 1 in Figure 3-5_Neutrophil Quantification_Breadloaf Method

Group	N	Missing	Median	25%	75%
Day10 WT	15	0	11.979	6.028	39.603
Day10 TSG-6 null	14	0	11.006	7.155	20.926

Mann-Whitney U Statistic= 93.000

T = 198.000 n(small)= 14 n(big)= 15 (P = 0.616)

The difference in the median values between the two groups is not great enough to exclude the possibility that the difference is due to random sampling variability; there is not a statistically significant difference (P = 0.616)

Figure 3-6:

No wound

t-test

Tuesday, September 24, 2019, 12:50:07 AM

Data source: Data 1 in Figure 3-6_TNFa WTvsTSG-6null ExW

Normality Test (Shapiro-Wilk) Passed (P = 0.879)

Equal Variance Test: Passed (P = 0.340)

Group Name	N	Missing	Mean	Std Dev	SEM
NoWound WT	5	0	0.542	0.348	0.156
NoWound TSG-6	5	0	1.010	0.562	0.251

Difference -0.469

t = -1.585 with 8 degrees of freedom. (P = 0.152)

95 percent confidence interval for difference of means: -1.150 to 0.213

The difference in the mean values of the two groups is not great enough to reject the possibility that the difference is due to random sampling variability. There is not a statistically significant difference between the input groups (P = 0.152).

Power of performed test with alpha = 0.050: 0.184

The power of the performed test (0.184) is below the desired power of 0.800. Less than desired power indicates you are less likely to detect a difference when one actually exists. Negative results should be interpreted cautiously.

12h Excisional wound

t-test

Tuesday, September 24, 2019, 12:50:14 AM

Data source: Data 1 in Figure 3-6_TNFa WTvsTSG-6null ExW

Normality Test (Shapiro-Wilk) Passed (P = 0.602)

Equal Variance Test: Passed (P = 0.258)

Group Name	N	Missing	Mean	Std Dev	SEM
12h WT	5	0	0.566	0.251	0.112
12h TSG-6 null	5	0	1.597	0.391	0.175

Difference -1.031

t = -4.959 with 8 degrees of freedom. (P = 0.001)

95 percent confidence interval for difference of means: -1.511 to -0.552

The difference in the mean values of the two groups is greater than would be expected by chance; there is a statistically significant difference between the input groups (P = 0.001).

Power of performed test with alpha = 0.050: 0.992

Day 3 Excisional wound

t-test

Tuesday, September 24, 2019, 12:50:22 AM

Data source: Data 1 in Figure 3-6_TNFa WTvsTSG-6null ExW

Normality Test (Shapiro-Wilk) Passed (P = 0.668)

Equal Variance Test: Passed (P = 0.807)

Group Name	N	Missing	Mean	Std Dev	SEM
Day3 WT	5	0	0.780	0.305	0.136
Day3 TSG-6 null	5	0	1.043	0.263	0.118

Difference -0.263

t = -1.460 with 8 degrees of freedom. (P = 0.182)

95 percent confidence interval for difference of means: -0.678 to 0.152

The difference in the mean values of the two groups is not great enough to reject the possibility that the difference is due to random sampling variability. There is not a statistically significant difference between the input groups (P = 0.182).

Power of performed test with alpha = 0.050: 0.149

The power of the performed test (0.149) is below the desired power of 0.800. Less than desired power indicates you are less likely to detect a difference when one actually exists. Negative results should be interpreted cautiously.

Day 5 Excisional wound

t-test

Tuesday, September 24, 2019, 12:50:32 AM

Data source: Data 1 in Figure 3-6_TNFa WTvsTSG-6null ExW

Normality Test (Shapiro-Wilk) Passed (P = 0.402)

Equal Variance Test: Passed (P = 0.239)

Group Name	N	Missing	Mean	Std Dev	SEM
Day5 WT	4	0	0.651	0.115	0.0577
Day5 TSG-6 null	4	0	0.941	0.416	0.208

Difference -0.290

t = -1.344 with 6 degrees of freedom. (P = 0.228)

95 percent confidence interval for difference of means: -0.819 to 0.238

The difference in the mean values of the two groups is not great enough to reject the possibility that the difference is due to random sampling variability. There is not a statistically significant difference between the input groups (P = 0.228).

Power of performed test with alpha = 0.050: 0.114

The power of the performed test (0.114) is below the desired power of 0.800. Less than desired power indicates you are less likely to detect a difference when one actually exists. Negative results should be interpreted cautiously.

Day 7 Excisional wound

t-test

Tuesday, September 24, 2019, 12:50:40 AM

Data source: Data 1 in Figure 3-6_TNFa WTvsTSG-6null ExW

Normality Test (Shapiro-Wilk) Passed (P = 0.833)

Equal Variance Test: Passed (P = 0.609)

Group Name	N	Missing	Mean	Std Dev	SEM
Day7 WT	5	0	0.432	0.443	0.198
Day7 TSG-6 null	4	0	2.457	0.850	0.425

Difference -2.026

t = -4.647 with 7 degrees of freedom. (P = 0.002)

95 percent confidence interval for difference of means: -3.056 to -0.995

The difference in the mean values of the two groups is greater than would be expected by chance; there is a statistically significant difference between the input groups (P = 0.002).

Power of performed test with alpha = 0.050: 0.977

Figure 3-7:

Day 5 Excisional wound

t-test

Tuesday, September 24, 2019, 12:54:41 AM

Data source: Data 1 in Figure 3-7_Macrophage Quantification_Breadloaf Method

Normality Test (Shapiro-Wilk) Failed (P < 0.050)

Test execution ended by user request, Rank Sum Test begun

Mann-Whitney Rank Sum Test

Tuesday, September 24, 2019, 12:54:41 AM

Data source: Data 1 in Figure 3-7_Macrophage Quantification_Breadloaf Method

Group	N	Missing	Median	25%	75%
Day5 WT	16	0	33.555	16.488	62.779
Day5 TSG-6 null	15	0	30.419	18.818	49.811

Mann-Whitney U Statistic= 113.000

T = 233.000 n(small)= 15 n(big)= 16 (P = 0.797)

The difference in the median values between the two groups is not great enough to exclude the possibility that the difference is due to random sampling variability; there is not a statistically significant difference (P = 0.797)

Day 7 Excisional wound

t-test

Tuesday, September 24, 2019, 12:54:48 AM

Data source: Data 1 in Figure 3-7_Macrophage Quantification_Breadloaf Method

Normality Test (Shapiro-Wilk) Passed (P = 0.331)

Equal Variance Test: Passed (P = 0.184)

Group Name	N	Missing	Mean	Std Dev	SEM
Day7 WT	13	0	73.701	36.368	10.087
Day7 TSG-6 null	21	0	57.190	27.341	5.966

Difference 16.512

t = 1.508 with 32 degrees of freedom. (P = 0.141)

95 percent confidence interval for difference of means: -5.798 to 38.821

The difference in the mean values of the two groups is not great enough to reject the possibility that the difference is due to random sampling variability. There is not a statistically significant difference between the input groups (P = 0.141).

Power of performed test with alpha = 0.050: 0.182

The power of the performed test (0.182) is below the desired power of 0.800. Less than desired power indicates you are less likely to detect a difference when one actually exists. Negative results should be interpreted cautiously.

Figure 3-8a:

t-test

Tuesday, September 24, 2019, 1:00:38 AM

Data source: Data 1 in Figure 3-8a_CD38 staining

Normality Test (Shapiro-Wilk) Passed (P = 0.931)

Equal Variance Test: Passed (P = 0.546)

Group Name	N	Missing	Mean	Std Dev	SEM
CD38/F480_WT	7	0	0.197	0.116	0.0440
CD38/F480_TSG-6 null	7	0	0.594	0.157	0.0593

Difference -0.397

t = -5.380 with 12 degrees of freedom. (P = <0.001)

95 percent confidence interval for difference of means: -0.558 to -0.236

The difference in the mean values of the two groups is greater than would be expected by chance; there is a statistically significant difference between the input groups (P = <0.001).

Power of performed test with alpha = 0.050: 0.999

Figure 3-8b:

t-test

Tuesday, September 24, 2019, 1:05:06 AM

Data source: Data 1 in Figure 3-8b_Arginase-1 staining

Normality Test (Shapiro-Wilk) Failed (P < 0.050)

Test execution ended by user request, Rank Sum Test begun

Mann-Whitney Rank Sum Test

Tuesday, September 24, 2019, 1:05:06 AM

Data source: Data 1 in Figure 3-8b_Arginase-1 staining

Group	N	Missing	Median	25%	75%
Arg-1/F480_WT	20	0	0.496	0.266	0.713
Arg-1/F480_TSG-6 null	21	0	0.209	0.0922	0.511

Mann-Whitney U Statistic= 116.000

T = 514.000 n(small)= 20 n(big)= 21 (P = 0.015)

The difference in the median values between the two groups is greater than would be expected by chance; there is a statistically significant difference (P = 0.015)

Figure 3-9c:

Two Way Analysis of Variance

Tuesday, September 24, 2019, 3:57:35 AM

Data source: rTSG-6 Wound Closure in Figure 3-9_Wound closure rTSG-6 Experiment

Balanced Design

Dependent Variable: Wound Area

Normality Test (Shapiro-Wilk) Passed (P = 0.212)

Equal Variance Test: Passed (P = 0.582)

Source of Variation	DF	SS	MS	F	P
Genotype	1	90.473	90.473	0.465	0.501
Treatment	1	58.801	58.801	0.302	0.587
Genotype x Treatment	1	2825.805	2825.805	14.529	<0.001
Residual	28	5445.818	194.493		
Total	31	8420.896	271.642		

Main effects cannot be properly interpreted if significant interaction is determined. This is because the size of a factor's effect depends upon the level of the other factor.

The effect of different levels of Genotype depends on what level of Treatment is present. There is a statistically significant interaction between Genotype and Treatment. (P = <0.001)

Power of performed test with alpha = 0.0500: for Genotype : 0.0500

Power of performed test with alpha = 0.0500: for Treatment : 0.0500

Power of performed test with alpha = 0.0500: for Genotype x Treatment : 0.958

Least square means for Genotype :

Group	Mean
WT	42.085
TSG-6 null	38.722

Std Err of LS Mean = 3.487

Least square means for Treatment :

Group	Mean
Vehicle Control	39.048
rTSG-6	41.759

Std Err of LS Mean = 3.487

Least square means for Genotype x Treatment :

Group	Mean
WT x Vehicle Control	31.332
WT x rTSG-6	52.838
TSG-6 null x Vehicle Control	46.764
TSG-6 null x rTSG-6	30.681

Std Err of LS Mean = 4.931

All Pairwise Multiple Comparison Procedures (Bonferroni t-test):

Comparisons for factor: Genotype	Diff of Means	t	P	P<0.050
----------------------------------	---------------	---	---	---------

WT vs. TSG-6 null	3.363	0.682	0.501	No
-------------------	-------	-------	-------	----

Comparisons for factor: Treatment

Comparison	Diff of Means	t	P	P<0.050
rTSG-6 vs. Vehicle Control	2.711	0.550	0.587	No

Comparisons for factor: Treatment within WT

Comparison	Diff of Means	t	P	P<0.05
rTSG-6 vs. Vehicle Control	21.505	3.084	0.005	Yes

Comparisons for factor: Treatment within TSG-6 null

Comparison	Diff of Means	t	P	P<0.05
Vehicle Control vs. rTSG-6	16.083	2.306	0.029	Yes

Comparisons for factor: Genotype within Vehicle Control

Comparison	Diff of Means	t	P	P<0.05
TSG-6 null vs. WT	15.431	2.213	0.035	Yes

Comparisons for factor: Genotype within rTSG-6

Comparison	Diff of Means	t	P	P<0.05
WT vs. TSG-6 null	22.157	3.178	0.004	Yes

Figure 3-9d:

Two Way Analysis of Variance

Tuesday, September 24, 2019, 4:01:12 AM

Data source: NeutRecruitment_12hours in Figure 3-9d_Neutrophil Quant_Breadloaf_rTSG-6 Experiment

General Linear Model

Dependent Variable: Neutrophils

Normality Test (Shapiro-Wilk) Passed (P = 0.110)

Equal Variance Test: Passed (P = 0.060)

Source of Variation	DF	SS	MS	F	P
Genotype	1	6928.113	6928.113	14.025	<0.001
Treatment	1	8.858	8.858	0.0179	0.894
Genotype x Treatment	1	4427.035	4427.035	8.962	0.003
Residual	100	49396.971	493.970		
Total	103	60380.444	586.218		

Main effects cannot be properly interpreted if significant interaction is determined. This is because the size of a factor's effect depends upon the level of the other factor.

The effect of different levels of Genotype depends on what level of Treatment is present. There is a statistically significant interaction between Genotype and Treatment. (P = 0.003)

Power of performed test with alpha = 0.0500: for Genotype : 0.963
 Power of performed test with alpha = 0.0500: for Treatment : 0.0500
 Power of performed test with alpha = 0.0500: for Genotype x Treatment : 0.813

Least square means for Genotype :

Group	Mean	SEM
WT	46.874	3.119
TSG-6 null	30.427	3.091

Least square means for Treatment :

Group	Mean	SEM
Vehicle Control	38.945	3.166
rTSG-6	38.357	3.043

Least square means for Genotype x Treatment :

Group	Mean	SEM
WT x Vehicle Control	53.741	4.738
WT x rTSG-6	40.006	4.058
TSG-6 null x Vehicle Control	24.148	4.200
TSG-6 null x rTSG-6	36.707	4.537

All Pairwise Multiple Comparison Procedures (Bonferroni t-test):

Comparisons for factor: Genotype

Comparison	Diff of Means	t	P	P<0.050
------------	---------------	---	---	---------

WT vs. TSG-6 null	16.447	3.745	<0.001	Yes
-------------------	--------	-------	--------	-----

Comparisons for factor: **Treatment**

Comparison	Diff of Means	t	P	P<0.050
Vehicle Control vs. rTSG-6	0.588	0.134	0.894	No

Comparisons for factor: **Treatment within WT**

Comparison	Diff of Means	t	P	P<0.05
Vehicle Control vs. rTSG-6	13.735	2.202	0.030	Yes

Comparisons for factor: **Treatment within TSG-6 null**

Comparison	Diff of Means	t	P	P<0.05
rTSG-6 vs. Vehicle Control	12.559	2.031	0.045	Yes

Comparisons for factor: **Genotype within Vehicle Control**

Comparison	Diff of Means	t	P	P<0.05
WT vs. TSG-6 null	29.593	4.674	<0.001	Yes

Comparisons for factor: **Genotype within rTSG-6**

Comparison	Diff of Means	t	P	P<0.05
WT vs. TSG-6 null	3.300	0.542	0.589	No

Figure 3-9e:

Kruskal-Wallis One Way Analysis of Variance on Ranks Tuesday, September 24, 2019, 4:45:34 AM

Data source: NeutRecruitment_Day7 in Figure 3-9e_Day7 Neutrophil Quant_Breadloaf_rTSG-6 Experiment

Normality Test (Shapiro-Wilk) Failed (P < 0.050)

Group	N	Missing	Median	25%	75%
WT Vehicle Control	24	0	2.842	1.554	6.603
WT +rTSG-6	18	0	2.759	1.975	4.355
TSG-6 Vehicle Control	23	0	9.466	3.795	19.826
TSG-6 null +rTSG-6	17	0	2.367	1.277	4.766

H = 21.518 with 3 degrees of freedom. (P = <0.001)

The differences in the median values among the treatment groups are greater than would be expected by chance; there is a statistically significant difference (P = <0.001)

To isolate the group or groups that differ from the others use a multiple comparison procedure.

All Pairwise Multiple Comparison Procedures (Dunn's Method) :

Comparison	Diff of Ranks	Q	P<0.05
TSG-6 Vehicle vs TSG-6 null +r	31.256	4.103	Yes
TSG-6 Vehicle vs WT +rTSG-6	25.053	3.343	Yes
TSG-6 Vehicle vs WT Vehicle Co	24.359	3.505	Yes
WT Vehicle Co vs TSG-6 null +r	6.897	0.914	No
WT Vehicle Co vs WT +rTSG-6	0.694	0.0935	Do Not Test
WT +rTSG-6 vs TSG-6 null +r	6.203	0.770	Do Not Test

Note: The multiple comparisons on ranks do not include an adjustment for ties.

Figure 4-7:

t-test

Tuesday, September 24, 2019, 4:38:57 AM

Data source: Data 1 in Figure 4-7_Adgre1_rtPCR_FACS sorted Macrophages

Normality Test (Shapiro-Wilk) Passed (P = 0.584)

Equal Variance Test: Passed (P = 0.053)

Group Name	N	Missing	Mean	Std Dev	SEM
dCt CD45 only	5	0	19.794	1.418	0.634
dCt CD45+F4/80+ Macrophages	6	0	13.541	0.422	0.172

Difference 6.253

t = 10.365 with 9 degrees of freedom. (P = <0.001)

95 percent confidence interval for difference of means: 4.888 to 7.618

The difference in the mean values of the two groups is greater than would be expected by chance; there is a statistically significant difference between the input groups (P = <0.001).

Power of performed test with alpha = 0.050: 1.000

Figure 5-3:

Kruskal-Wallis One Way Analysis of Variance on Ranks Tuesday, September 24, 2019, 5:01:00 AM

Data source: Data 1 in Figure 5-3_Leukocyte rolling behavior_WT vs TSG6 null

Normality Test (Shapiro-Wilk) Failed (P < 0.050)

Group	N	Missing	Median	25%	75%
WT Acetone Control	10	0	0.000	0.000	29.066
WT Croton Oil	10	0	49.144	8.137	75.882
TSG-6 null Acetone Control	11	0	25.281	0.000	35.088
TSG-6 null Croton Oil	11	0	17.937	8.621	49.881

H = 6.888 with 3 degrees of freedom. (P = 0.076)

The differences in the median values among the treatment groups are not great enough to exclude the possibility that the difference is due to random sampling variability; there is not a statistically significant difference (P = 0.076)

Figure 5-4:

Kruskal-Wallis One Way Analysis of Variance on Ranks Tuesday, September 24, 2019, 5:01:36 AM

Data source: Data 1 in Figure 5-4_Leukocyte adhesion behavior_WT vs TSG6 null

Normality Test (Shapiro-Wilk) Failed (P < 0.050)

Group	N	Missing	Median	25%	75%
WT Acetone Control	10	0	0.000	0.000	4.167
WT Croton Oil	10	0	14.787	4.245	18.904
TSG-6 null Acetone Control	11	0	0.000	0.000	0.000
TSG-6 null Croton Oil	11	0	17.647	7.692	25.000

H = 18.951 with 3 degrees of freedom. (P = <0.001)

The differences in the median values among the treatment groups are greater than would be expected by chance; there is a statistically significant difference (P = <0.001)

To isolate the group or groups that differ from the others use a multiple comparison procedure.

All Pairwise Multiple Comparison Procedures (Dunn's Method) :

Comparison	Diff of Ranks	Q	P<0.05
TSG-6 null Cr vs TSG-6 null Ac	17.545	3.354	Yes
TSG-6 null Cr vs WT Acetone Co	14.509	2.707	Yes
TSG-6 null Cr vs WT Croton Oil	1.509	0.282	No
WT Croton Oil vs TSG-6 null Ac	16.036	2.992	Yes
WT Croton Oil vs WT Acetone Co	13.000	2.370	No
WT Acetone Co vs TSG-6 null Ac	3.036	0.566	No

Note: The multiple comparisons on ranks do not include an adjustment for ties.